ADVANCED ELECTRIC THRUSTER (A SPACE ELECTRIC RAMJET)

Gordon L. Cann

Technion, Incorporated

Prepared for:

Air Force Rocket Propulsion Laboratory

April 1973

NOTICES

When U.S. Government drawings, specifications, or other data are used for any purpose other than a definitely related government procurement operation, the Government thereby incurs no responsibility nor any obligation whatsoever, and the fact that the Government may have formulated, furnished, or in any way supplied the said drawings, specifications or other data, is not to be regarded by implication or otherwise, or in any manner licensing the holder or any other person or corporation, or conveying any rights or permission to manufacture use, or sell any patented invention that may in any way be related thereto.

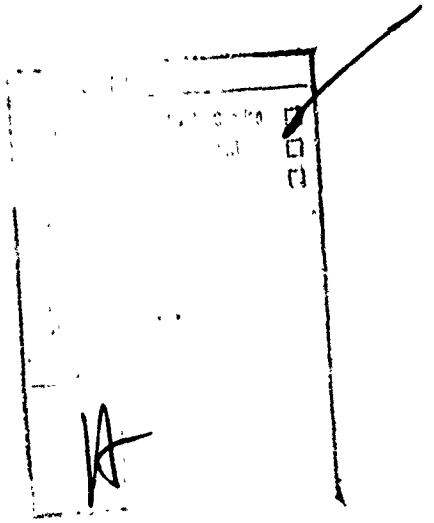

Security Classification

DOCUMENT CONTROL DATA - R & D

(Security classification of title, body of abstract and indexing annotation must be entered when the overall report is classified)

1. ORIGINATING ACTIVITY (Corporate author) AFRPL-Edwards AFB	2a. REPORT SECURITY CLASSIFICATION UNCLASSIFIED 2b. GROUP DCAS

3. REPORT TITLE

ADVANCED ELECTRIC THRUSTER

4. DESCRIPTIVE NOTES (Type of report and inclusive dates)

FINAL

5. AUTHOR(S) (First name, middle initial, last name)

GORDON L. CANN

6. REPORT DATE APRIL 1973	7a. TOTAL NO. OF PAGES ~~105~~ 117	7b. NO. OF REFS 19
8a. CONTRACT OR GRANT NO. F 04611-73-C-0020 b. PROJECT NO. 10-003 c. d.	9a. ORIGINATOR'S REPORT NUMBER(S) AFRPL-TR-73-12 9b. OTHER REPORT NO(S) (Any other numbers that may be assigned this report) FQ7623	

10. DISTRIBUTION STATEMENT

"Approved for public release; distribution unlimited"

11. SUPPLEMENTARY NOTES Details of illustrations in this document may be better studied on microfiche.	12. SPONSORING MILITARY ACTIVITY AIR FORCE

13. ABSTRACT

Laboratory experiments have established that axisymmetric plasma accelerators using a solenoidal magnetic field can produce thrust by recycling the ambient material of the vacuum tank in which they were operated, indicating that an electromagnetic accelerator on a satellite at low altitude should be able to ionize and accelerate air streaming by it and produce thrust for drag make up. This principle is the basis of the Space Electric Ramjet, (SERJ/Advanced Electric Thruster). Utilization of solar cell arrays to supply power gives the system a theoretical unlimited total impulse, otherwise limited by engine cathode and anode lifetimes. These lifetimes can be very long, however.

Minimum system performance requirements for drag make up in the 100-300 miles altitude range are computed. Present solar cell technology places a lower limit of about 120 miles altitude for successful solar-powered drag makeup under conditions of minimum drag by the cell arrays (alignment parallel to line of flight).

Basic design parameters for system components (anode, cathode, magnet coil, insulators) and power requirements are calculated. An analysis shows an engine of less than 10 pounds weight should make up drag of a 1 meter x 1 meter cylindrical satellite for one year at altitudes of 120 miles and higher.

Comments are made on integration of the propulsion system into a satellite, and on possible mechanical and electromagnetic interference effects. Facility and instrumentation requirements to conduct an experimental feasibility and performance program are outlined.

DD FORM 1 NOV 65 1473

UNCLASSIFIED
Security Classification

14. KEY WORDS	LINK A		LINK B		LINK C	
	ROLE	WT	ROLE	WT	ROLE	WT

FOREWORD

Recent satellite advanced have allowed mission planners to pursue mission goals that are more ambitious than ever thought possible. Consequently, there has been a considerable impace on satellite propulsion systems. Future systems will be forced to accomplish missions involving large total impulses. To reasonable achieve this performance level, the ambient atmosphere should be used whenever possible to supply the thruster propellant. Provided that adequate plasma can be generated from the atmosphere, electromagnetic techniques can be employed for drag make-up and other low thrust maneuvers, using power collected from solar cell arrays. The system herein described has the potential of producing extremely large total impulses, extending the lifetimes of low orbit satellites by many times.

This technical report has been reviewed and is approved.

WALTER A. DETJEN, Chief
Engine Development Branch

ACKNOWLEDGEMENTS

This propulsion concept took definitive form while the author was engaged as a visiting scientist at the Thermo-Mechanics Laboratory at Aerospace Research Laboratories, WPAFB. He would like to thank Mr. Eric Soehngen and Mr. Ken Cramer of that laboratory for many valuable discussions that helped to crystallize the concept.

Ever since the initial idea was presented to the Rocket Propulsion Laboratory, Major S. Baty has been extremely helpful in suggesting ideas and providing enthusiastic support for the study. This help is gratefully acknowledged.

Discussions were held with Dr. Dan Goldin of TRW on problems associated with integrating the propulsion system into the spacecraft. His valuable suggestions are acknowledged with thanks.

LIST OF FIGURES

LIST OF SYMBOLS

a	radius of spacecraft body
A_θ	vector potential
A_i	cross-sectional area
B	magnetic field strength
C_D	drag coefficient
C_T	coefficient of thrust
C_V	voltage coefficient
$\|e\|$	charge on the electron
E	electric field strength
$E(k^2)$	elliptic function
F_D	drag force
F_T	thrust force
$F(k)$	grouping of elliptic functions (see Eq.4.10)
i	induced current
I	electric current (discharge and/or magnet)
J_{ℓ}	axial moment of inertia of satellite
k	gas constant
k^2	parameter in elliptic function, $= \frac{4R}{(1 + R)^2 + Z^2}$
$K(k^2)$	elliptic function
l	length of anode ring
L	length of magnet wire
m_V	satellite mass

m	particle mass
$\dot{m}$	mass flow rate
M	mass of magnet
M^*	Mach number
n	number density of particles
N	number of turns on magnet coil
p	pressure
P	power
$\left(\frac{dP}{dA}\right)_s$	solar radiant power per unit area at earth's orbit
q_{eI}	cross section for electron-ion colisions
q_{ea}^{I}	cross section for ionizing collisions
r	radius
R	non-dimensional radius
R^*	resistance of electric circuit
R_e	Reynold's number
S	non-dimensional satellite velocity $= \frac{v}{\sqrt{\frac{2kT}{m}}}$
t	time
t_Y	number of seconds in one year
T	temperature
v_i	gas velocity
v_{cr}	critical or Alfvén velocity $= \sqrt{\frac{2\lvert e\rvert V_I}{m_I}}$
V	electric potential drop
V_I	ionization potential

z	axial coordinate
Z	number of charges on ions
Z_A	non-dimensional axial coordinate
	various coefficients, defined *in situ*
$\frac{\alpha}{p}$	ionization rate parameter
γ_A	ratio of anode area to solar cell area
θ	angular displacement
ϕ	magnetic flux
Φ	angular displacement
χ	work function of metal
σ_W	electrical conductivity of magnet wire
σ	Stefan-Boltzmann constant
ϵ	emissivity of surface
μ	viscosity of gas; magnetic moment
μ_o	permeability of free space
ρ	gas density
ρ_W	density of magnet wire material
ϵ^*	fraction of atoms ionized
σ'	surface reflection coefficient for normal momentum transfer
σ''	surface reflection coefficient for shear momentum transfer
η_{sc}	solar cell efficiency
τ	period for reversal of magnetic field

τ_e	collision time for electrons
τ_I	collision time for ions
ω_e	cyclotron frequency for electrons
ω_I	cyclotron frequency for ions

TABLE OF CONTENTS

1. Introduction

The thrust to conduct the maneuvers associated with satellite reorientation, orbit modification and drag make-up has up to the present been provided by any one of a number of means:

cold gas jets
hydrazine jets
ion engines
arc jets and plasma thrusters carrying their own propellant
chemical rocket propulsion systems
colloid thrusters.

The problems and disadvantages of these systems are many and diverse, but they have in common the critical problem that the total impulse available is proportional to the mass of propellant carried on the space craft. Mission life-times must hence be programmed from the point of view of this limitation, rather than from the mission requirements. Utilization of ambient atmosphere as propellant eliminates this problem.

Studies have been conducted to determine the feasibility of collecting air at high altitudes for use in chemical or electric propulsion systems. The most extensive investigations were those of S.T.Demetriades and colleagues on the Air-Scooping Orbital Rocket (A-SCOR) (Ref. 1-4). Similar studies were carried out elsewhere (Ref.5-9). These studies indicated that the system was feasible provided that a power source of considerable size (several Megawatts) was available to assist in the collection process and to heat the air (thermally or electrically) used as propellant in the thruster system. The lack of an adequate power source appears to be the main obstacle to the implementation of this system.

The ideal propulsion system for satellites would be one for which both power and propellant were available *in situ*. Rapid improvements in solar cell technology and in the technology of axisymmetric plasma accelerators over the past ten years make it desirable at this time to investigate the feasibility of such a truly infinite total impulse propulsion system. Obviously, unless extremely large solar cell arrays are

utilized (on the order of square kilometers), the power level available will be low (under 10 kilowatts), so that the cryogenic collection and storage of propellant--as suggested in the above-mentioned studies -- will not be feasible. An alternate means of propellant handling is obtained through the use of a space-electric ram jet, which device is herein investigated. The SERJ utilizes a solenoidal magnetic field and the ionization of the ambient air in an electric discharge, as the basic elements of the operation of a plasma propulsion engine, for which power is supplied by solar cell arrays. This system would have an infinite total impulse.

1.1 Axisymmetric Plasma Accelerators--Background

During the decade from 1956 to 1966 both the USAF and NASA funded extensive programs to develop low-thrust electric propulsion systems. Hampered by lack of a definitive theory of operation, the axisymmetric plasma accelerators lagged behind the development of thermal arc jets, ion engines and colloid thrusters. Indeed, phenomena were observed that appeared to intimately couple the plasma engine operation and performance with the test environment (Refs. 10-13). A great deal of effort was expended in attempting to decouple the engine from its environment by continually reducing the ambient pressure into which the engine was exhausted. Due to problems of this nature the plasma thruster has been viewed with distrust by potential users, and other systems have been given priority by the development agencies. However, the unique characteristics of the magnetoplasmadynamic (MPD) arc or axisymmetric accelerator endow it with some very desirable features for low orbit missions, in that it appears very probable that it can utilize the ambient atmosphere as propellant--in other words, instead of attempting to decouple the engine from its environment, use the interaction as a propulsion mechanism. Many tests in various laboratories in this country have established that the following phenomena occur:

1. Thrust is produced by the expulsion of high-velocity ions from the engine.
2. The ions are produced by collisons between atoms and

energetic electrons throughout the volume of the discharge.

3. The electrical discharge extends a considerable distance downstream of the electrodes, and hence transfers most of the energy to the gas far from the engine. Viscous interaction with the engine components can therefore be neglected. Thermal conduction effects to all engine components other than the cathode can also be neglected.
4. The solenoidal magnetic field that is applied acts as a magnetic nozzle for any plasma that is produced by the discharge. That is, all forms of electron and ion energy (exclusive of ionization and radiation) are converted into axial and radial ion velocities by expansion out of the magnetic field. This indicates that all the electrical power of the discharge can be converted into beam power except for the anode and cathode power losses, and the power used in ionizing the propellant.
5. All of the beam energy cannot be converted into axial kinetic energy (propulsion), since the ions must have some tangential velocity to balance the torque produced on the accelerator by the discharge current in crossing the applied magnetic field. Also, there will be some radial velocity of the ions due to the shape of the magnetic nozzle.
6. A large fraction of the thrust reaction occurs on the magnet, indicating that azimuthal currents must be flowing in the plasma column.
7. As the mass flow injected through the engine is reduced, the discharge envelope grows larger and encompasses more mass. The high energy electrons in the discharge ionize some of this gas and use it as propellant. Eventually the discharge ionizes enough material to make up a

minimum-potential mode mass flow rate for the engine. Under certain operating conditions, this total flow -- below called the critical mass flow, or $\dot{m}_{cr}$ -- can be obtained from the ambient gas.

8. Under a wide range of operating conditions, some fraction of the discharge current is observed to be confined to a long reentrant filament that spins very rapidly (20khz-500khz) through the gas. The filament can be considered as an ionization front.

2. Engine Design and Operating Mechanisms

2.1 Configuration

The space electric ramjet (Advanced Electric Thruster) consists of the following elements (see Fig.2.1): a component for producing an axisymmetric magnetic field[1], an anode ring[2], a cathode assembly[3], and a power supply[4]. The magnetic field may be produced by either permanent magnets or by a solenoidal coil. The current to operate the latter is obtained from an auxilliary power supply or by the same used to supply the arc current. The magnets or solenoidal coil may be placed around the spacecraft, or at one or both ends. The anode ring consists of one or more metallic rings placed concentric to the magnetic field. The rings can be made from any suitable material (e.g. brass, copper, aluminum, molybdenum, iron, etc.) depending on the power and discharge level. The size of the anode ring is determined primarily by the magnitude of the discharge current, the following relation holding:

$$I = \alpha_1 \frac{(n_e)_A |e|}{4} \sqrt{\frac{8kT_e}{\pi m_e}} \; A_A \qquad (2.1)$$

where

I = discharge current

A_A = area of anode ring or rings

$(n_e)_A$ = electron density near anode face

$|e|$ = charge on the electron

k = gas constant

m_e = mass of the electron

T_e = electron temperature near anode face

$\alpha_1 = \dfrac{\text{anode attachment area}}{\text{anode area}}$

The cathode is designed to produce electrons on the center line of the device at a rate adequate to carry the discharge current in the vicinity of the cathode and "cathode jet". The cathode may consist of any one of

the following configurations, or any combination thereof:

1. A thermionic emitter heated from some external source.
2. A thermionic emitter heated by energy from the discharge. This energy can come from ion bombardment or thermal conduction.
3. A field-emission type cathode.

The cathode configuration should be confined to as small a cross-sectional area on the center line (i.e. concentric with the anode ring) as feasible.

Electrical power to operate the thruster can come from a number of sources. The most effective method of obtaining electric power is through the use of solar cells and a storage battery, the former either on the body of the spacecraft or on arrays that are deployed out some distance from the satellite. A very effective method of using this type of power is to place the satellite in an eccentric orbit. During most of the orbit energy is being collected and stored while the thruster is not operating. Only near perigee, when the satellite is at altitudes below 400 miles, is the engine activated and the resultant thrust used for drag make-up, orbit shifts, attitude control, etc. Power can also be obtained from any other source aboard the spacecraft, such as fuel cells, batteries, nuclear reactors, etc. A promising new energy source for this specific application may be the use of high power lasers to beam power from stations at the surface to the spacecraft.

2.2 Modes of Operation

The thruster can be designed to operate either on a steady state basis, intermittently, or pulsed. The type of thrust program employed will depend upon many factors, such as power availability, possible communications interference, etc. One possible mode of operation that would be very efficient would be operation of the thruster at altitudes where the ambient ionization level is near its peak, i.e. in the region between 200 and 300 km altitude. By properly designing the magnetic field configuration, the discharge could encompass a large cross-section in space and utilize only the existing ions and electrons. In this manner the thrust is produced without any accompanying ionization energy loss.

Also, in this mode, it will be possible to operate at much higher electric potentials and hence at much higher specific impulses.

2.2.1 The Minimum Power Hypothesis

For many plasma engines it has been found that the performance data can best be correlated and understood if the assumption is made that the engine operates at a minimum arc potential (see References 16,17,18). In order to accomplish this, the power input to the beam and to the production of charged particles is equipartitioned, i.e.

$$\frac{F^2}{2\dot{m}} = \dot{m}\frac{|e|}{m_a}\left(V_I^1 + V_I^2 + \ldots\right)$$

When this occurs, the exhaust beam velocity is the Alfvén speed

$$v_{Al} = \sqrt{\frac{2|e|\left(V_I^1 + V_I^2 + \ldots\right)}{m_a}} \qquad (2.2.1)$$

The mass flow rate in the exhaust beam adjusts itself to equal a "critical mass flow rate

$$\dot{m}_{cr} = \frac{F}{v_{cr}} = \frac{F}{v_{Al}} \qquad (2.2.2)$$

This "adjustment" can be accomplished in a number of ways (see Reference 16). For the mode of operation under discussion in this report, the discharge is assumed to spread out in the volume behind the engine until it encompasses enough volume to ionize gas at a rate sufficient to produce the critical mass flow rate. Needless to say, this type of behavior has been observed on many occasions and often the size of the vacuum tank was the factor that limited the

growth of the discharge volume.

2.3 Plasma Acceleration Mechanisms

A very thorough discussion of these phenomena is given in References 13-15, and rather than reproducing it here, the relevant parts of one of the reports (Ref.13) are appended to this report.

For the specific case where a deliberate attempt is made to use only the ambient gas as propellant and thus operate a Space Electric Ramjet, the following brief discussion outlines the engine mechanisms involved.

There are a number of modes of operation for a plasma thruster of this type, the particular mode depending to some extent upon the environment and the configuration. The discussion here presented outlines the generally accepted views of the phenomena involved and the mechanisms responsible for the production of thrust when operating in a very low density environment.

Figure 2.1 illustrates the mechanisms of the engine. Part of the current may be carried in a "filament" (which can be many centimeters in diameter) that extends out from the cathode and loops back to the anode. This loop encompasses all of the magnetic flux lines inside the anode ring. The "loop" current rotates rapidly (200-800khz) and, because of the high electron concentration and temperature within it, acts as an ionization front, ionizing the atoms of the ambient gas as it spins through them. The ions that are produced are then accelerated (electrostatically) toward the axis and join with electrons from the cathode jet to form the exhaust beam that escapes from the magnetic field and produces a net axial thrust and a torque on the engine. It is also possible to consider that the thrust is produced by j x B forces, in which case the axial thrust results from the interaction of the azimuthal current with the radial component of the applied magnetic field.

The distance that the current loop extends out into the space behind the engine depends upon the ambient pressure, the applied magnetic field strength, and the total current. In some cases (very low pressures) it

can be many meters long and several meters in diameter at its widest.

It is obvious that the current can be broken up into two components: the spinning loop that ionizes the ambient gas, and the ion current that produces the thrust. The efficiency of the thruster depends upon the fraction of the total current carried by the ions. This is usually between 1/2 and 1/4 of the total current.

The engine produces a torque that is equal to

$$T_q = \frac{B_A I(r_A^2 - r_c^2)}{2} \tag{2.2}$$

where

B_A = magnetic field strength at anode
r_A = radius of anode ring
r_c = radius of cathode.

In order to have no torque on the average, the magnetic field must be reversed periodically. Naturally, use can be made of the torque for spinning or despinning the vehicle.

There are a number of equivalent ways to calculate the thrust produced by the engine. That most generally used is a semi-empirical law that reads

$$\text{thrust } F = C_T B_A I r_A \tag{2.3}$$

where C_T = coefficent of thrust, usually near 1. Another method is to compute the electrostatic thrust

$$F = \frac{m_I}{|e|} I_I \sqrt{\frac{2|e|V}{m_I}} \tag{2.4}$$

where

$\frac{m_I}{|e|}$ = mass-charge ratio of the ions
I_I = ion current
V = anode-to-cathode voltage

$$B_A r_A v_{cr} C_v \quad (\text{with } C_v = \text{voltage coefficient} \tag{2.5}$$
$$v_{cr} = \frac{2eV_I}{m_I}$$
V_I = ionization potential of ambient gas).

Equations (2.3), (2.4), and (2.5) can be combined to determine the ration of ion current to total electric current:

$$\frac{I_I}{I} = C_T \left\{ \frac{|e| B_A r_A}{2 m_I v_{cr} C} \right\}^{\frac{1}{2}} \tag{2.6}$$

This equation illustrates the very important design criterion that the product $B_A r_A$ should always be kept low enough so that

$$\frac{|e| B_A r_A}{2 m_I v_{cr}} < 1 \tag{2.7}$$

since otherwise the thrust coefficient will drop to low values. This inequality can be written another way:

$$V_{\cdot} = B_A r_A v_{cr} < 4 V_I \tag{2.7a}$$

In order to operate with high specific impulse and simultaneously with high potential drops, it could be advantageous to multiply ionize the propellant so that

$$V_I = V_I^{(1)} + V_I^{(2)} + \ldots\ldots \tag{2.8}$$

where

$V_I^{(1)}$ = 1st ionization potential

$V_I^{(2)}$ = 2nd ionization optential

etc.

⋮

2.4 Ion Production Rate

The ion production is assumed to occur entirely in the volume behind the engine where the magnetic field is sufficently strong to contain the discharge. Assuming that the ions formed all spiral into the cathode jet, the ion current can be written as

$$I_I = Z |e| \dot{n} \text{ Vol.} \tag{2.9}$$

where

I_I = ion current

$Z|e|$ = charge on ion

$\dot{n}$ = ion production rate

and Vol. = volume of discharge.

For electrical discharges in a low pressure environment, the ion production rate can be expressed as

$$\dot{n} = \left(\frac{\alpha}{p}\right) n_e v_e p_a \tag{2.10}$$

where

$\dot{n}$ = ions produced per c.c. per sec.

n_e = electron density per c.c.

v_e = electron thermal velocity, cm/sec

p_a = gas pressure, mm Hg

$\frac{\alpha}{p}$ = ion pairs per c.c. per mm Hg.

The volume required by the discharge to produce adequate ions to carry an ion current I_I is given by

$$\text{Vol.} = \frac{I_I}{Z|e|\,(\alpha/p) n_e v_e p_a} \tag{2.11}$$

The electron thermal velocity can be expressed in terms of an average electron energy e V as follows (T_e is the electron temperature)

$$v_e^2 = \frac{8}{\pi} \frac{kT_e}{m_e} \tag{2.12}$$

and

$$\frac{5}{2} kT_e = |e|V \tag{2.13}$$

so that

$$v_e = \sqrt{\frac{16}{5\pi} \frac{|e|V}{m_e}}\,. \tag{2.14}$$

From experimental data, the value of α/p for air approaches 10 ion pairs per c.c. per mm Hg for high values of E/p (where E is the electric field, and $p \ll 1$ mm Hg). In MKS units

$$\alpha/p = 10 \text{ ion pairs} \frac{1}{\text{cm}} \cdot \frac{100\text{cm}}{\text{m}} \cdot \frac{1}{\text{mmHg}} \cdot \frac{760 \text{ mmHg}}{10^5}$$

$$= 7.6(\text{ion pairs/m})/(\text{newton/m}^2)$$

If we assume the following, that

$$I_I = I/2$$

$$n_e = n/2$$

$$p_a = \frac{n}{2} kT$$

and $V = 5.6$ volts,

we find that

$$v_e = 10^6 \text{ m/sec}$$

and

$$\text{Vol.} = \frac{I}{2 Z \times 7.6\times10^{6}\times1.6\times10^{-19} \times \frac{n^4}{4} kT}$$

$$= \frac{I}{Z \left(\frac{n}{10^{16}}\right)^2 \left(\frac{T}{1000}\right)} m^3 \qquad (2.15)$$

3. Electrode Performance

The anode and cathode structures for the SERJ will be investigated so that the following parameters can be established:

1. Size and weight
2. Operating temperature.
3. Power requirements and losses
4. Mass loss rate and lifetimes.

In some cases, empirical information will be necessary to accurately establish some of the above quantities.

Since acceleration of the plasma occurs by the discharge current crossing magnetic flux lines, it is important that as much of the flux as feasible be concentrated between the anode and cathode structures. Examination of the flux lines in Figure 4.2 indicates that the cathode structure can probably be made to encompass less than 5% of the flux ϕ_o, where $\phi_o = 4\pi\mu_o aNI$. To accomplish this, the cathode must be positioned slightly in front of the plane of the magnet coil, on the centerline, and have a diameter less than 0.2a. The concentrating of the flux lines around the coil places severe restrictions on the size and position of the anode. To have 75% of the flux between the two electrode structures, the anode must be confined to the coil side of the 0.80 flux line, as might be accomplished by an anode built as a surface of revolution on the $\phi/\phi_o = 0.80$ line, with a length adequate to carry the current. However, a short cylinder of diameter 2a would probably be adequate.

Both electrodes must be placed in regions of strong magnetic field to ensure that no purely radial current flows between them. Also, to prevent surface currents from flowing over the insulator between them, the anode cylinder or ring should be separated axially by a gap from the magnet and insulator.

3.1 The Anode

A number of possible anode configurations are available. Two that have been much used in laboratory work are shown in Figures (3.1a)

and (3.1b). The collection area needed by the anode in this application would seem to indicate that the ring configuration should be used.

The anode collects electrons from the plasma to complete the current circuit. There are essentially three modes in which it could operate:

1. Collection of the current uniformly over the anode surface with no enhanced ion production near the surface and no sheath formation.
2. Concentration of the current in a filament and formation of an attachment point. This point would rotate rapidly around the anode cylinder due to the j x B forces from the applied magnetic field. The current concentration can occur only if mass is available to be ionized in the filament near the anode surface. This matter could be ambient material, or mass eroded from the anode by the high heat flux at the attachment point.
3. If the electron flux to the anode surface is such that it would carry more than the total discharge current, then a sheath will form to repell some of the electrons.

Because of the low ambient density, the low current and the large anode surface area, it is extremely unlikely that mode 2 will ever occur in this device. Further, mode 3 requires high plasma densities relative to those available. Therefore, the analysis will be carried out on the basis of mode 1 operation.

The impingement rate of electrons on the anode is

$$\frac{n_e v_e}{4} A_A$$

and they carry a current

$$I = \frac{|e| n_e v_e}{4} A_A \qquad (3.1)$$

where

$|e|$ = electron charge

n_e = electron number density

v_e = electron thermal velocity

$= \left(\frac{8kT_e}{\pi m_e}\right)^{\frac{1}{2}}$

A_A = anode area.

The power loss to the anode is the sum of the work function energy and enthalpy carried by the electrons into the metal:

$$P_A = I \left(\chi + \frac{5}{2}\frac{kT_e}{|e|}\right) \tag{3.2}$$

The anode temperature can be estimated by equating the sum of the power dissapated and solar impingent power, to the power radiated by the anode

$$e\,\sigma T_A^4 = \frac{1}{2}\left(\frac{dP}{dA}\right)_s + \frac{|e|\,n_e v_e}{4}\left(\chi + \frac{5}{2}\frac{kT_e}{|e|}\right) \tag{3.3}$$

where it is assumed that 1/2 of the anode is exposed directly to the solar radiation.

The anode lifetime can be estimated by finding the evaporation rate of the material at its operating temperature T_A. Since the vapor pressure is given in atmospheres in Figure 3.2, the mass loss rate per year of continuous operation is

$$\frac{m_{loss}}{year} = 4\,p_a\,t_y\left(\frac{p}{p_a}\right)_A \frac{al}{v_a} \quad \text{kgm/yr}$$

where

p_a = atmospheric pressure = 10^5 newtons/meter^2

v_a = thermal speed of atoms = $\sqrt{\frac{8kT_a}{nm_a}}$

t_y = number of seconds/year = 3.15×10^7

l = anode length

so that

$$\frac{m_{loss}}{year} = 1.26 \times 10^{13}\left(\frac{p}{p_a}\right)_A \frac{al}{v_a}\,. \tag{3.4}$$

For example, if the anode is aluminum, with an area of 1/4 meters^2, and runs at 1000°K, then

$$v_A = 883 \text{ m/sec}$$

$$\left(\frac{p}{p_a}\right)_A = 7 \times 10^{-11}$$

and

$$\frac{\dot{m}_{loss}}{year} = \frac{1.26 \times 10^{13} \times 7 \times 10^{-11}}{4 \times 883}$$

$$= 0.250 \text{ kgm/yr} = 0.55 \text{ lbs/yr}.$$

3.2 The Cathode

The conventional cathode for this type of accelerator would be a conical cathode made of thoriated tungsten. This type has the advantages of rugged construction and resistance to breakage, and it does not require a separate heater, since power to liberate the electrons comes from the electric discharge through thermal conduction and ion bombardment. However, such cathodes have been operated only at current and pressure levels considerably higher than is anticipated here, and there is reason to doubt that the same kind of performance can be obtained at pressures less than 10^{-5} atm and currents of under 10 amperes. Also, since the SERJ device would be operating in air, the tip oxidation would probably be rapid.

For low currents (under 10 amperes) it will probably be best to design the cathode with an independent heating device. Use of a thorium or oxide coated surface would minimize the temperature and heating required.

An "L"-type cathode configuration, such as that shown in Figure 3.3, would probably be optimal. With good insulation, the conduction power loss can be kept to the level of the radiation loss through the orifice, hence the total power loss will be

$$P_K = \sigma T_K^4 A_K \qquad (3.5)$$

where

T_K = temperature in the cathode

A_K = cathode orifice area

P_K = power loss to the cathode.

Because of the position of the anode relative to the cathode and since the potential drop will be less than 100 volts, space charge effects will limit the current of a pure thermionic cathode to a few milliamperes. It will therefore be necessary to have an ion density in the cathode cavity (see Figure 3.3) that is comparable to the electron density. These ions will consist of the material used to coat the cathode surface. The density will be low enough so that the mean free path of the ion-electron collisions will be much larger than the cavity diameter, so that equations for free particle flow, rather than diffusion equations, will be used to describe the ion and electron flow rates out of the cavity. If both electrons and ions escape through the orifice at thermal velocity the current can be written as

$$I = |e| \left(\frac{n_e v_e}{4} - \frac{n_I v_I}{4} \right) A_K$$

$$= \frac{|e| n_e v_e}{4} A_K \left(1 - \frac{n_I}{n_e} \frac{v_I}{v_e} \right)$$

$$\approx \frac{|e| n_e v_e A_K}{4} \qquad (3.6)$$

since the ion velocity is several orders of magnitude smaller than the electron velocity.

Cathode operation at a current density of 10 - 20 amps/cm^2 through the orifice requires cathode temperatures of about 2000°K, so the electron thermal velocity would be

$$v_e = \left\{ \frac{8 \times 1.38 \times 10^{-23} \times 2000}{3.14 \times 0.91 \times 10^{-31}} \right\}^{\frac{1}{2}}$$

$$= 2.78 \times 10^5 \text{ meters/sec.}$$

The electron density in the cavity is hence, from Equation (3.6)

$$n_e = \frac{4 \times 2 \times 10^5}{1.6 \times 10^{-19} \times 2.78 \times 10^5}$$

$$= 1.80 \times 10^{19}/m^3.$$

In order to cancel out space charge effects, an ion density comparable to this value must exist in the cavity, and this material will flow out of the cathode orifice resulting in a significant rate of loss of material:

$$\dot{m}_c = \frac{\sqrt{m_I m_e}}{|e|} I \qquad (3.7)$$

For thorium and a current of 10 amperes, the mass loss per year would be

$$\frac{m_{loss}}{year} = \frac{(232 \times 1.67 \times 10^{-27} \times 0.91 \times 10^{-30})^{\frac{1}{2}}}{1.6 \times 10^{-19}} \times 10 \times 3.15 \times 10^7$$

$$= 1.17 \text{ kgm/yr} = 2.58 \text{ lbs/yr.}$$

Equation (3.7) indicates that the mass loss rate is proportional to the square rood of the atomic weight of the cathode coating material. For this reason, the feasibility of using a low molecular weight substance rather than thorium should be investigated. For instance, if lithium were feasible, then the mass loss rate per year could be reduced to a value of

$$\left(\frac{m_{loss}}{year}\right)_{Li} = 1.17\sqrt{\frac{7}{232}}$$

$$= 0.203 \text{ kg/yr} = 0.448 \text{ lb/yr.}$$

The momentum conserva ion equation places a further constraint on the current level at which the L-type cathode can operate. This equation indicates that the following inequali y must be obeyed:

$$pA \geq \frac{\mu_0 I^2}{8\pi} \qquad (3.8)$$

(See Appendix 2.) From Equation (3.6) an expression for pA can be obtained as follows:

$$I = \frac{|e|\, n_e\, v_e}{4p}\, pA$$

$$= \frac{|e|}{8}\, \frac{v_e}{kT}\, pA \quad \text{since } p_e \approx p_I = \frac{p}{2} = n_e kT.$$

Also, since $v_e^2 = \frac{8kT}{\pi m_e}$

$$I = \frac{|e|}{\pi m_e}\, \frac{pA}{v_e} \,. \tag{3.9}$$

Combining Equations (3.8) and (3.9):

$$\frac{\mu_o I}{8\pi} \leq \frac{\pi m_e}{|e|}\, v_e \tag{3.10}$$

or

$$I \leq \frac{8\pi^2 m_e}{\mu_o |e|}\, v_e \,. \tag{3.10a}$$

For a cathode temperature of 2000°K, this places a maximum limit on the current:

$$I \leq \frac{6.28 \times 10^7 \times 0.91 \times 10^{-30} \times 2.78 \times 10^5}{1.6 \times 10^{-19}}$$

$$\leq 99.3 \text{ amperes.}$$

4. Magnetic Field Considerations

There are several alternative ways of producing the required magnetic field. The three most feasible systems would be

1. Permanent magnets.
2. Solenoidal coil with its own power supply.
3. Solenoidal coil connected in series with the discharge.

Since a permanent magnet would have no power consumption , it might at first glance appear optimal. However, torques act on the vehicle that are proportional to the strength of the magnetic field and the calculations in Section 6 indicate that these torques can seriously affect the orientation of the vehicle in a relatively short time. The only feasible method of cancelling these torques is to operate the engine for equal times with the two polarities of the magnetic field direction. In that it would not appear practicable to reverse the field of a permanent magnet configuration on a space vehicle, and because of the weight disadvantage of permanent magnets, such magnets would appear unsuited to this application.

Of the two solenoidal magnets, the series-connected appears to offer the most advantage. It gives the electric discharge a positive characteristic so that it can be connected directly in series with the solar cells, eliminating any power conditioning need, and it facilitates the cancellation of the torques by ensuring equality of the opposite torques (see Section 6) in that there is only one current.

4.1 Characteristics of a Dipole Magnetic Field

The magnetic coil configuration that is most convenient and probably near optimum in weight is a short solenoid where the coil length is equal to its thickness. As long as one does not approach too close to the coil, it may be considered a single turn of wire with a current of NI amperes, where N is the total number of turns. The vector potential of the coil is given by (c.f. Jackson, Classical

Electrodynamics, p 142)

$$A_\theta = \frac{4\mu_o NIa}{(a^2 + z^2 + r^2 + 2ar)^{\frac{1}{2}}} \quad \frac{(2-k^2)\,K(k) - 2E(k)}{k^2} \qquad (4.1)$$

where

$$k^2 = \frac{4ar}{a^2 + z^2 + r^2 + 2ar} \qquad 1 > k \geq 0 \qquad (4.2)$$

K(k) and E(k) are elliptic integrals whose values are tabulated (as in Handbook of Chemistry and Physics). The magnetic flux ϕ through any area πr^2 is given by

$$\begin{aligned}\phi &= 2\pi r A_\theta \\ &= 4\pi\mu_o NI \sqrt{ar}\ \frac{(2-k^2)\,K(k) - 2E(k)}{k}\end{aligned} \qquad (4.3)$$

The magnetic field components are given by

$$B_z = \frac{1}{r}\ \frac{\partial}{\partial r}(rA_\theta) \qquad (4.4)$$

$$B_r = -\frac{\partial A_\theta}{\partial z} \qquad (4.5)$$

or

$$2\pi r B_z = \frac{\partial \phi}{\partial r} \qquad (4.4a)$$

$$2\pi r B_r = -\frac{\partial \phi}{\partial z} \qquad (4.5a)$$

When $k \approx 0$ (that is, for positions near the z-axis or far from the coil), the magnetic field parameters can be expressed simply as

$$A_\theta = \mu_o \pi a^2 NI\ \frac{r}{(a^2 + z^2 + r^2 + 2ar)^{3/2}} \qquad (4.6)$$

$$B_z = \mu_o \pi a^2 NI\ \frac{2(a^2 + z^2) - r^2 + ar}{(a^2 + z^2 + r^2 + 2ar)^{5/2}} \qquad (4.7)$$

$$B_r = \mu_o \pi a^2 NI \frac{3zr}{(a^2 + z^2 + r^2 + 2ar)^{5/2}} \tag{4.8}$$

$$\phi = \mu_o \pi a^2 NI \frac{2\pi r^2}{(a^2 + z^2 + r^2 + 2ar)^{3/2}} \tag{4.9}$$

The vector potential and flux can be evaluated for the region around the wire, numerically. Defining

$$F(k) = \frac{(2 - k^2)K(k) - 2E(k)}{k} \tag{4.10}$$

then

$$\phi = 4\pi\mu_o NI \sqrt{ar}\, F(k) \ . \tag{4.3a}$$

The function F(k) is plotted in Figure 4.1. For values of $k < 0.5$, the function F(k) can be expressed accurately by a series

$$F(k) \sqrt{2}\pi \left(\frac{k^2}{8}\right)^{3/2} \left\{1 + 6\left(\frac{k^2}{8}\right) + \frac{75}{2}\left(\frac{k^2}{8}\right)^2 + 245\left(\frac{k^2}{8}\right)^3 \ldots\ldots\right\} \tag{4.11}$$

The coordinates of constant flux lines are shown in Table 4.1. Lines of constant flux are plotted in Figure 4.2.

4.2 Engine Performance with a Dipole Magnetic Field

At this point, it is desirable to express the engine performance in terms of the magnetic dipole parameters. Using the results from Appendix 2, the torque on the engine can be expressed as

$$T = \frac{I\,\phi_{AC}}{2\pi} \tag{4.12}$$

where

I = current of discharge

and ϕ_{AC} = minimum flux enclosed between the anode and cathode surfaces.

Equation (4.12) is a generalization of Equation (2.2). A generalized expression for the thrust to replace Equation (2.3) can also be written

in terms of the magnetic flux, as follows:

$$F = C_T \frac{I \phi_{AC}}{\pi r_A} \tag{4.13}$$

or alternatively

$$F = \frac{I \phi_{AC}}{\pi r_F} \tag{4.13a}$$

where r_F = reference radius. If a cylindrical anode is used, the minimum value of r_F would be the anode radius r_A. The maximum radius r_F could have would be the radius at which the flux line through the rear of the anode is perpendicular to the coil centerline. This value can be determined from Table 4.1. In general, the reference radius will increase as the ambient density decreases, hence less thrust is produced in a low density environment than would be produced in one of higher density. For this reason we shall use the most pessimistic value for $(r_F)_{max}$--i.e. the value that gives the minimum thrust for a given amount of magnetic flux, ϕ_{CA} between the cathode and anode.

In order to estimate the size of the magnet required, the following assumptions are made:

1. The magnet and engine are run in series so that the magnet current and discharge current are the same.
2. The anode is a cylinder of 1 meter diameter and 1/4 meter long, and insulated on the outside.
3. The magnet coil has an average diameter of 1 meter.
4. The front end of the anode is placed near the magnet coil.
5. The flux encompassed by the cathode is negligible.

The minimum magnetic flux passing through the anode can now be evaluated, using Equation (4.3a):

$$\phi_{AC} = 4\pi \mu_o NIa\sqrt{R_A}\, F(k_A) \tag{4.14}$$

where $R_A = \frac{r_A}{a} = 1$

and

$$k_A^2 = \frac{4R_A}{(1 + R_A)^2 + Z_A^2} = 0.9412$$

$$Z_A = \frac{z_A}{a} = 0.50.$$

Using the tables for evaluation ;. $F(k_A)$ is found to be 0.888. Hence

$$\phi_{AC} = 0.888 \times 4\pi\mu_o NIa \qquad (4.14a)$$

Following the flux line that passes through the rear of the anode, it is seen to become perpendicular to the magnet centerline at approximately

$$Z_M = 0.59$$

$$R_M = 1.38.$$

The thrust equation (4.17a) can now be rewritten as

$$F = \frac{I \times 4\pi\mu_o NIa \times 0.888}{1.38\pi a}$$

$$\boxed{F = 2.57\,\mu_o NI^2} \qquad (4.15)$$

$$F = 3.23 \times 10^{-6} NI^2.$$

This equation can be used to evaluate the number of turns N required on the magnet.

4.3 Mass of the Magnet

The mass of the magnet can now be estimated. Using Ohm's Law

$$I = \frac{\sigma_W A_W V}{L}$$

where

σ_W = electrical conductivity of magnet wire

A_W = cross-sectional area of magnet wire

V = voltage drop across the magnet coil

L = length of magnet wire.

The mass M of the magnet coil can be written as

$$M = \sigma_W A_W L \tag{4.17}$$

Eliminating A_W between Equations (4.16) and (4.17) gives

$$M = \frac{\rho_W}{\sigma_W} L^2 \frac{I}{V}$$

$$= \frac{\rho_W}{\sigma_W} \frac{L^2 I^2}{P_M} \tag{4.18}$$

If the magnet is wound with a diameter close to that of the vehicle

$$L = \pi DN$$

and the magnet mass can be written as

$$M = \frac{\rho_W}{\sigma_W} \frac{(\pi DNI)^2}{P_M} \tag{4.18a}$$

The parameter that determines the best material to use for the magnet is the ratio of the density to the electrical conductivity. Values of this parameter for verious metals are presented in Table 4.2. The values indicate that the lightest magnet would be made of sodium, which metal, if used, would require enclosure by a tube (e.g. of stainless steel) to prevent breaks in the circuit due to melting or reacting of the sodium.

4.4 Magnet Cooling

The magnet will be radiation cooled. The temperature at which the coil must be run in order to handle the power can be computed from Stefan's Law:

$$P_M = A_s e_R \sigma' T^4 \tag{4.19}$$

where

P_M = power radiated

A_s = surface area of wire

σ' = Stefan-Boltzmann constant

T = wire temperature

e_R = emissivity of wire surface.

The surface area of the wire is given by

$$A_s = 2\pi r_w \cdot 2\pi aN \tag{4.20}$$

where r_w is the wire radius. But

$$M = \rho_w \pi r_w^2 (2\pi aN)^{\frac{1}{2}}$$

so that

$$r_w = \left(\frac{1}{2\pi aN}\right)^{\frac{1}{2}} \left(\frac{M}{\pi\rho_w}\right)^{\frac{1}{2}} \tag{4.21}$$

Hence we have

$$A_s = 2\pi \left(\frac{M}{\pi\rho_w}\right)^{\frac{1}{2}} (2\pi aN)^{\frac{1}{2}}$$

$$= 2\pi \left(\frac{2aMN}{\rho_w}\right)^{\frac{1}{2}} \tag{4.21a}$$

If the coil is wound in a single spiral, the surface area that can radiate heat will be approximately half the total wire surface. When there are many turns, the coil must be ound in layers, and if it is wound so that its thickness and width are equal, the surface area will be given by

$$(A_s)_{min} = 8 \left(\frac{2aM}{\rho_w}\right)^{\frac{1}{2}} \tag{4.21b}$$

5. Vehicle Drag and Solar Cell Performance

The drag force that must be balanced by the engine thrust consists of the drag on the space vehicle itself and that on the solar cells and other engine components which supply the power to the engine. The formulae needed to estimate the drag are given below.

The pressure on a surface due to molecular impingement is given by

$$p = \frac{\frac{1}{2}\rho v^2}{S^2}\left[\frac{(2-\sigma')S'}{\pi^{\frac{1}{2}}} + \frac{\sigma'}{2}\left(\frac{T_W}{T}\right)^{\frac{1}{2}} e^{-(S')^2} + \left\{(2-\sigma')\left(S'^2 + \frac{1}{2}\right) + \frac{\sigma'}{2}\left(\frac{\pi T_W}{T}\right)^{\frac{1}{2}} S'\right\}\left\{1 + \operatorname{erf}(S')\right\}\right] \tag{5.1}$$

The shear stress on the surface is

$$= \frac{1}{2}\frac{\rho v^2 \sigma'' \cos\psi}{\pi^{\frac{1}{2}} S}\left\{e^{-(S')^2} + \pi^{\frac{1}{2}} S'(1 + \operatorname{erf}(S'))\right\} \tag{5.2}$$

where

$S^2 = \frac{mv^2}{2kT}$

$S' = S \sin\psi$

v = satellite velocity

T_W = satellite surface temperature

ψ = angle between surface and incident beam

T = gas temperature

$$\operatorname{erf}(S') = \frac{2}{\pi^{\frac{1}{2}}}\int_0^{S'} e^{-(S')^2} dS'$$

σ', σ'' = surface reflection coefficient for normal momentum transfer, shear momentum transfer

As reference drag force for the vehicle we will assume that the vehicle shape is that of a cylinder one meter in diameter and one meter

in length, and that it is aligned so that the cylinder axis is parallel to direction of flight. Formulae (5.1) and (5.2) reduce, under these assumptions, to

$$p = 2\,(2 - \sigma')\,\frac{1}{2}\rho\, v_v^2 \tag{5.1a}$$

$$\tau = -\,\frac{\sigma}{\pi^{\frac{1}{2}} S}\,\frac{1}{2}\rho\, v_v^2 \tag{5.2a}$$

The total drag force on the cylinder can therefore be computed and is given by

$$F_D = \left\{2(2 - \sigma')\frac{\pi}{4} D^2 + \frac{\sigma}{\pi^{\frac{1}{2}} S}\pi DL\right\}\frac{1}{2}\rho v_v^2 \tag{5.3}$$

$$= \left\{2(2 - \sigma') + \frac{\sigma}{\pi^{\frac{1}{2}} S}\frac{4L}{D}\right\}\frac{\pi}{4} D^2\,\frac{1}{2}\rho\, v_v^2 \tag{5.3a}$$

This allows us to compute the drag coefficient C_D:

$$C_D = 2(2 - \sigma') + \frac{\sigma}{\pi^{\frac{1}{2}} S}\frac{4L}{D} \tag{5.4}$$

$$= 2(2 - 0.885) + \frac{0.385}{1.77 \times 7.9} \times 4$$

$$= 2.23 + 0.25$$

$$= 2.48.$$

If solar cell arrays are used to collect power to run the propulsion system, their drag must be computed. This drag is strongly dependent on the orientation of the array relative to the direction of satellite motion. If they are perpendicular to the motion they will have a drag coefficient $C_{Dsc} = 2.23$, while alignment parallel to the motion gives $C_{Dsc} = 0.127$. The type of orbit that is used will determine the angle of the solar cells, so that no attempt to find optimum angles is made here. Rather performance capability for both normal and parallel orientation will be presented.

The power collected from the solar cells can be written as

$$P = \left(\frac{dP}{dA}\right)_s \eta_{sc} A_{sc} \tag{5.5}$$

where

$\left(\frac{dP}{dA}\right)_s$ = power density of solar energy

η_{sc} = efficiency of solar cells

A_{sc} = cross-sectional area of solar cells.

Assuming equipartition of the power between losses and beam power, the power used by the engine can be written as

$$P = P_M + 2\frac{F^2}{2\dot{m}} + P_E \qquad (5.6)$$
$$= P_M + \frac{F^2}{\dot{m}} + P_E$$

where P_E = electrode power

P_M = magnet power

F = thrust

$\dot{m}$ = mass flow rate.

For preliminary estimates we can let the sum of the magnet and electrode power be equal to the engine power, so that the overall efficiency of the engine is 25%. Later, the weight of the magnet required to permit this performance will be estimated.

The thrust F can be written as

$$F = \dot{m} v_{cr} = \dot{m} (v_e - v_v) \qquad (5.7)$$

Equating this to the total drag gives the power balance

$$\left(\frac{dP}{dA}\right)_s \eta_{sc} A_{sc} = 2 v_{cr} \times \text{Drag}$$
$$= 2 v_{cr} \frac{1}{2} \rho v_v^2 \left\{ (C_D)_v A_v + (C_D)_{sc} A_{sc} + (C_D)_A A_A \right\} \qquad (5.8)$$

The drag of the anode has been added. Since it is the only other major component of any size required for the propulsion system, the total drag of the vehicle and propulsion system has been found.

The anode can be designed in several ways, one an annular plate with the outside diameter approximately equal to that of the vehicle (see Figure 3.1a). This design has the disadvantage that the anode surface area is limited and may not be large enough to collect all of the current. An alternative design is a thin cylinder with a diameter approximately equal to that of the vehicle (Figure 3.1b), a configuration permitting large surface areas with minimum drag. For such anode configuration the surface area A_A needed to collect the current can be expressed in terms of the solar cell surface area A_{sc} as follows:

$$I_I = \frac{Z|e|}{m} \dot{m} = \text{ion current} \tag{5.9}$$

$$I = \frac{|e| n_e v_e}{4} A_A = \text{total current} \tag{5.10}$$

Combining Equations (5.7), (5.9), and (5.10) gives

$$A_A = \frac{4}{|e| n_e v_e} \frac{I}{I_I} \frac{Z|e|}{m} \frac{F}{v_{cr}}$$

$$= \frac{4Z}{m n_e v_e} \frac{I}{I_I} \frac{F}{v_{cr}} \tag{5.11}$$

Using Equation (5.8), this can be written as

$$A_A = \frac{4Z}{m n_e v_e} \frac{I}{I_I} \frac{1}{2v_{cr}^2} \left(\frac{dP}{dA}\right)_s \eta_{sc} A_{sc} \tag{5.11a}$$

But $n_e = \bar{e}^* Zn$, so that

$$A_A = \frac{2}{\bar{e}^* v_e} \frac{I}{I_I} \frac{I}{v_{cr}^2} \left(\frac{dP}{dA}\right)_s \eta_{sc} A_{sc} \tag{5.12}$$

Defining $$\gamma_A = \frac{2}{\epsilon \rho v_e v_{cr} Z} \frac{I}{I_I} \left(\frac{dP}{dA}\right)_s \eta_{sc} \tag{5.13}$$

gives

$$A_A = \gamma_A A_{sc} \tag{5.14}$$

γ_A can be evaluated as a function of altitude once values are assumed for ϵ and I/I_I. In the following calculations we will assume

$$\epsilon = \frac{1}{2}$$

$$I_I = 2.$$

With the anode cylinder aligned parallel to the direction of motion, the drag coefficient of the anode $(C_D)_A$ will be the same as that for the solar cells. This permits calculation of the solar cell area using Equation (5.8):

$$A_{sc} = \frac{(F_D)_v}{\left(\frac{dP}{dA}\right)_s \frac{\eta_{sc}}{2v_{cr}} - \frac{1}{2}\rho v_v^2 (C_D)_{sc}(1+\gamma_A)} \tag{5.8a}$$

When the solar cells are normal to the line of flight, the maximum density at which the solar cells can supply adequate energy for drag make up is

$$\rho_{Max} = \frac{\left(\frac{dP}{dA}\right)_s \frac{\eta_{sc}}{2 v_{cr}}}{2.23 \; v_v^2/2} \tag{5.15}$$

The solar energy constant is

$$\left(\frac{dP}{dA}\right)_s = 1300 \text{ watts/m}^2$$

and for the other quantities we can take as approximate values

$$\eta_{sc} = 0.10$$

$$v_v = 8000 \text{ meters/sec}$$

$$v_{cr} = 1.6 \times 10^4 \text{ meters/sec}$$

and obtain

$$\rho_{Max} = \frac{1.3 \times 10^3 \times 10^{-1}}{2 \times 1.6 \times 10^4} \cdot \frac{1}{1.11 \times 0.64 \times 10^8}$$

$$= 5.7 \times 10^{-11} \text{ kgm/m}^3.$$

This corresponds to an altitude of approximately 300 km (186 mi). For a critical velocity v_{cr} of 2.4×10^4 meters/sec (doubly ionized atoms) the solar cells can supply power to make up their own drag only at higher altitudes (above 210 mi) if the solar panels are normal to line of flight.

6. Torques and Deflections

6.1 Engine Torque and Roll Angle

The engine's electromagnetic torque will tend to spin the vehicle, and if for a particular satellite this spin is considered undesirable, periodic magnet current reversal will be necessary to keep the angular rotation or roll ϕ about the vehicle axis to within prescribed limits. The equation of motion for this deflection is

$$J_t \frac{d^2\phi}{dt^2} = T_t \tag{6.1}$$

where $J_t = m_v \frac{a^2}{2}$ is the axial moment of inertia of the vehicle in terms of its outer radius a, and $T_t = \frac{I\phi_{AC}}{2\pi}$ from Equation (4.12). Integrating equation (6.1) and specifying a maximum permitted angle ϕ_m of roll for the vehicle, the period τ for reversing the magnet current can be estimated

$$\tau \leq \left\{ 4\pi \frac{m_v a^2 \phi_m}{2I \phi_{AC}} \right\}^{\frac{1}{2}} \tag{6.2}$$

From equation (3.14a)

$$\phi_{AC} = .888 \times 4\pi \mu_o NIa$$

so that

$$\tau \leq \left\{ \frac{m_v a \phi_m}{1.776 \mu_o NI^2} \right\}^{\frac{1}{2}} \tag{6.2a}$$

As an example, let

$$\phi_m \approx \frac{1}{60} \text{ radians (about 1 degree)}$$

$$m_v = 100 \text{ kgm}$$

$$a = 1/2 \text{ meter}$$

$$NI = 100 \text{ ampere-turns}$$

and $$I = 10 \text{ amperes}.$$

These give

$$\tau \leq \left\{ \frac{100 \times .5 \times 1}{1.776 \times 1.25 \times 10^{-6} \times 60 \times 10^3} \right\}^{\frac{1}{2}}$$

$$\leq 15 \text{ sec.}$$

6.2 Interaction of the Earth's Magnetic Field and Engine Magnetic Field

There will be two torques on the vehicle due to the engine magnet interacting with the earth's magnetic field. When the coil has an applied current flowing through it there will be a torque tending to line up the two fields. There will also be a " damping" torque on the vehicle due to the induced current in the coil caused by the change in flux through the coil as the vehicle rotates in the earth's magnetic field.

The torque caused by the current through the magnet can be easily evaluated: it is the product of the magnetic moment of the coil (μ) and the terrestrial field strength (B_e) times the sine of the angle between them (θ),

$$T_1 = \pm \mu B_e \sin \theta \qquad (6.3)$$

where

$$\mu = NI_a A_c \qquad (6.4)$$

N = number of turns on coil

and A_c = area of coil.

If the fields are antiparallel, the negative sign should be used in (6.3), and if parallel, the positive sign.

The damping force can be evaluated by using the induction equation

$$iR^* = -N \frac{d\phi}{dt} \qquad (6.5)$$

where

$R^* = \frac{2\pi aN}{A_w \sigma_w}$ is the wire resistance

with

i = induced current

ϕ = flux through coil = $\pi a^2 B_e \cos\theta$

A_w = cross-section area of magnetic wire

σ_w = conductivity of magnet wire

a = radius of coil.

The induced current can therefore be expressed as

$$i = \frac{A_w \sigma_w}{2na} \pi a^2 B_e \sin\theta \frac{d\theta}{dt} \qquad (6.6)$$

$$= \frac{A_w \sigma_w a B_e \sin\theta}{2} \frac{d\theta}{dt} ,$$

$$T_2 = \pm i \pi a^2 N B_e$$

$$= \frac{\pi A_w \sigma_w}{2} a^3 N B_e^2 \sin\theta \frac{d\theta}{dt} \qquad (6.7)$$

A differential equation for the motions of the vehicle due to these torques can be set up:

$$J \frac{d^2\theta}{dt^2} + \frac{\pi}{2} A_w \sigma_w a^3 N B_e^2 \sin\theta \frac{d\theta}{dt} + NI\pi a^2 B_e \sin\theta = 0 \qquad (6.8)$$

where $J = \frac{19}{12} ma^2$ is the moment of inertia of the vehicle about one end, assuming vehicle of length 2a. Equation (6.8) can be rewritten as

$$\frac{d^2\theta}{dt^2} + \frac{6\pi}{19} \frac{A_w \sigma_w a N B_e^2}{m_v} \sin\theta \frac{d\theta}{dt} + \frac{12\pi}{19} \frac{NIB_e \sin\theta}{m} = 0 \qquad (6.8a)$$

which is an equation very similar to that describing the motion of a simple pendulum under gravity. Exact solutions are not possible, but approximate solutions can be obtained. The case of small deflections from either the stable position ($\theta \approx 0$), where the fields are aligned antiparallel, the orthogonal position ($\theta \approx \frac{\pi}{2}$), and the unstable equilibrium position ($\theta \approx \pi$) are considered below. The first and third of these cases would correspond approximately to a satellite in a polar orbit, and the second to one in an equatorial orbit.

6.3 Perturbations About Equilibrium

In this case we make the approximation that $\sin\theta = 0$ and neglect the damping term. Then

$$\frac{d^2\theta}{dt^2} + \frac{12\pi}{19} \frac{NIB_e}{m_v} \theta = 0 \qquad (6.8b)$$

and so

$$\theta = \theta_1 \sin\sqrt{\frac{12\pi}{19} \frac{NIB_e}{m_v}}\, t + \theta_2 \cos\sqrt{\frac{12\pi}{19} \frac{NIB_e}{m_v}}\, t \qquad (6.9)$$

representing oscillations with a period of

$$\tau = 2\pi\sqrt{\frac{19}{12n}\frac{m_v}{NIB_e}} \qquad (6.10).$$

As an example, let

m_v = 100kg (220 lb)

NI = 100 ampere-turns

$B_e = 10^{-4}$ Tesla (1 gauss).

These values give

τ = 445 seconds.

6.4 Deflections from Perpendicular Magnetic Field Position

In this case, $\sin\theta = 1$. If the damping is neglected, then the solution to the Equation (6.8a) is found to be

$$\theta = \frac{6n}{19}\frac{NIB_e}{m_v}t^2 \qquad (6.11)$$

The time τ_o required for a deflection of an angle θ_m away from the orthogonal position can now be computed to be

$$\tau_o = \left(\frac{19}{6n}\frac{m_v\theta_m}{NIB_e}\right)^{\frac{1}{2}} \qquad (6.12)$$

Using the same values as given previously and permitting a deflection of $\theta_m = \frac{1}{60}$ (about 1 degree), the time τ_o becomes

$$\tau_o = \sqrt{\frac{19 \times 100}{100 \times 60 \times 10^{-4} \times 18.85}} \text{ seconds}$$

$$= 12.9 \text{ seconds}.$$

For a vehicle in an equatorial orbit, the magnetic field should hence be reversed about once every 10-20 sec in order to keep this deflection lower than 1-2 degrees from the desired orientation.

6.5 Deflections from the Unstable Equilibrium Position

Here, $\theta \simeq \pi$ and any deflection generates a force tending to increase the angle between the terrestrial field and the axis of the magnet. For angles near $\theta = \pi$, the solution to the differential equation is

$$\theta = \pi' \cosh\sqrt{\frac{12n}{19}\frac{NIB_e}{m_v}}\, t \qquad (6.13)$$

and for small t

$$\theta \approx \pi' \left(1 + \frac{12n}{19}\frac{NIB_e}{m_v}\frac{t^2}{2}\right)$$

or

$$\frac{\theta_m}{\pi'} = \frac{12n}{19}\frac{NIB_e}{m_v}\frac{t^2}{2}$$

so that

$$t \approx \left\{\frac{19}{6n^2}\frac{m\theta_m}{NIB_e}\right\}^{\frac{1}{2}}$$

as the time for a deflection θ_m to be attained. Again using the values given above, we find a time of about 7.3 sec for a deflection of about 1 degree to occur.

7. Procedure and Formulae for Evaluating Engine Performance. Results.

The procedure and formulae for evaluating the engine performance capability are summarized in this section. The MKS system of units is used in all calculations.

7.1 Satellite Drag (Equation (5.3a))

If the satellite is assumed to have a radius a and a length 2a, then the drag is

$$(F_D)_v = (C_D)_v \pi a^2 \frac{1}{2} \rho v_v^2 \tag{7.1}$$

Equation (5.4) gives the drag coefficient

$$(C_D)_v = 2.48.$$

We take as satellite dimensions a = 0.5 meters, and satellite velocity v_v = 8000 meters/sec. Using values of ρ from the ARDC model atmosphere (see Appendix 1) the drag force on the vehicle can be evaluated as a function of altitude. The results are shown in Figure 7.1.

7.2 Ratio γ_A of Anode Area to Solar Cell Area (Equation 5.13)

We have

$$\gamma_A = \frac{2}{\epsilon \rho v_e} \frac{I}{I_I} \frac{1}{v_{cr}^2} \left(\frac{dP}{dA} \right)_s \eta_{sc} \tag{7.2}$$

where

ϵ = fraction of ambient atmosphere that is ionized
= 0.5

v_e = thermal velocity of electrons
= 10^6 meters/sec

I/I_I = ratio of total current to ion current
= 2.0

$\left(\frac{dP}{dA}\right)_s$ = solar constant
= 1300 watts/sq. meter

η_{sc} = solar cell efficiency
= 0.10

v_{cr} = Alfven speed of ions

$(v_{cr})_1 = 1.6 \times 10^4$ meters/sec (singly ionized Nitrogen)

$(v_{cr})_2 = 2.4 \times 10^4$ meters/sec (doubly ionized Nitrogen)

Using the values of ρ from the ARDC tables, the values of γ_A can be determined as function of altitude for both values of the Alfven speed. Results are shown in Figure 7.2.

7.3 Solar Cell Area required when Cell Array Parallel to Line of Flight (Equation 5.8a)

$$A_{sc} = \frac{(F_D)_v}{\left(\frac{dP}{dA}\right)_s \frac{\eta_{sc}}{2v_{cr}} - \frac{1}{2}\rho v_v^2 (C_D)_{sc}(1+\gamma_A)} \tag{7.3}$$

where from Equation (5.2a)

$$(C_D)_{sc} = \frac{2\sigma''}{\pi^{\frac{1}{2}} S}$$

$$= \frac{2 \times 0.885}{1.772 \times 7.9}$$

$$= 0.127$$

The other parameters are given above. The values of the solar cell areas needed for the two Alfven values of the exhaust velocity are shown as a function of altitude in Figure 7.3. This calculation indicates that the system will not operate below some critical altitude, shown here to be about 110 miles.

7.4 Anode Area Required (Equation(5.14))

$$A_A = \gamma_A A_{sc} \tag{7.4}$$

Since γ_A and A_{sc} are computed above, this equation can be evaluated immediately. Values of the anode area A_A are shown as a function of altitude in Figure 7.4.

7.5 Total Power Required by the Propulsion System (Equation 5.5)

$$P = \left(\frac{dP}{dA}\right)_s \eta_{sc} A_{sc} \tag{7.5}$$

All of the necessary values for computing P are above. The power requirements are shown as function of altitude in Figure 7.5.

7.6 Total Drag on the Vehicle (satellite + solar cells + anode) (Equation 5.8)

$$(F_D)_T = \frac{P}{2v_{cr}} \tag{7.6}$$

Once again this equation can be evaluated using values computed above. The results are shown in Figure 7.6.

7.7 Total Current in the Electric Discharge (Equations (5.9), (2.2.2))

$$I = 2I_I = \frac{2\,Z\,e}{m_a}\,\dot{m} = \frac{2\,Z\,e}{m_a}\,\frac{(F_D)_T}{v_{cr}} \tag{7.7}$$

where

Z = number of positive charges on the ion

e = electronic charge = 1.6×10^{-19} coulombs

m_a = mass of the atom = $14 \times 1.67 \times 10^{-27}$ kg for Nitrogen

Using the values for the total drag computed above and remembering that Z = 1 for $(v_{cr})_1$, and Z = 2 for $(v_{cr})_2$, the discharge current can be computed as a function of altitude. The results are shown in Figure 7.7.

7.8 Minimum Cross-Sectional Area for the Discharge πR^2 in order to have adequate mass for the exhaust beam. (Equation (5.7))

$$(\dot{m})_{cr} = e^{*}\int \rho\, v_v\, \pi R^2 = \frac{(F_D)_T}{v_{cr}}$$

so that

$$\pi R^2 = \frac{1}{e^{*}\int \rho v_v}\,\frac{(F_D)_T}{v_{cr}} \tag{7.8}$$

or, using Equation (7.7)

$$\pi R^2 = \frac{m_a}{2eZ\,|e|}\,\frac{I}{\int \rho v_v} \tag{7.8a}$$

This equation can be immediately evaluated and the results are shown in Figure 7.8. It should be emphasized that the values computed are the minimum values for the cross-sectional area of the discharge. If the ionization rate is such that less than 1/2 of the atoms passing through the discharge are ionized, then $\epsilon < 0.5$ and the cross-sectional area must be larger.

7.9 Number of Turns on Magnet to produce the required thrust. (Equation (4.15))

$$N = \frac{(F_D)_T}{3.23 \times 10^{-6} I^2} \tag{7.9}$$

The results of this evaluation are shown in Figure 7.9. The numbers of ampere-turns, NI, for the magnet are shown in Figure 7.9a.

7.10 Mass of the Magnet (Equation (4.18a))

$$M = \frac{\rho_W}{\sigma_W} \frac{(2\pi a NI)^2}{P/2} \tag{7.10}$$

Once the material for the magnet has been selected, this equation can be evaluated. Examination of Table 4.2 indicates that a magnet made of sodium clad in stainless steel would likely result in a minimum weight magnet. For this case

$$\frac{\rho_W}{\sigma_W} = 0.417 \times 10^{-4} \frac{\text{kg-ohm}}{\text{m}^2}$$

The mass of the magnet is shown in Figure 7.10 as a function of altitude.

7.11 Surface Area of the Magnet that is effective in radiation cooling the coil. (Equation (4.21b))

$$(A_s)_{Min} = 8\left\{\frac{2aM}{\rho_W}\right\}^{\frac{1}{2}} = 0.257\, M^{\frac{1}{2}} \text{ for Sodium} \tag{7.11}$$

This area can be evaluated using the magnet mass M from Section 7.10. The magnet surface area is shown in Figure 7.11 vs. altitude.

7.12 Magnet Equilibrium Temperature using the power dissipation and solar energy as inputs and radiation as energy output. Assume that half of the magnet surface is directly radiated by the sun. (Equation (4.19))

$$\frac{P}{2} + \left(\frac{dP}{dA}\right)_S \frac{(A_S)_{Min}}{2} = (A_S)_{Min}\, e_R\, \sigma' T_S^4 \qquad (7.12)$$

where

e_R = emissivity of wire surface
= 1.0

σ' = Stefan-Boltzmann constant
= 5.69×10^{-8} watts/meter^2 $^oK^4$.

The magnet surface temperature is shown in Figure 7.12 vs. altitude.

7.13 Volume of the Discharge Necessary to produce ions at the rate required through inelastic collisions of electrons and atoms. (Equation (2.11))

$$\text{Vol.} = \frac{I_I}{Z\,|e|\,n_e\,v_e\,p_a\,(\alpha/p)} \qquad (7.13)$$

where

I_I = ion current in exhaust beam
= I/2

n_e = average electron density in volume of discharge
= n/2

p_a = ambient pressure of atoms
= p/2

(α/p) = experimentally determined ionization parameter for air
= 7.6 (ion pairs/m) / (newton/m^2)

v_e = electron thermal velocity
= 10^6 meters/sec.

Therefore we have

$$\text{Vol.} = 164.5\, \frac{I}{Z\left(\frac{n}{10^{16}}\right)\left(\frac{p}{10^{-6}}\right)} \text{ meters}^3 .$$

8. Discussion of the Calculations

Several important inferences can be drawn from the calculations. One of the most important is that the use of solar energy to power the Advanced Electric Thruster will result in sufficient thrust for drag make up at altitudes only above about 100 miles. It should be emphasized, however, that the engine will work well and probably better at lower altitudes, but that some source of power other than or in addition to solar power would be needed. The discharge will operate at a potential of between 25 and 30 volts under the conditions specified in the calculations. This matches well with voltages available from solar cell arrays. Further, if the magnet and discharge are operated in series, then the discharge will have a strong positive characteristic and can be connected directly to the power source without power conditioning.

The performance has been calculated on the assumption that no shock wave occurs due to the very large value of the mean free path (more than 1 meter) of the gas particles in the altitude range under consideration. In fact, effects due to shock wave formation would improve engine performance: for example, increased density would improve ionization efficiency.

The maximum axial magnetic field strength needed on the axis of the coil is about 57 gauss for accelerating singly charged ions, and about 43 gauss for accelerating doubly charged ions. These field strengths are independent of the altitude, as indicated by Figure 7.9a. In practice, there is little or nothing that can be done to restrict operation to one of either the singly ionized or the doubly ionized mode. As the ambient density decreases, the electron temperature will tend to rise, leading to the onset of higher multiple ionizations.

9. Pulsed Operation

The Advanced Electric Thruster can be operated in a pulsed mode as well as steady-state. However, several problems are introduced by pulsed operation:

1. The thrust level must be higher by the ratio of the orbit period to the operating time during the orbit. This requires a larger cross-sectional area of interaction in order to intersect enough propellant. This can be accomplished by using a magnet with a larger magnetic moment.
2. The magnet current must be operated in a pulsed mode as well as the discharge in order to use the power efficiently. This can be accomplished by using a condenser to store the magnet power and arranging to open the circuit between the magnet coil and the condenser when all of the energy is stored back in the condenser.

There is a potential advantage possible from pulsed operation. If the satellite is operating in the ionosphere, it may be possible that a considerable number of charged particles will be accumulated by the magnetic field and carried along. The particles will be accelerated in the exhaust beam when the discharge current is turned on.

10. Integration of the Advanced Electric Thruster into the Spacecraft

10.1 Possible Configurations

In order to ensure minimum interference between sensors, etc. on the satellite and the AET components, the thruster will be positioned on the rear of the satellite or if desired mounted up to 0.5 meters from the body of the satellite. The coil outer diameter should be approximately equal to the diameter of the satellite, and the anode should have a similar diameter. An insulator plate placed concentrically around the cathode will extend radially out to the anode radius to prevent metal components in the satellite from shorting out the radial electric field between the electrodes. As mentioned above, an axial gap between the insulator and the anode ring will be necessary to prevent the flow of surface currents which would quickly erode the insulator.

10.2 Mechanical and Electromagnetic Interference Effects

Placing the Advanced Electric Thruster at or beyond the rear of the satellite should make possible designing out any mechanical interference problems between AET and satellite components.

The d.c. magnetic field of the engine might offer some problems of interaction with moving ferromagnetic components of the satellite, and possibly with electromagnetic devices, especially under conditions of the field reversals. There are various ways of shielding the susceptible devices--ferromagnetic shielding, suitable design and alignment of components, and so on, or even alternating engine operation with that of the device or devices.

Alteration to some degree of the engine magnetic field by the presence of ferromagnetic etc. materials in the vehicle should not degrade engine performance appreciably, and may possibly be so designed as to enhance performance.

11. Requirements for Wind-Tunnel and/or Flight Test of the Advanced Electric Thruster (AET) Concept

11.1 Critical Engine Parameters Requiring Investigation

11.1.1 Engine Components

The engine consists of three major components: the anode, the magnet coil, and the cathode. The design parameters for the first two are well-known and can be fabricated once the material for construction is chosen. However, some preliminary experimental work should be undertaken to investigate cathode design parameters. These should determine the following:

1. The best method of ensuring that the cathode coating material is injected into the cathode cavity at the proper rate.
2. Which coating material should be used.
3. The relation between the mass loss rate from the cathode, and the current.
4. The minimum power input necessary to ensure proper cathode performance.
5. Optimum radiation shielding configurations.

11.1.2 Performance Parameters

11.1.2.1 Ionizing Efficiency

The most critical phenomena relative to the engine operation that requires experimental investigation is the effectiveness with which the ambient material is ionized by the electric discharge. To assess this, it is necessary to conduct a test in an environment with the ambient density close to that found at the altitudes of interest, i.e. those over 100 miles.

11.1.2.2 Anode Operation

Anode shape, size and positioning require experimental study. The anode must be placed in such a position as to prevent the discharge from enveloping the vehicle, i.e. the discharge current must be confined to

the space behind the plane of the magnet. The outer surface of the anode ring will undoubtedly have to be covered with insulating material to ensure that this does occur. Anode shape and size, and other factors involving positioning would require study for performance analysis and optimization.

11.2 Scaling

There are a number of non-dimensional parameters associated with the performance of a device of the AET type. Some are:

1. The ratio of the electron and ion cyclotron frequencies to the collision frequency:

$$\omega_e \tau_e = \frac{|e| B}{m_e} \frac{1}{n_I q_{eI} v_e} \tag{11.1}$$

and

$$\omega_I \tau_I = \frac{|e| B}{m_e} \frac{1}{n_e q_{eI} v_I} \tag{11.2}$$

2. The ratio of the electron and ion cyclotron radii to the vehicle radius, a:

$$\frac{v_e}{\omega_e a} = \sqrt{\frac{8kT_e}{nm_e}} \frac{m_e}{|e| B a} \tag{11.3}$$

and

$$\frac{v_I}{\omega_I a} = \sqrt{\frac{2|e| V_I}{m_I}} \frac{m_I}{|e| B a} \tag{11.4}$$

3. The ratio of the magnetic pressures to the gas pressure:

For the applied magnetic field: $\frac{B^2}{2 \mu_o p}$ (11.5)

For the induced magnetic field: $\frac{\mu_o I^2}{8 \pi A_c p}$ (11.6)

4. The ratio of the ionizing mean free path to the vehicle radius:

$$\frac{v_a}{n_a q_{ea}^I v_e a} \tag{11.7}$$

5. The ratio of the atom-atom mean free path to the vehicle radius:

$$\frac{1}{n_a q_a a} \tag{11.8}$$

6. The Mach number:

$$M^* = \frac{v_v}{\sqrt{\frac{\delta k T_a}{m_a}}} \tag{11.9}$$

7. The Reynold's number:

$$R_e = \frac{\rho v_v a}{\mu} \tag{11.10}$$

Because there is such a large number of these parameters, designing a reduced scale experiment would be very difficult ; hence it appears that a full scale experiment would be the only feasible method of testing the concept.

11.3 Size of the Testing Vacuum Tank

The tank should be sufficiently large that the magnetic field will drop to values at least as low as that of the earth's magnetic field,at the walls. If the experiment is placed at the center of the tank, minimum values of tank length and diameter can be termined by specifying the minimum value of the ampere turns of the magnet. The calculations in Section 7 indicate that NI should be about 400 ampere turns, so that using Equation (4.7), the tank length 2aZ can be found:

$$B_e = \frac{\mu_o \pi NI}{a} \frac{2}{(1 + Z^2)^{3/2}} \tag{11.11}$$

where

B_e = earth's magnetic field
$\simeq 0.5 \times 10^{-4}$ Tesla

NI = 400 ampere turns

a = radius of test equipment
= 0.5 meter

Hence

$$(1 + Z_A^2)^{3/2} = \frac{6.28 \times 1.256 \times 10^{-6} \times 400}{0.5 \times 0.5 \times 10^{-4}}$$

$$= 126.2$$

and

$$Z_A = 4.92$$

so that, since 2a=1, the tank length should be no less than 4.92 meters (16ft).

For a dipole magnet, the far field radially out in the plane of the magnet is minus one half its value on the axis for the same distance from the center of the coil. The tank diameter can hence be estimated by the equation

$$B_e = \frac{\mu_o \pi N I}{2a} \frac{2}{(1 + R^2)^{3/2}} \qquad (11.12)$$

or

$$(1 + R^2)^{3/2} = 63.10$$

$$R = 3.85.$$

Thus the tank diameter should be more than 3.85 meters (12.5ft) (for a vehicle of 1 meter diameter).

11.4 The Test Environment

The test engine must be placed in an air flow where the mass, momentum, and energy fluxes are as close as possible to that encountered by satellites at altitudes between 100 and 300 miles. An electron density of between 10^{11} and 10^{12} electrons/ meter^3 needs to be present in the flow.

In the altitude range mentioned, the mean free path varies from 5 meters to 23,000 meters. Because of this and since the size of vehicle under consideration is 1 meter, little or no significant shock wave effects will be present, such as increases in density, pressure and temperature over the ambient values, even though the vehicle would be travelling at Mach numbers between 8 and 10.

Accurate simulation of this high-altitude flow field is not feasible in existing facilities. Figure 11.1 illustrates an experimental configuration which should offer a satisfactory approximation to the conditions required. In it, an arc heater with a conical nozzle expands the flow to a Mach number of between 2 to 4, and opens to a large vacuum tank with the best available pumping capacity, so that the flow will continue to expand, decreasing the density in the flow to as low a value as possible. If it is assumed that the flow cross-sectional area at the test position is about 18 meters^2, then the mass flow rate of air through the arc heater should vary from 0.16 gm/sec to 3.18 x 10^{-4} gm/sec. The power required by the arc heater would be from about 20 kw down to less than 100 watts.

It appears at present possible only to produce wind-tunnel flows simulating the satellite environment at altitudes under 100 miles due to the limitations of the available vacuum facilities and the technology of producing extremely low density flows,

11.5 Test Facilities Available

Because existing facilities in the USA do not appear capable of the accurate high-altitude flow simulation desired for the full scale test, certain compromises and/or auxilliary devices would be necessary. The following facilities appear to be the best available for consideration for testing the Advanced Electric Thruster.

11.5.1 A.E.D.C. Low Density Tunnel M

This tunnel has a nitrogen flow from an arc heater expanding through a conical nozzle into a text section tank 8 ft in diameter. A balance is available for measuring drag or thrust from 0 to 100 milli-pounds. The tunnel has the disadvantage that the mass flux rate, ρu, is more than 10^4 too high. Further, the tank is too small, and since pumping is accomplished by air injectors it is unlikely that a low enough density could be achieved for meaningful tests.

11.5.2 A.E.D.C. Aerospace Chamber (10V)

This chamber is designed for--among other things--space propulsion testing. The chamber pressure characteristics (shown in Figure 11.1, as taken from Reference) indicate that the density can be maintained at a level of 10^{-5} torr at the flow rate anticipated from the arc heater. This is about 1 order of magnitude too high for simulation of 100 miles altitude. The tank is 10 feet in diameter, compared with the minimum of 12.5 feet desired. If under certain compromises this tank were used, a small nitrogen arc heater would have to be designed and built as part of the experiment.

11.5.3 A.E.D.C. Aerospace Environmental Chamber (Mark I)

This tank is approximately 34 feet in diameter and 65.5 feet long, and so is clearly large enough. It also has a pumping capacity adequate to conduct a test at a pressure of 10^{-7} torr, simulating an altitude of 100 miles. The maximum throughput of nitrogen at this pressure would be only a few milligrams/sec. This means that the arc heater must operate at as low a power as feasible, probably about 1 kw. Once again, if this tank were used, the arc heater and balance would have to be designed and built as part of the experiment.

11.5.4 N.A.S.A. Lewis Electric Propulsion Facility

Meaningful tests could be conducted in this facility if it could be made available. It is possible that one of the NASA Lewis MPD arcs could be used as the arc heater. Balances are available to measure the drag and thrust.

11.5.5 Other Facilities

There are a number of facilities in industry and at other government installations that might be considered, such as the EOS-USAF electric propulsion facility, and the WPAFB electric propulsion facility. However, they appear well below the previously mentioned facilities in meeting standards of suitability for the experiment as described.

12. Proposed Experimental Program

The following program is recommended as the next phase of this study. It is so constructed that each section could be done as an independent study.

12.1 Cathode Studies

A cathode structure, similar to that shown in Figure 3.3, should be designed and built, and tests conducted in a small vacuum chamber to determine relations among the following variables:

1. temperature of the cathode cavity
2. material used to coat the cathode.
3. mass loss rate through the orifice
4. strength of the applied solenoidal magnetic field

all as functions of the total current carried between the cathode cavity and an anode placed at least 10 cm from the cathode.

12.2 Investigation of Engine Performance in a Flow Field with a Low Level of Ionization

This experiment could be conducted on a transient pressure basis, in that the tests would be initiated in the tank at its highest vacuum and data accumulated before jet influxes increased pressure excessively. The objective would be to determine the extent to which the accelerator can utilize the ionized fraction of gas at the atmospheric E-layer as propellant and to provide discharge breakdown nucleii. The tests would also determine variation of the discharge as ambient pressure is reduced.

The facilities and components needed to conduct this series of tests would be

1. a vacuum chamber at least 10 ft in diameter that has a pumping system capable of reducing the tank pressure to under 10^{-7} torr.
2. a small (1-10kw) arc jet that can operate on a pulsed basis (0-10sec). This would be used as a pulsed, point source of gas and plasma. The conical expansion of this

flow will reduce electron density and mass flux at the test engine to the desired values.

3. a test propulsion engine consisting of a magnet coil, an anode assembly, a cathode assembly and a battery power supply of approximately 1 kw capability.

These tests would also determine the feasibility of operating the engine by acceleration only of the existing ions in the flow, and determine the current and voltage levels at which this can be done, as a function of the magnetic field strength and the flow parameters.

12.3 Investigation of Engine Performance in Simulated Flow Field

This series of tests would place the thruster on a balance to measure drag, thrust, and torque. The tests would be conducted in a facility that could simulate the required mass flux rate and electron on a steady basis (i.e. for 1 minute or more).

REFERENCES

1. Demetriades, S.T., and Kretschmer, C.B., "The Use of Planetary Atmospheres for Propulsion", Armed Services Technical Info. Agency Doc.AD 154-132, (April 1958)

2. Demetriades,S.T., " A Novel System for Space Flight Using a Propulsive Fluid Accumulator", J.British Interplanetary Soc. 17, 114-119, (1959).

3. Demetriades, S.T., " Orbital Propulsion System for Space Maneuvering (PROFAC)", Astronaut.Sci. Rev. 1, 17-18 (1959)

4. Demetriades, S.T., and Young, C.F., "Orbital Refuling Satelloid", Soc. Automotive Engrs./Air Force Office Sci. Research Paper 230H (October 1960)

5. Berner, F. and Camac, M., "Air Scooping Vehicle", Avco-Everett Research Lab. Research Rept. 76, Air Force Ballistic Missle Div. TR 59-17 (August 1959)

6. Camac, M. and Berner, F., " An Orbital Air Scooping Vehicle", Astronautics 6, 28-29, 70-71, (August 1961).

7. French, E.P., "Operation of an Electric Ramjet in a Planetary Atmosphere", Am.Astronaut. Soc. Preprint, 60-90, (August 1960).

8. Glassmeyer, J.M., AFRPL "Ideagram", A-SCOR, (3 May 1970).

9. Corliss, W.R., Propulsion Systems for Space Flight, McGraw-Hill Book Co., Inc. 1960.

10. Jahn, R.G., Physics of Electric Propulsion, McGraw-Hill Book Co.,Inc. 1968.

11. Ducati, A.C.,et al, "Recent Progress in High Specific Impulse Thermo-Ionic Acceleration", AIAA 2nd Aerospace Sciences Meeting, New York January 1965, (AIAA Paper 65-96).

12. Bennett, S.c et al, "MPD Arc Jet Engine Performance", AIAA 2nd Annual Meeting, San Francisco, July 1965, (AIAA Paper 65-296).

13. Cann, G.L., et al, "Hall Current Accelerator", Final Report NASA Contract #NAS 3-5909.

14. Cann, G.L. et al, " Follow-On Investigation of a Steady State Hall Current Accelerator", Final Report Nasa Contract #NAS 3-3568.

15. Moore, R.A., et al, "High Specific Impulse Thermal Arc Jet Thruster Technology", Technical Reports AFAPL-TR-65-48, Parts I and II.

16. Cann, G.L. and Harder, R.L., "Thrust Efficiencies of Electromagnetic Engines", AIAA Journal, Vol.6 No. 3, March 1968, pp 559-560.

17. Cann, G.L., "The Use of E.M.Accelerators in High Pressure Test Facilities", ARL Report 72-0061, May 1972.

18. Kogelshatz, U., "Doppler-Shift Measurements of Axial and Rotational Velocities in an MPD Arc", AIAA Journal, Vol.8, No. 1, pp 150-154, January 1970.

19 Test Facilities Handbook, 9th Edition, Arnold Engineering Development Center, Tennessee July 1971.

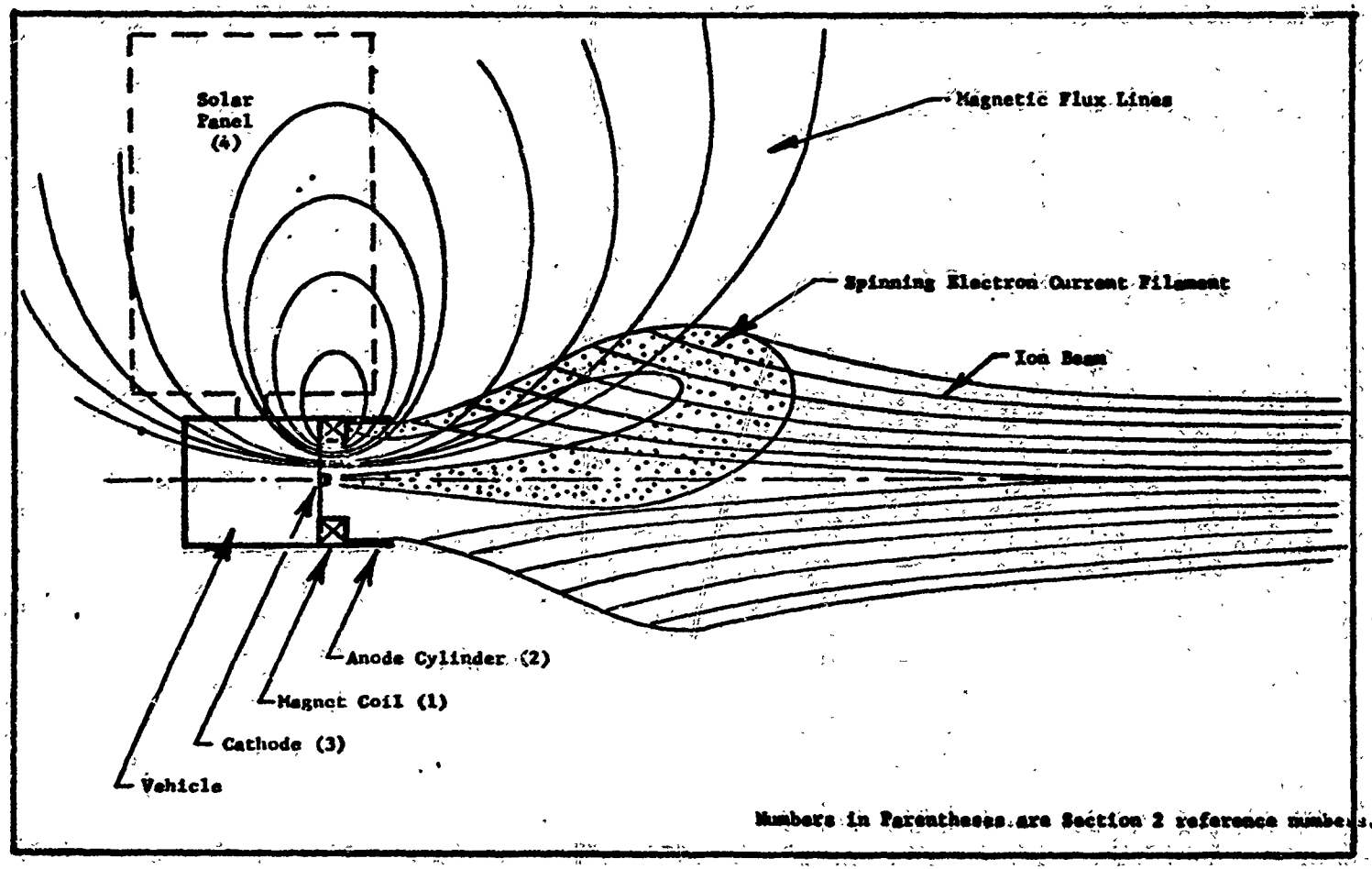

Figure 2.1 Schematic of Advanced Electric Thruster (SERJ)

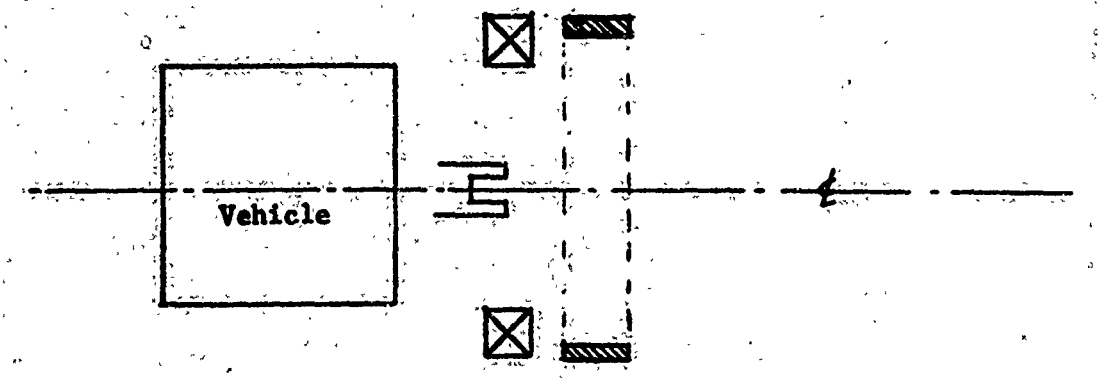

(a) Cylindrical Anode

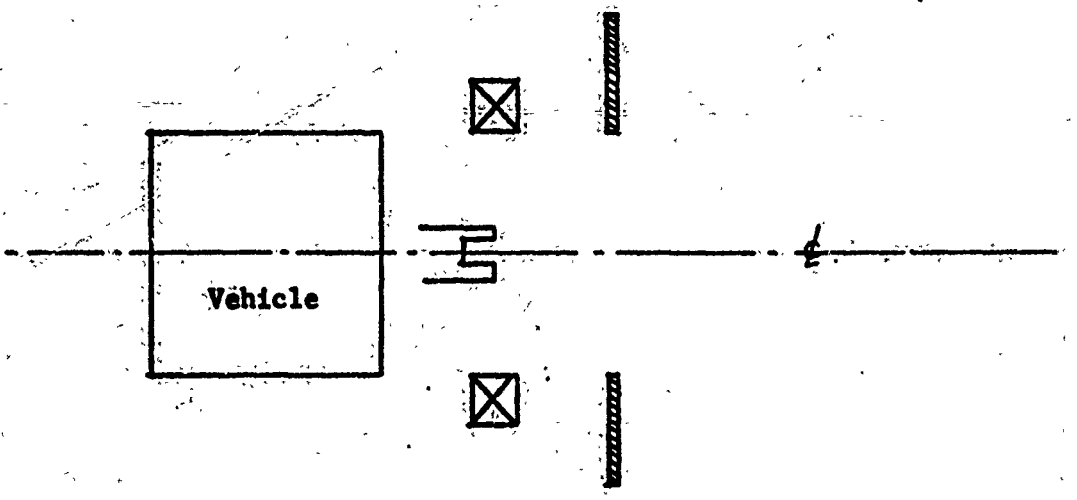

(b) Disc Anode

Figure 3.1

Anode Configurations

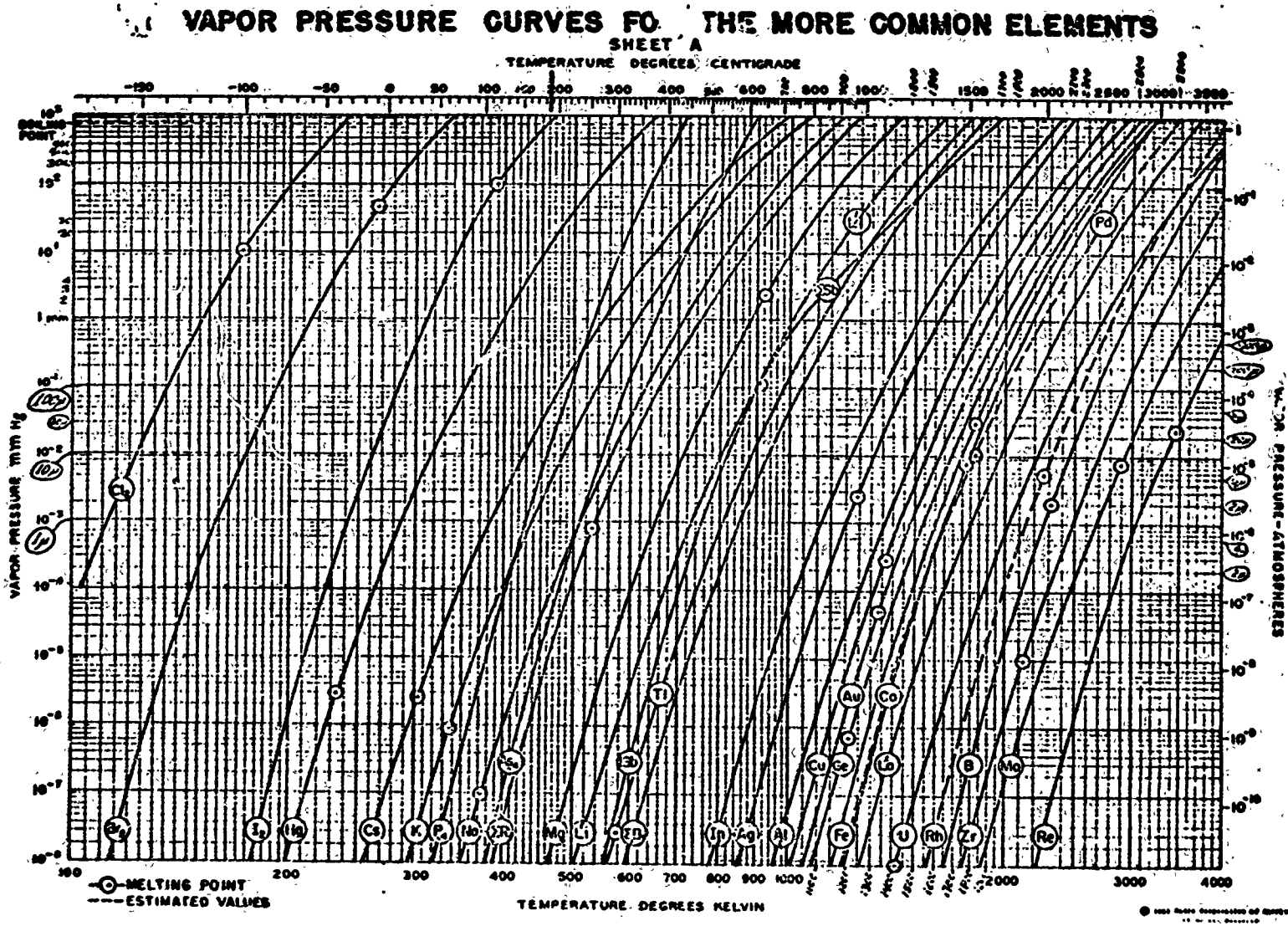

Figure 3.2 Vapor Pressure Curves for the More Common Elements (RCA)

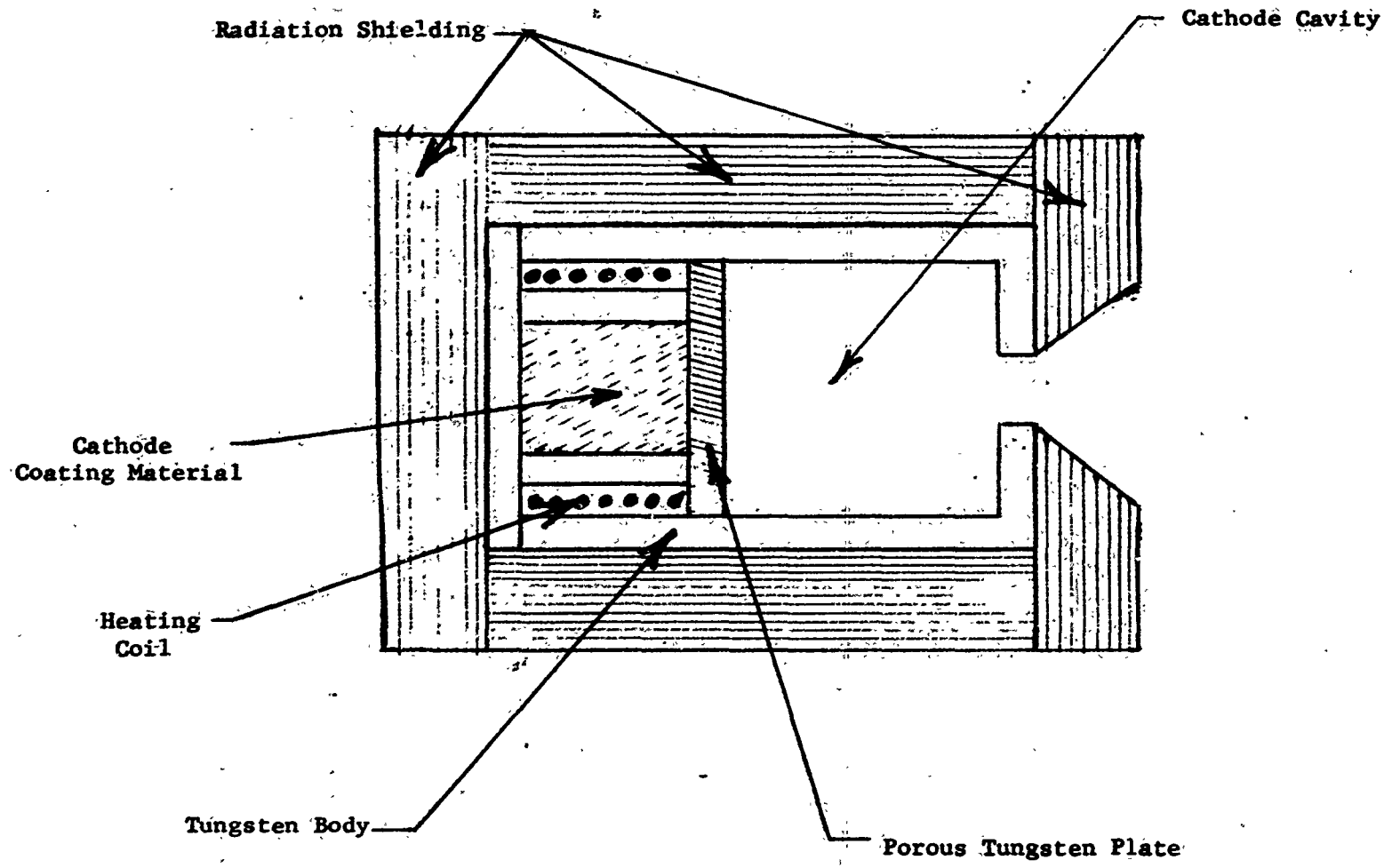

Figure 3.3 "L"-Type Cathode Configuration

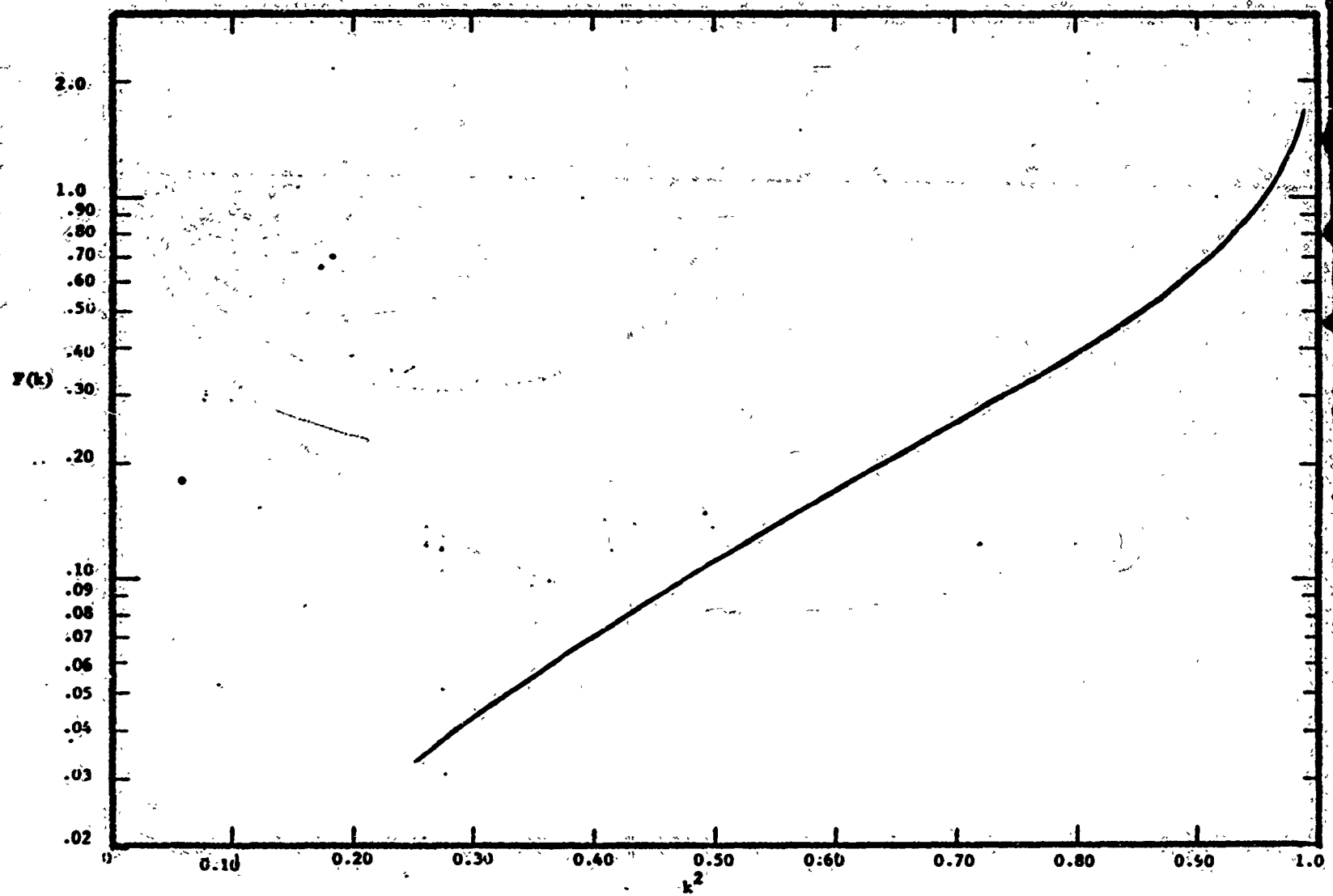

Figure 4.1 Evaluation of F(k)

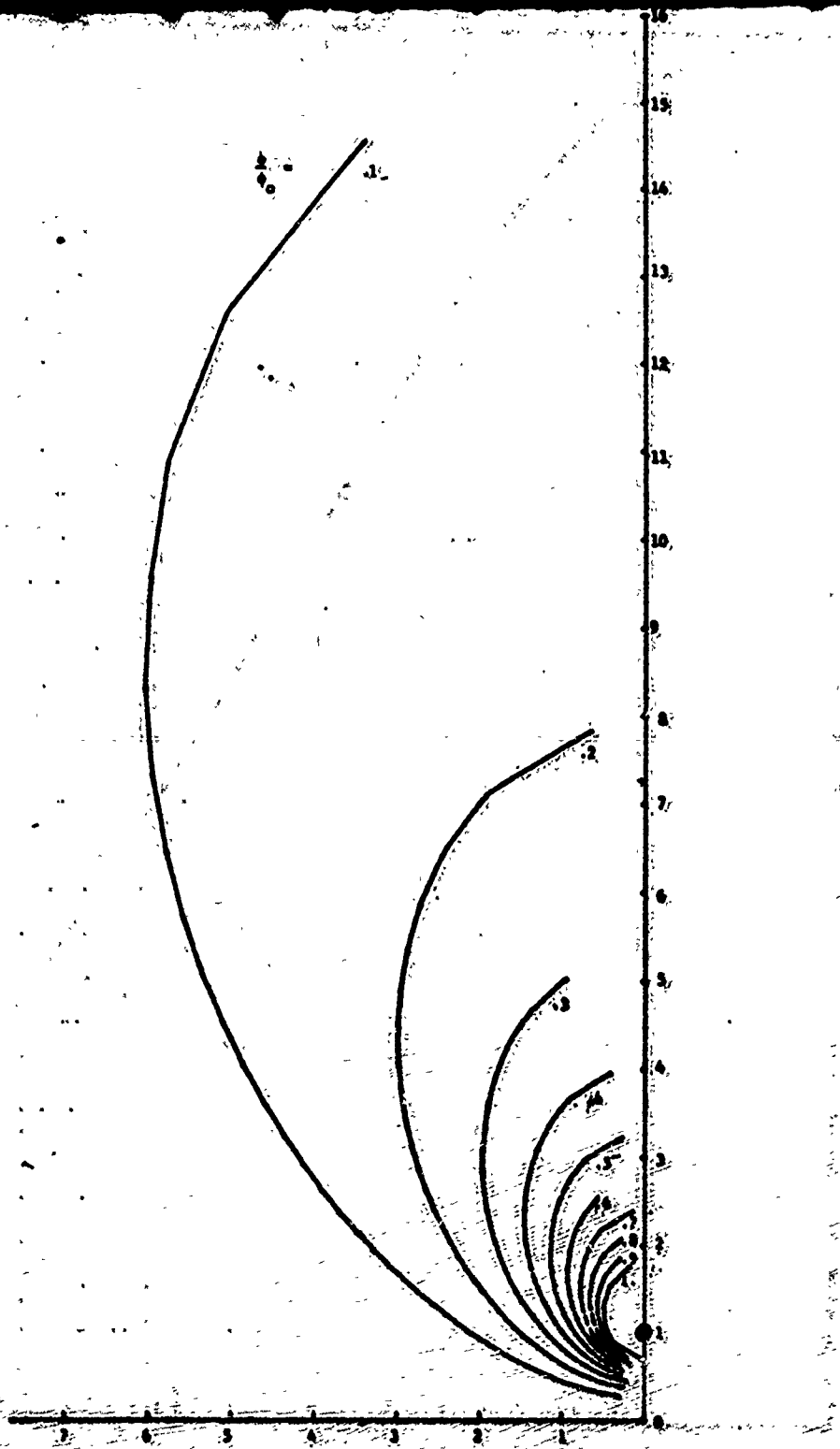

Figure 4.2 Lines of Constant Flux for Dipole Magnetic Field

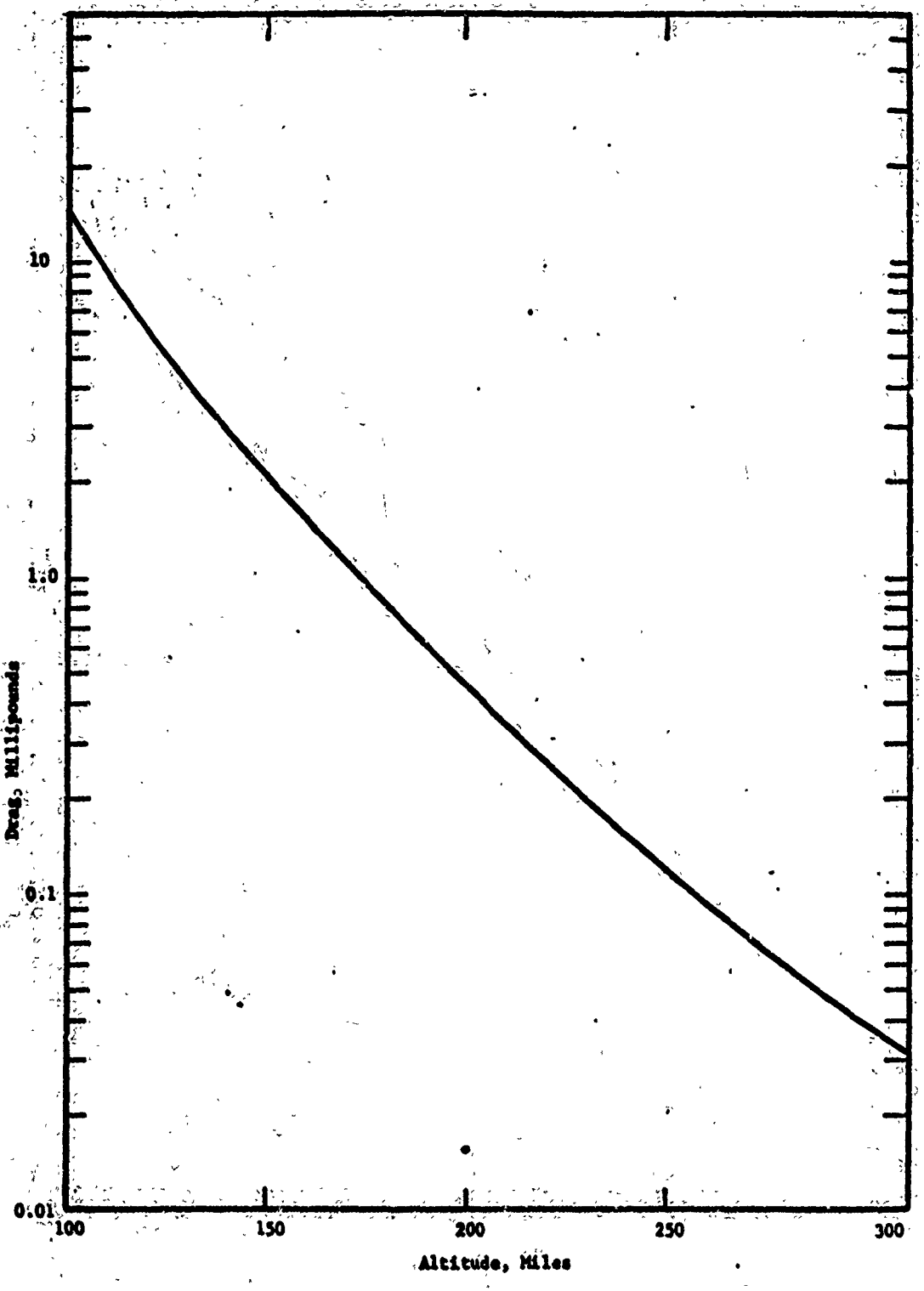

Figure 7.1 Satellite Drag, Vehicle Only.

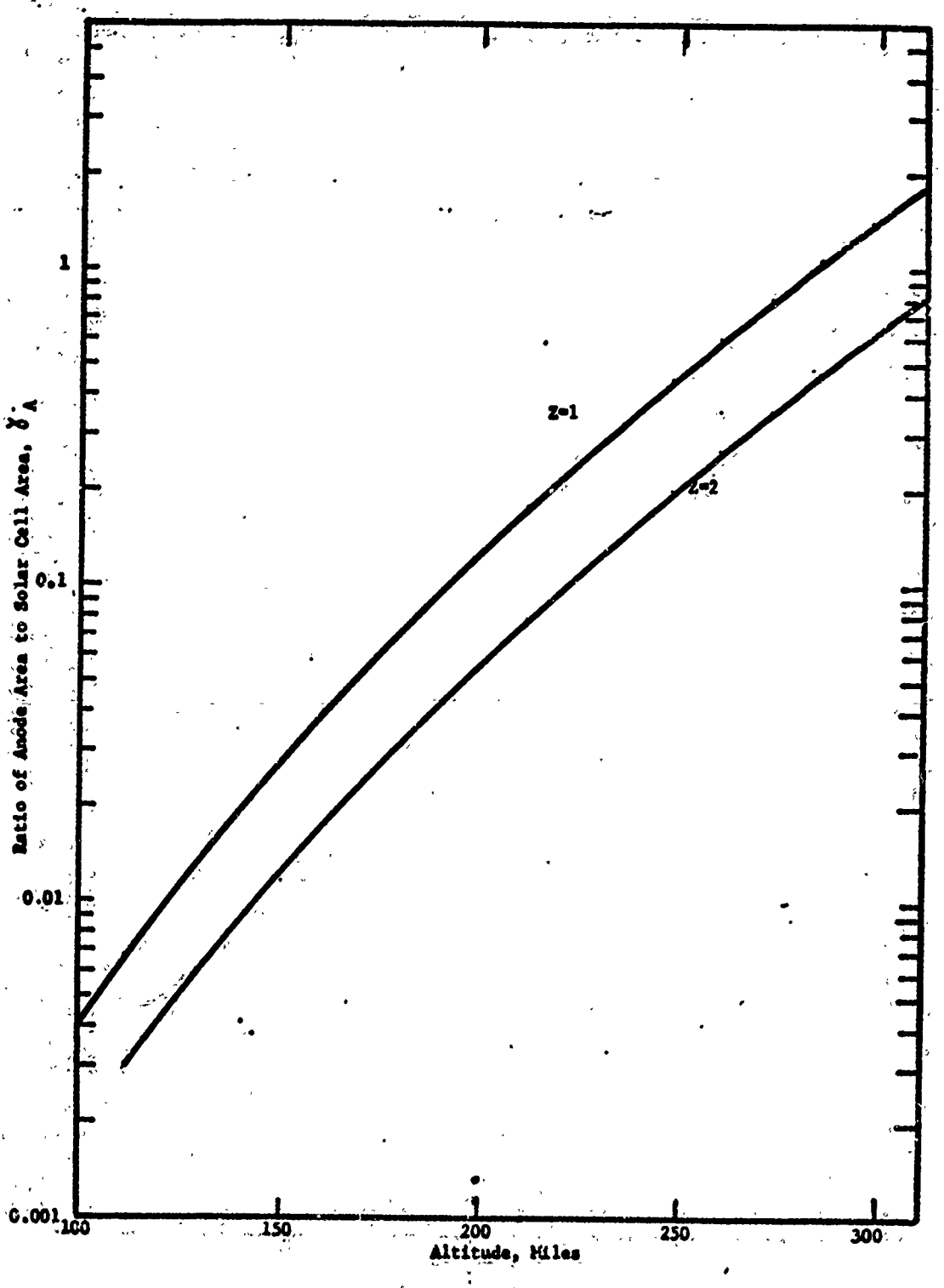

Figure 7.2 Ratio of Anode to Solar Cell Areas, γ_A

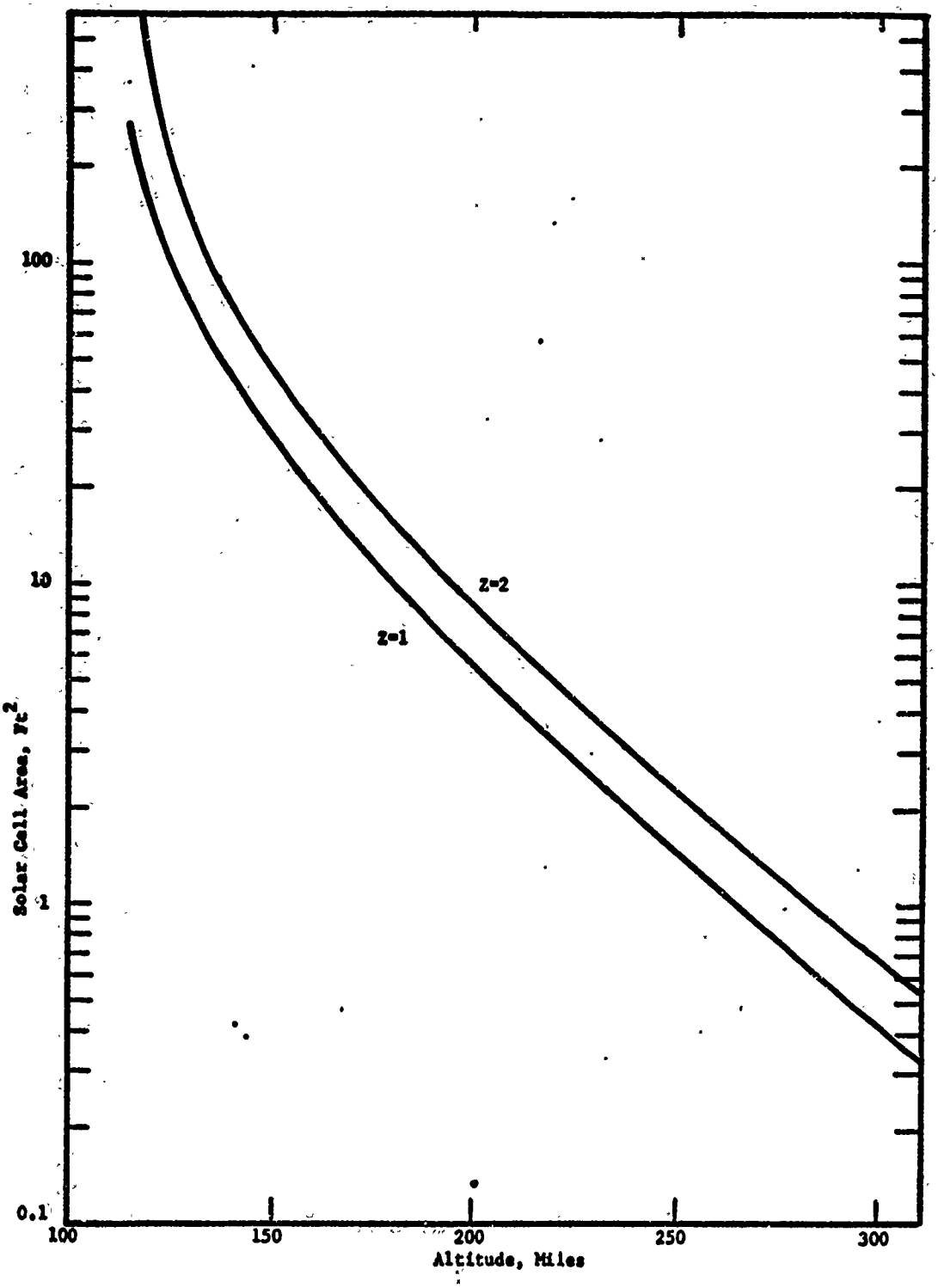

Figure 7.3 Solar Cell Area

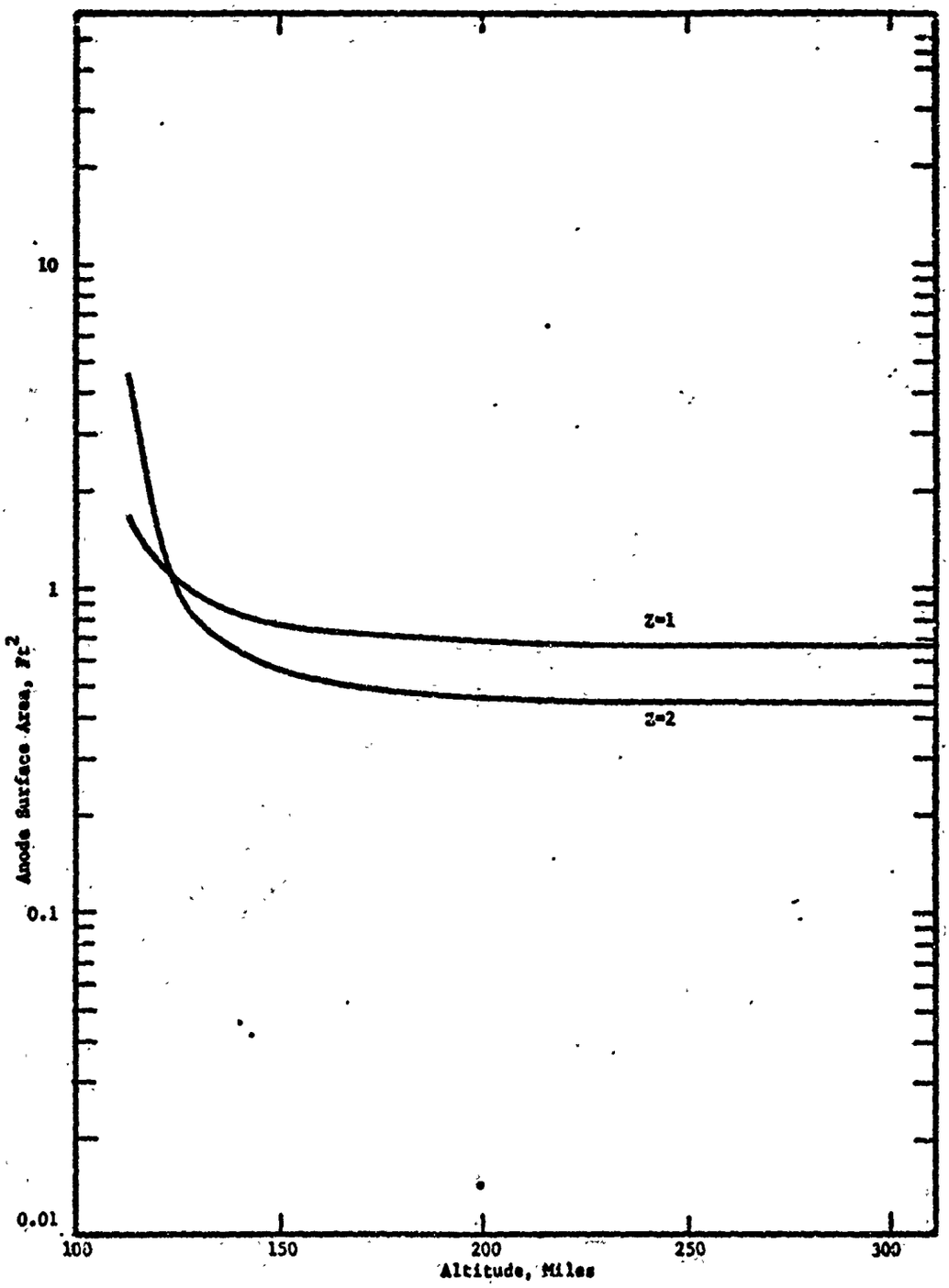

Figure 7.4 Anode Surface Area

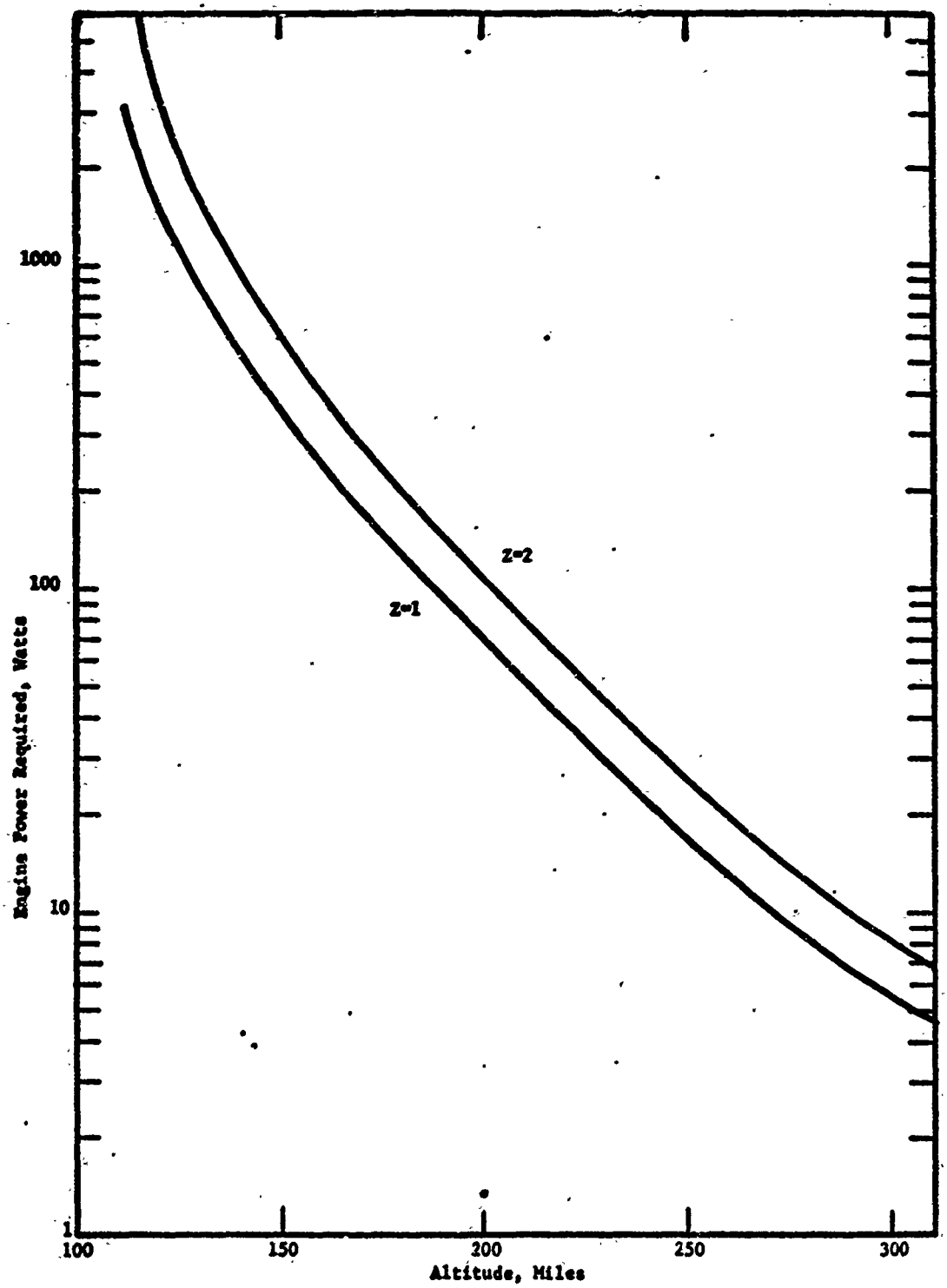

Figure 7.5 Engine Power Required

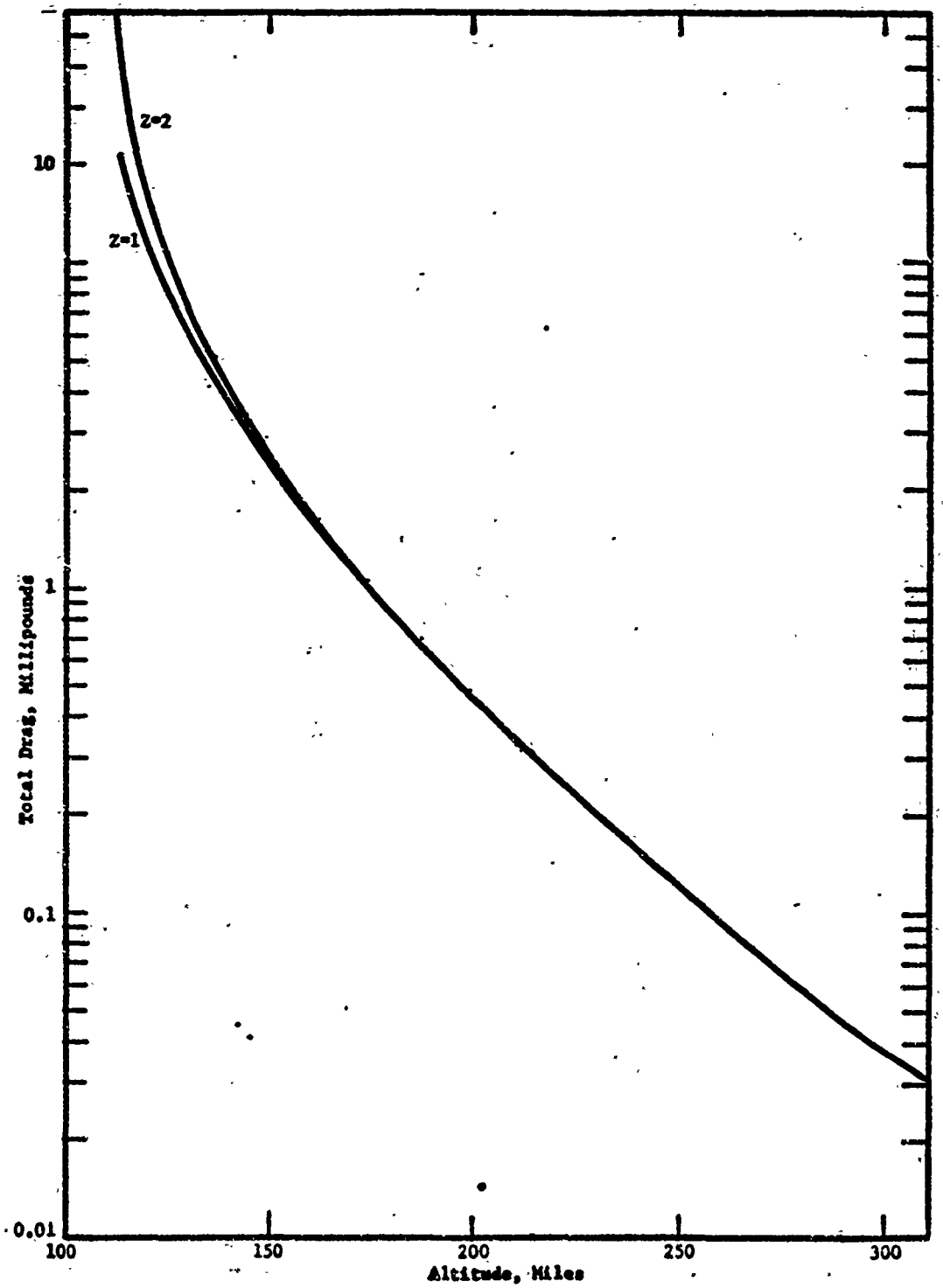

Figure 7.6 Total Drag

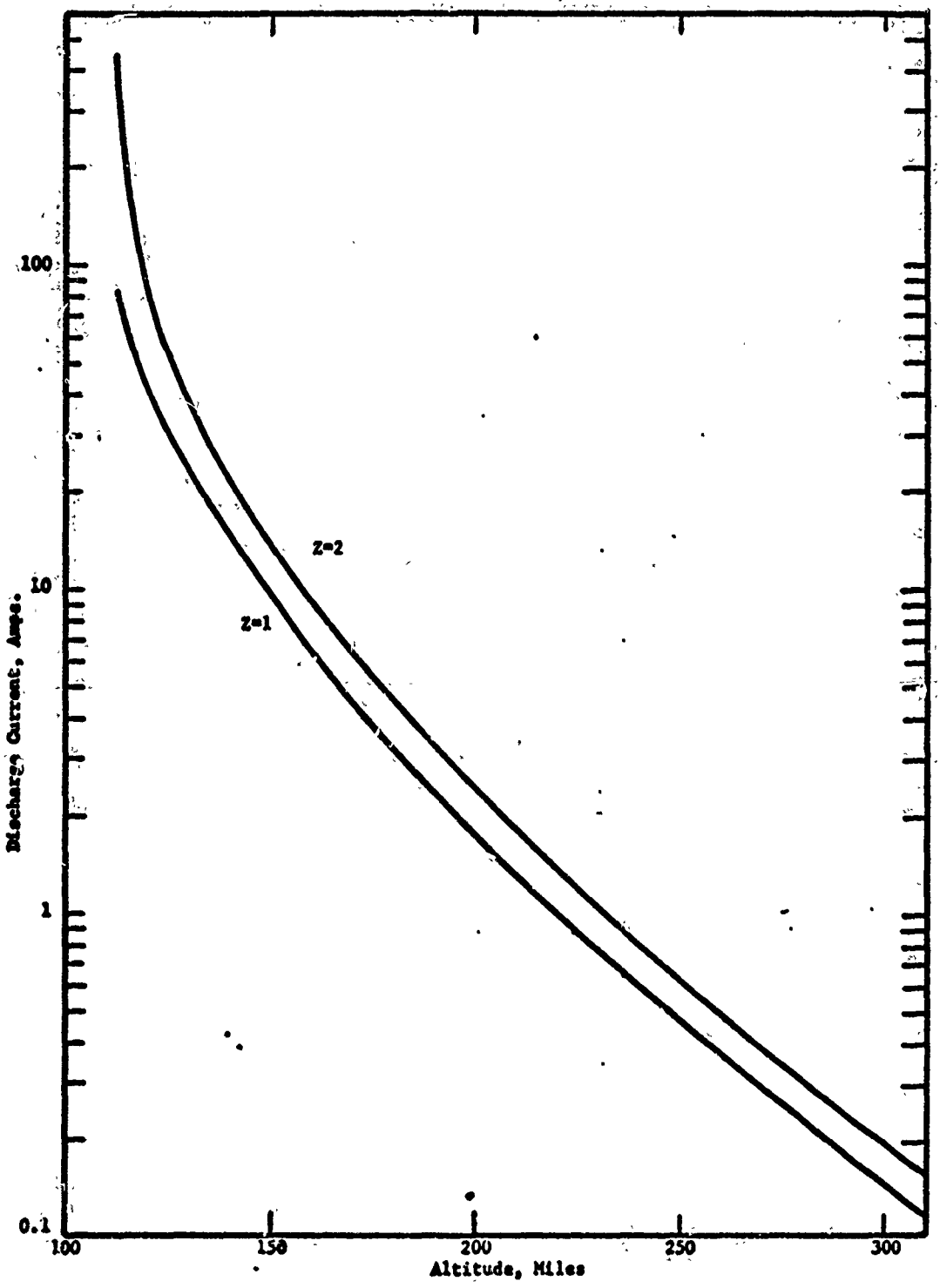

Figure 7.7 Discharge Current Required

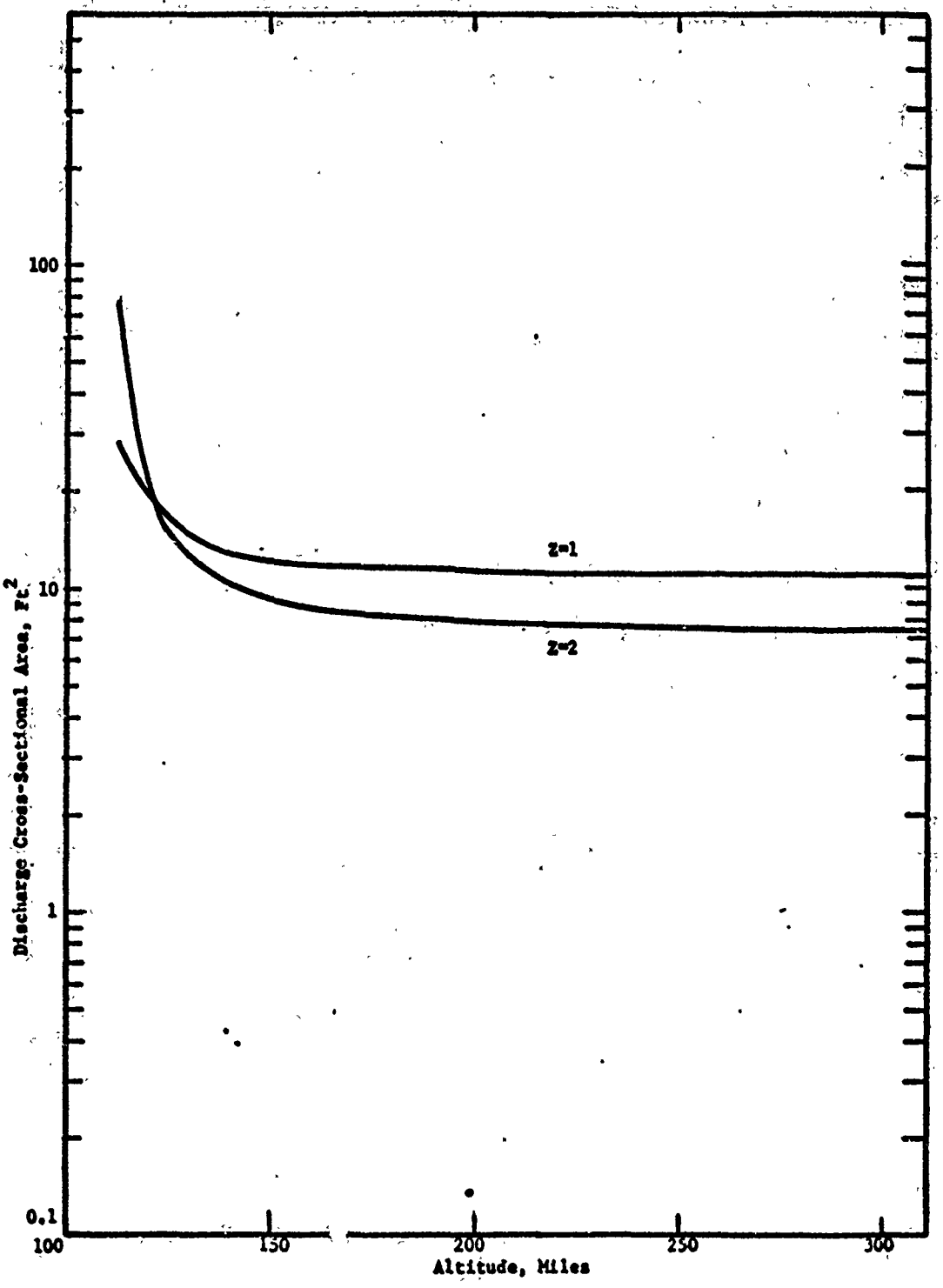

Figure 7.8 Discharge Cross-Sectional Area, Minimum Required

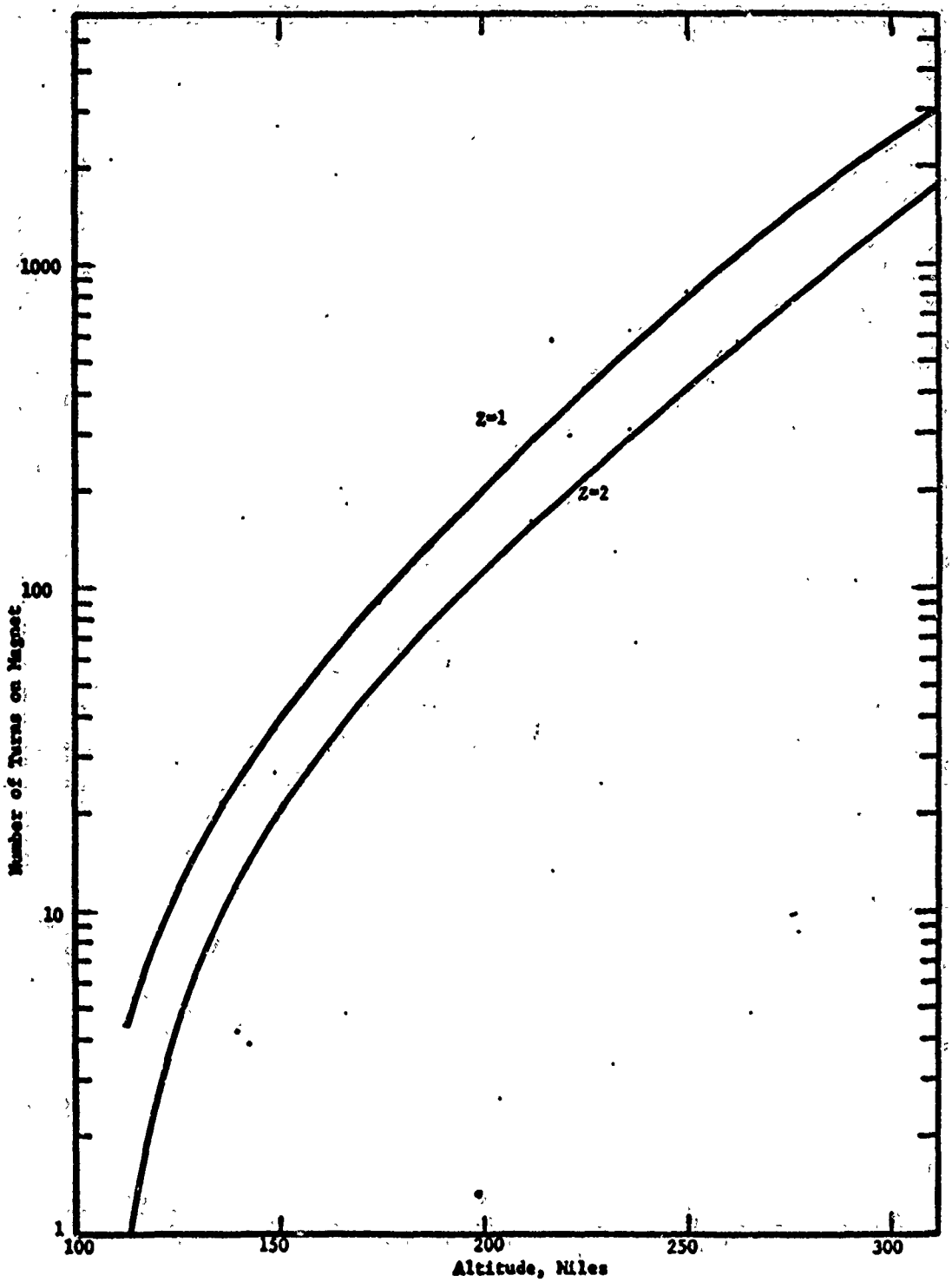

Figure 7.9 Number of Turns on Magnet

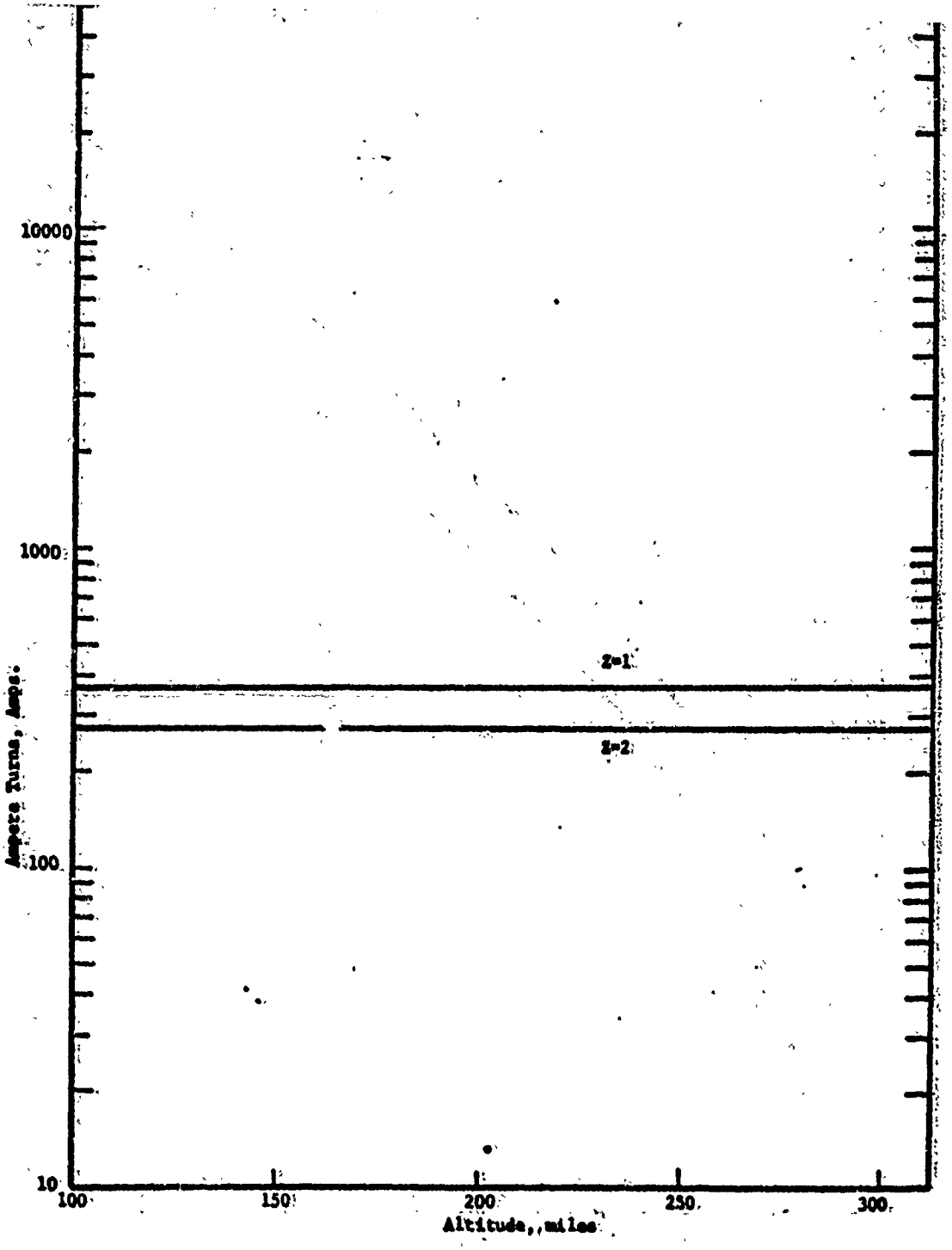

Figure 7.9a: Ampere Turns.

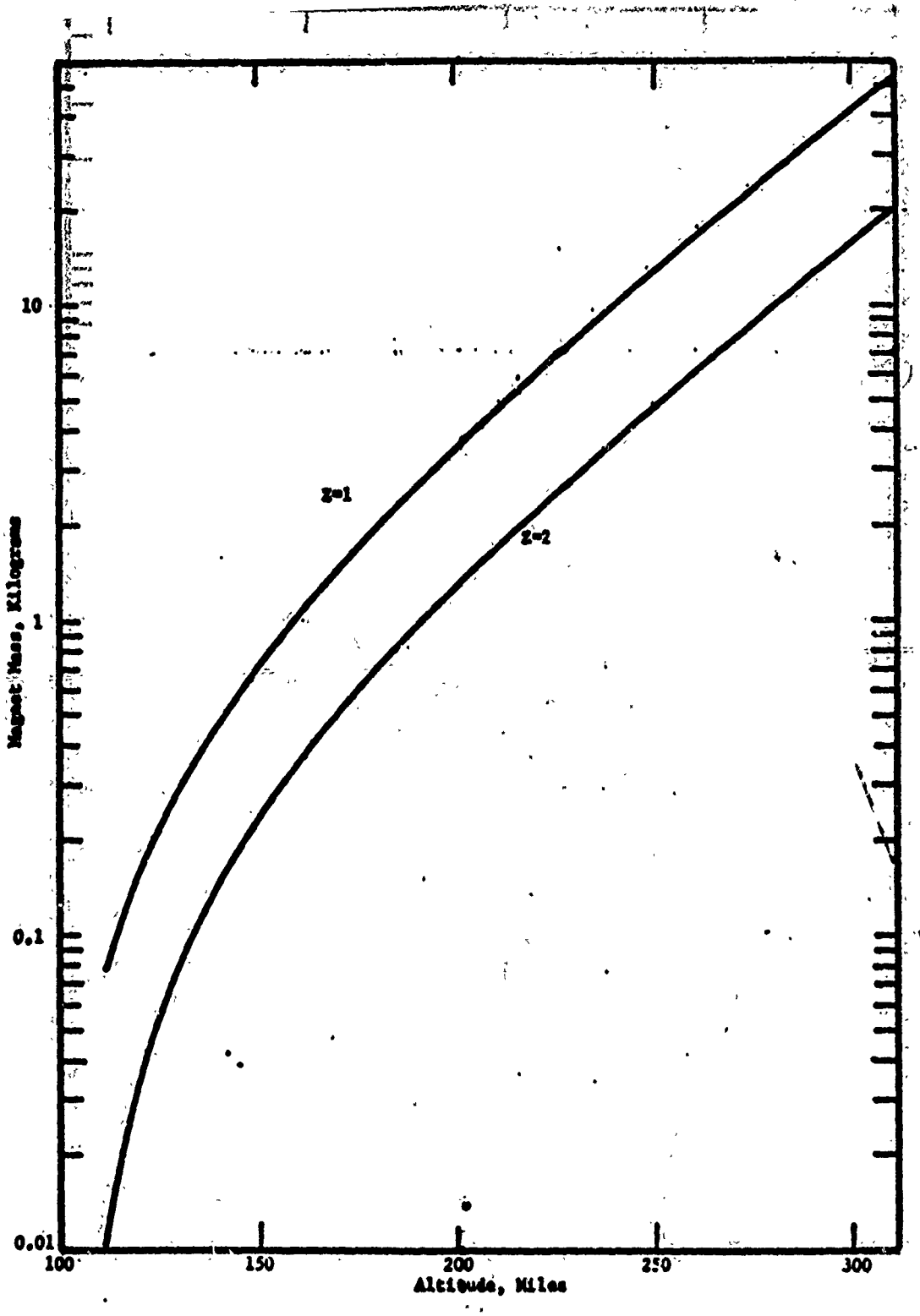

Figure 7.10 Magnet Mass

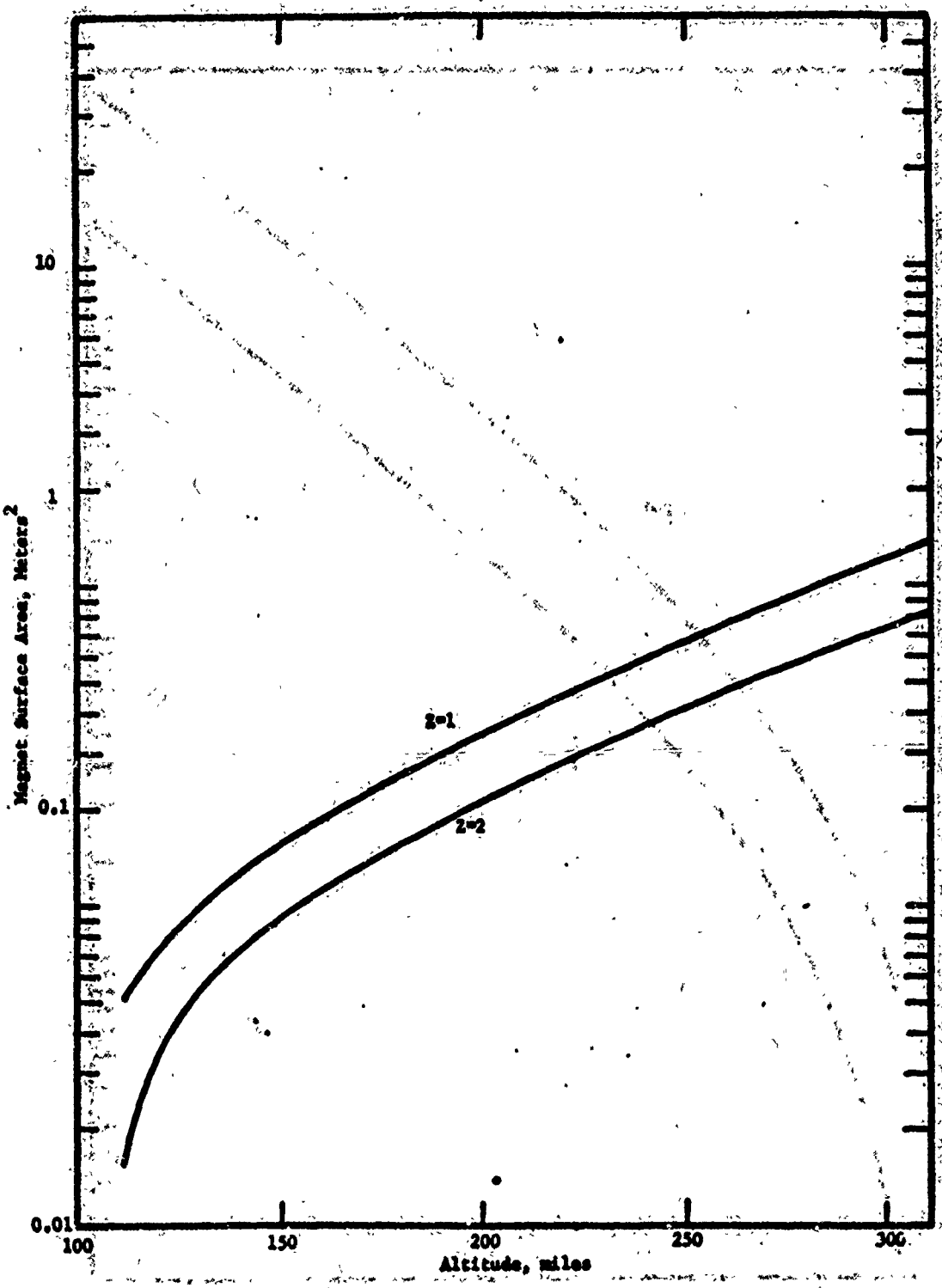

Figure 7.11 Magnet Surface Area

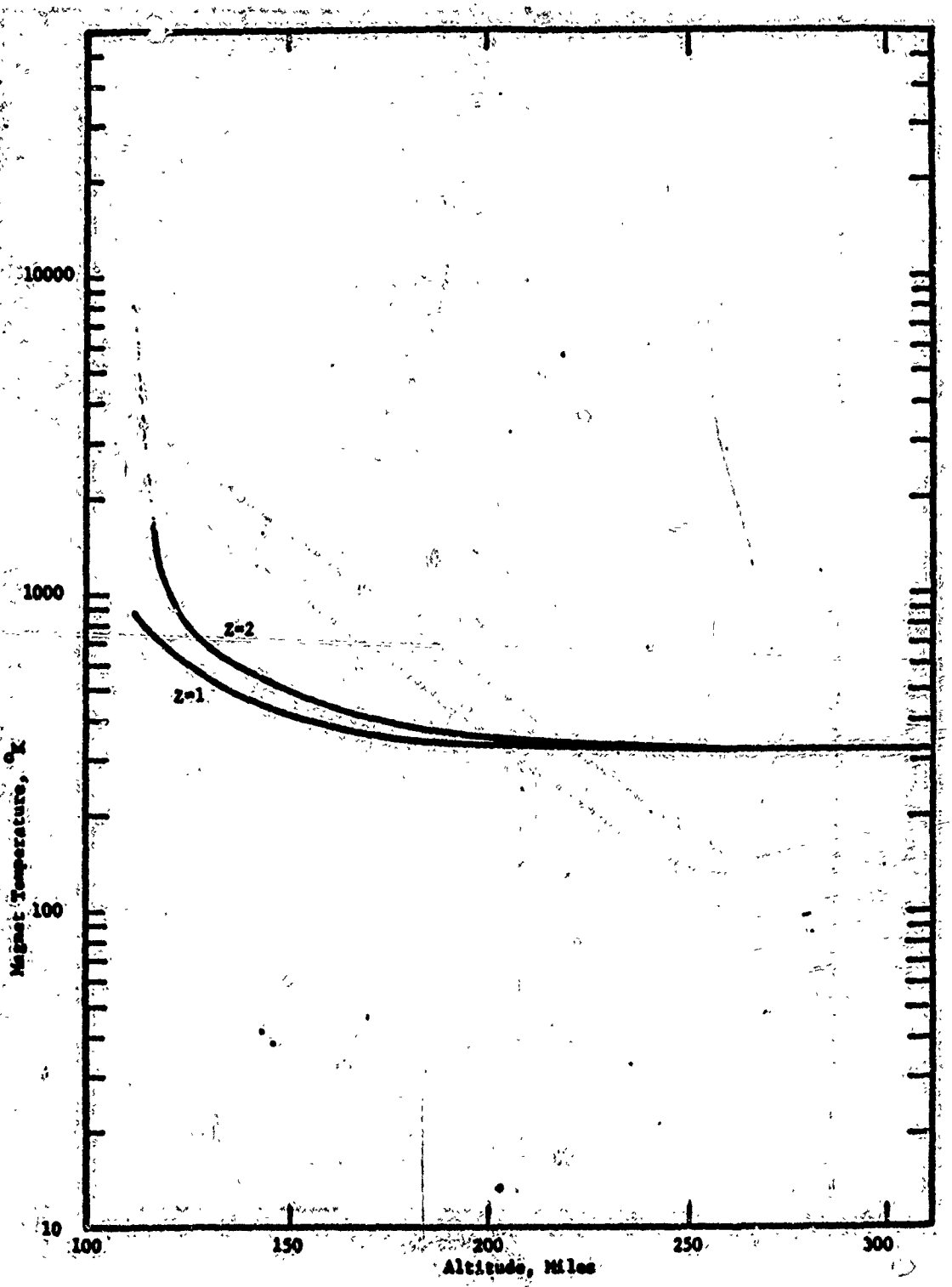

Figure 7.12 Magnet Temperature

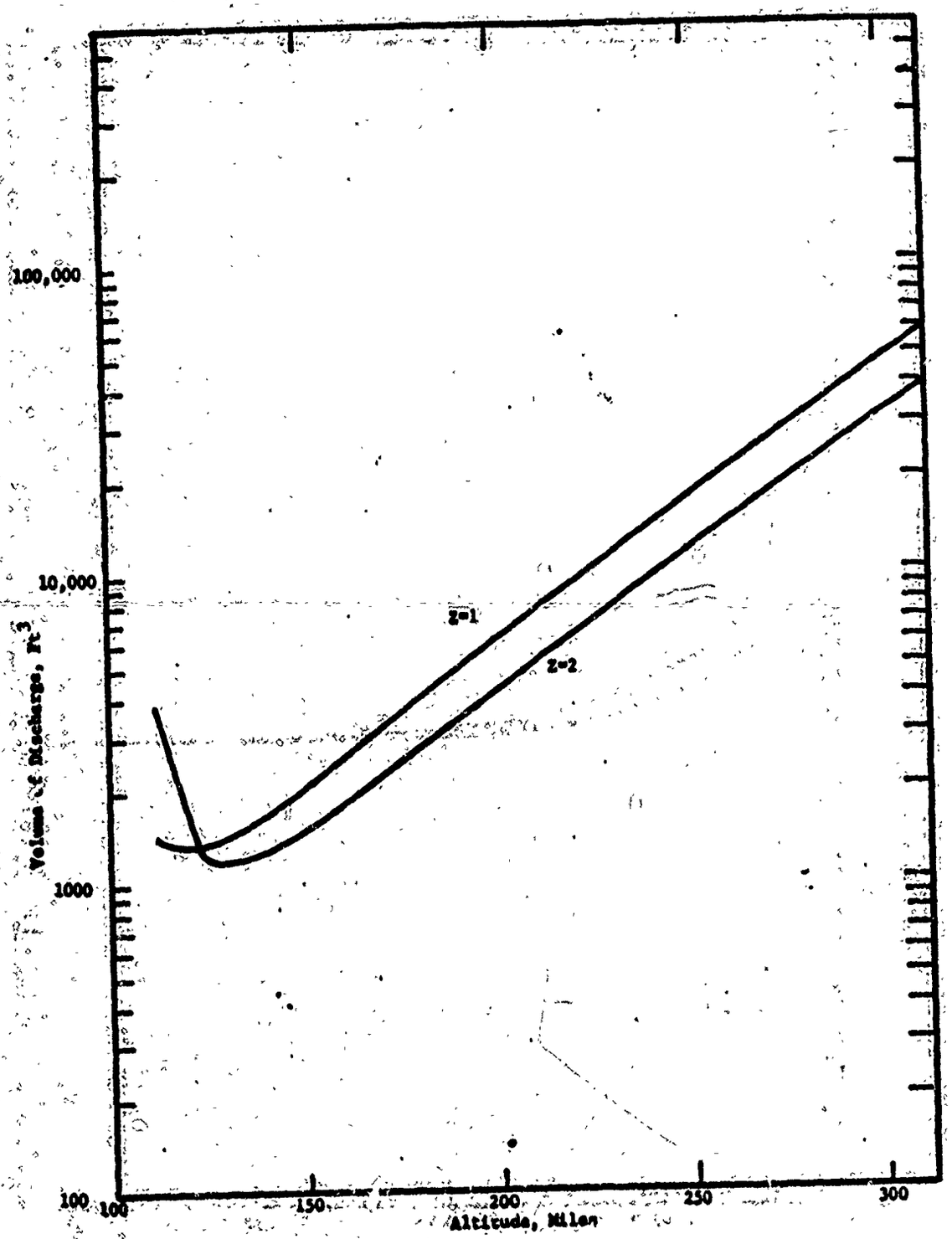

Figure 7.13 Volume of Discharge

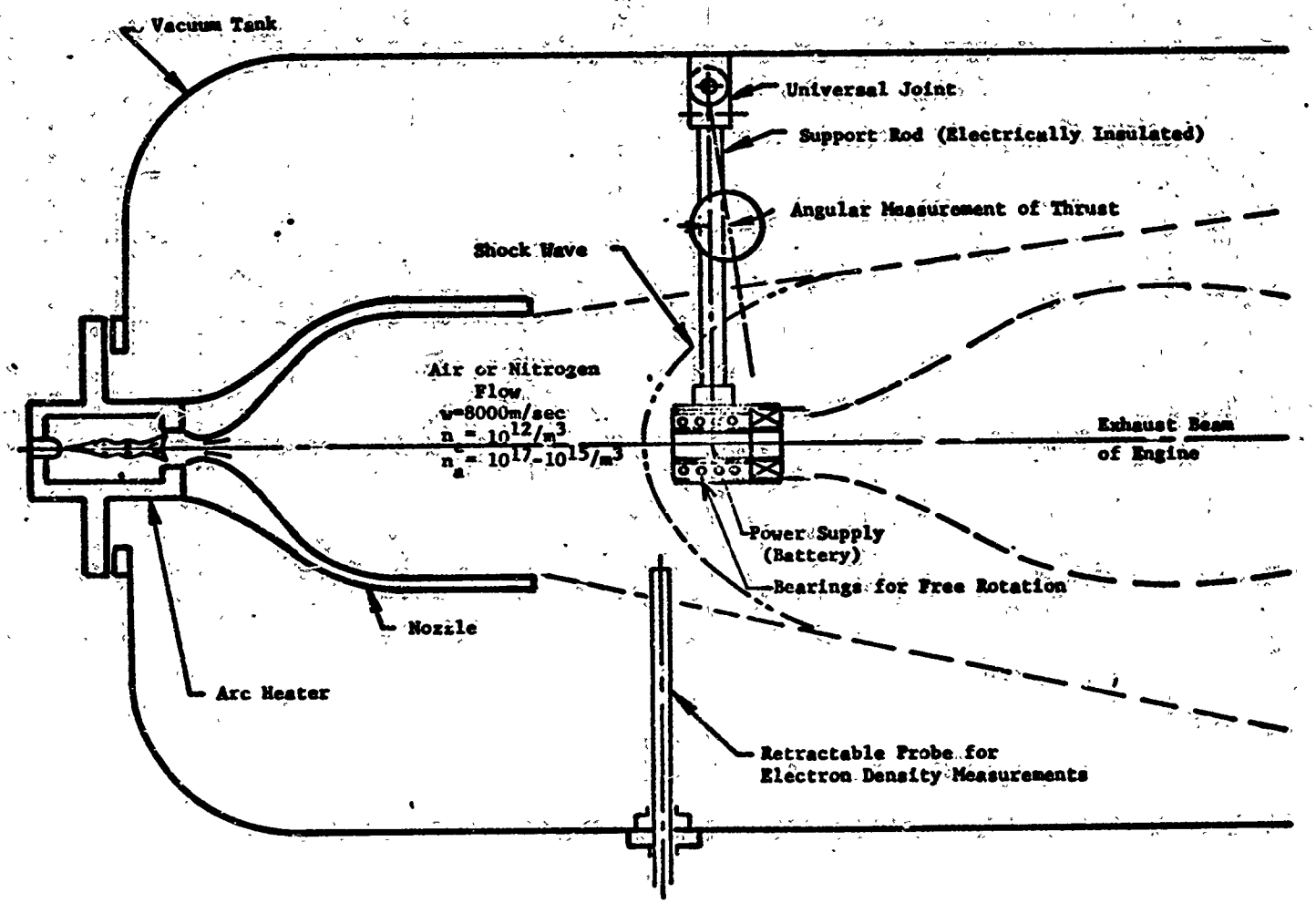

Figure 11.1 Schematic of Test Configuration

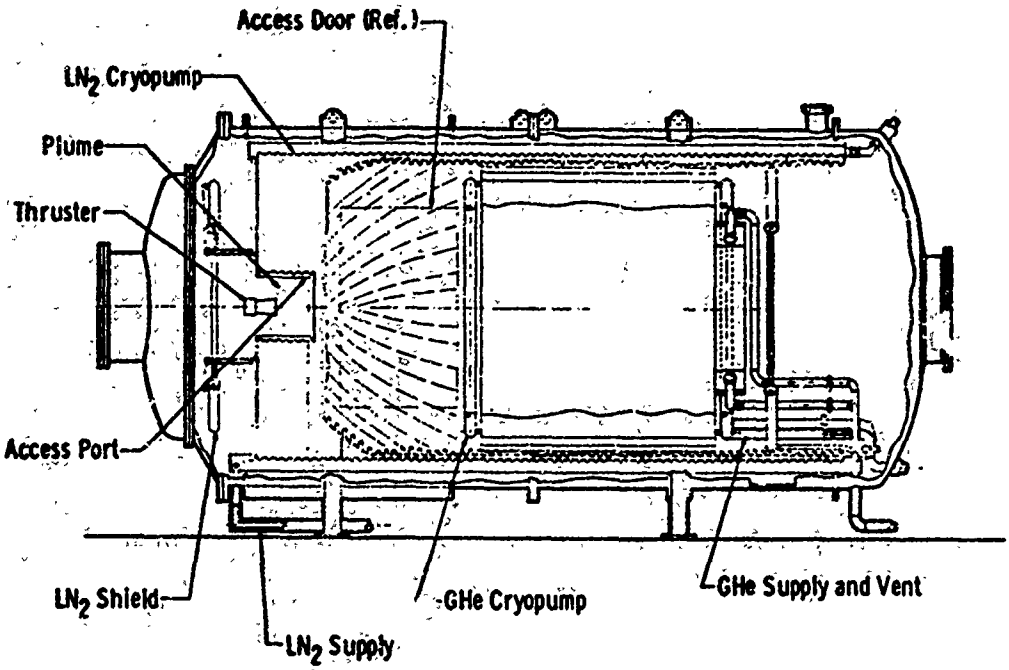

Fig. 12.4 Aerospace Chamber (10V) Operating as a Space Propulsion Test Facility

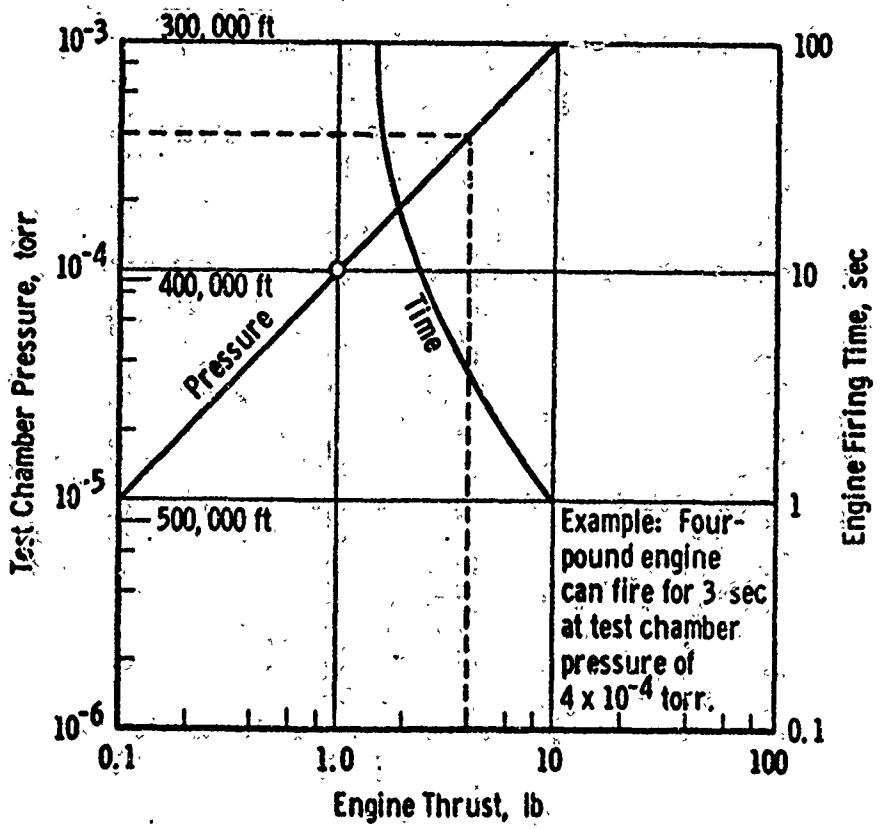

Fig. 11.2 Performance of Aerospace Chamber (10V) for Space Propulsion Testing

TABLE 4.2

Material	ρ kgm/m^3	$1/\sigma$ ohm-m	ρ/σ kgm-ohm/m
Silver	10.5 x10^{3}	1.63x10^{-8}	1.7 x10^{-4}
Copper	8.89 "	1.72 "	1.53 "
Aluminum	2.70 "	2.69 "	0.725 "
Magnesium	1.74 "	4.46 "	0.778 "
Lithium	0.534 "	8.55 "	0.457 "
Sodium	0.971 "	4.30 "	0.417 "
Potassium	0.870 "	6.10 "	0.531 "

APPENDIX I

Relevant parameters of the ARDC STANDARD ATMOSPHERE

Table 1-4 (cont.)

ALTITUDE		SCALE HEIGHT	NUMBER DENSITY	PART. SPEED	COLL. FREQ.	MEAN FREE PATH
Z, m	H, m'	H_s, km	n, m^{-3}	V, m sec^{-1}	ν, sec^{-1}	L, m
64000	63362	7.0484	4.5546 + 21	415.36	1.1198 + 6	3.7093 - 4
66000	65322	6.7893	3.5435	407.53	8.5476 + 5	4.7677
68000	67280	6.5300	2.7301	399.55	6.4564	6.1883
70000	69238	6.2706	2.0813	391.41	4.8217	8.1175
72000	71194	6.0110	1.5685	383.10	3.5567	1.0771 - 3
74000	73148	5.7512	1.1674	374.61	2.5886	1.4472
76000	75102	5.491	8.571 + 20	365.9	1.857	1.971
78000	77054	5.231	6.199	357.1	1.310	2.725
80000	79006	4.972	4.410	348.0	9.082 + 4	3.831
82000	80956	4.975	2.949	348.0	6.075	5.728
84000	82904	4.978	1.973 + 20	348.0	4.064 + 4	8.562 - 3
86000	84852	4.981	1.321	348.0	2.720	1.279 - 2
88000	86798	4.984	8.840 + 19	348.0	1.821	1.911
90000	88743	4.987	5.918	348.0	1.219	2.855
92000	90687	5.073	3.904	350.9	8.108 + 3	4.327
94000	92630	5.310	2.540	358.9	5.395	6.652
96000	94572	5.548	1.684	366.7	3.655	1.003 - 1
98000	96512	5.786	1.136	374.3	2.516	1.488
100000	98451	6.023	7.783 + 18	381.8	1.759	2.171
102000	100389	6.261	5.413	389.2	1.247	3.121
104000	102326	6.500	3.816 + 18	396.4	8.953 + 2	4.428 - 1
106000	104261	6.738	2.724	403.5	6.506	6.202
108000	106196	7.555	1.830	427.1	4.626	9.233
110000	108129	8.731	1.240	459.0	3.368	1.363 + 0
112000	110061	9.908	8.823 + 17	488.8	2.553	1.915
114000	111991	11.09	6.525	516.9	1.996	2.589
116000	113921	12.26	4.975	543.5	1.600	3.396
118000	115849	13.44	3.890	568.8	1.310	4.343
120000	117777	14.62	3.105	593.1	1.090	5.441
125000	122589	17.57	1.899	649.7	7.301 + 1	8.898
130000	127395	20.53	1.254 + 17	701.7	5.208 + 1	1.347 + 1
135000	132192	23.49	8.764 + 16	750.0	3.891	1.928
140000	136983	26.46	6.395	795.3	3.010	2.642
145000	141766	29.43	4.829	838.1	2.395	3.499
150000	146542	32.40	3.748	878.8	1.950	4.507
155000	151310	35.38	2.977	917.6	1.617	5.675
160000	156071	38.36	2.411	954.7	1.363	7.007
165000	160825	41.10	1.998	987.4	1.168	8.456
170000	165572	42.62	1.722	1005.	1.024	9.813
175000	170311	44.11	1.495	1021.	9.036 + 0	1.130 + 2
180000	175043	44.91	1.324 + 16	1030.	8.070 + 0	1.276 + 2
185000	179768	45.71	1.177	1039.	7.234	1.435
190000	184485	46.51	1.050	1046.	6.503	1.609
195000	189196	47.31	9.385 + 15	1055.	5.858	1.800
200000	193899	48.12	8.406	1063.	5.288	2.010
205000	198595	48.92	7.545	1071.	4.782	2.239
210000	203284	49.58	6.805	1077.	4.339	2.483
215000	207965	50.16	6.154	1083.	3.944	2.745
220000	212640	50.75	5.573	1088.	3.589	3.032
225000	217307	51.34	5.052	1094.	3.270	3.344

79

Table 1-4 (cont.)

ALTITUDE		SCALE HEIGHT	NUMBER DENSITY	PART. SPEED	COLL. FREQ.	MEAN FREE PATH
Z, m	H, m'	H_s, km	n, m^{-3}	V, m sec^{-1}	ν, sec^{-1}	L, m
230000	221968	51.93	4.585 + 15	1099.	2.983 + 0	3.685 + 2
240000	231267	53.12	3.790	1110.	2.489	4.458
250000	240539	54.31	3.145	1120.	2.086	5.372
260000	249782	55.50	2.620	1131.	1.754	6.448
270000	258998	56.69	2.191	1141.	1.480	7.712
280000	268185	57.89	1.838	1152.	1.253	9.193
290000	277345	59.09	1.547	1162.	1.064	1.092 + 3
300000	286478	60.29	1.306	1172.	9.056 - 1	1.294
310000	295583	61.50	1.105	1182.	7.731	1.528
320000	304661	62.71	9.385 + 14	1191.	6.618	1.800
330000	313711	63.92	7.989 + 14	1201.	5.680 - 1	2.115 + 3
340000	322735	65.14	6.818	1211.	4.886	2.478
350000	331731	66.36	5.834	1220.	4.213	2.896
360000	340701	67.59	5.003	1229.	3.641	3.377
370000	349644	68.81	4.301	1239.	3.154	3.928
380000	358561	70.04	3.706	1248.	2.738	4.558
390000	367451	71.28	3.201	1257.	2.382	5.278
400000	376315	72.52	2.770	1266.	2.076	6.098
410000	385152	73.76	2.403	1275.	1.813	7.031
420000	393964	75.00	2.088	1284.	1.587	8.090
430000	402749	76.25	1.819 + 14	1292.	1.391 - 1	9.289 + 3
440000	411509	77.50	1.587	1301.	1.222	1.064 + 4
450000	420243	78.75	1.388	1310.	1.076	1.217
460000	428951	80.01	1.216	1318.	9.485 - 2	1.390
470000	437634	81.27	1.067	1327.	8.377	1.584
480000	446291	82.54	9.380 + 13	1335.	7.411	1.801
490000	454923	83.81	8.262	1343.	6.568	2.045
500000	463530	85.08	7.290	1351.	5.830	2.318
510000	472111	86.35	6.443	1359.	5.184	2.622
520000	480668	87.63	5.704	1367.	4.616	2.962
530000	489200	88.91	5.057 + 13	1375.	4.117 - 2	3.341 + 4
540000	497707	90.19	4.492	1383.	3.677	3.761
550000	506189	91.48	3.995	1391.	3.290	4.229
560000	514647	92.77	3.559	1399.	2.947	4.747
570000	523080	94.07	3.176	1407.	2.644	5.320
580000	531489	95.37	2.837	1414.	2.375	5.955
590000	539874	96.67	2.539	1422.	2.136	6.655
600000	548235	97.97	2.275	1429.	1.924	7.427
610000	556571	99.28	2.041	1437.	1.736	8.278
620000	564884	100.6	1.834	1444.	1.567	9.214
630000	573173	101.9	1.650 + 13	1451.	1.417 - 2	1.024 + 5
640000	581438	103.2	1.486	1459.	1.283	1.137
650000	589680	104.5	1.340	1466.	1.163	1.261
660000	597898	105.9	1.210	1473.	1.055	1.396
670000	606092	107.2	1.094	1480.	9.585 - 3	1.544
680000	614263	108.5	9.904 + 12	1487.	8.718	1.706
690000	622411	109.9	8.975	1494.	7.938	1.882
700000	630536	111.2	8.143	1501.	7.235	2.075

80

Table 1-2 (cont.)

ALTITUDE		TEMPERATURE		PRESSURE		
Z, m	H, m'	T, °K	$T_{M'}$ °K	P, mb	P, kgf m^{-2}	P, mm Hg
64000	63362	236.03	236.03	1.4838 - 1	1.5131 + 0	1.1130 - 1
66000	65322	227.21	227.21	1.1113	1.1332	8.3354 - 2
68000	67280	218.40	218.40	8.2298 - 2	8.3920 - 1	6.1728
70000	69238	209.59	209.59	6.0209	6.1396	4.5160
72000	71194	200.79	200.79	4.3470	4.4327	3.2605
74000	73148	191.99	191.99	3.0937	3.1547	2.3204
76000	75102	183.2	183.2	2.167	2.210	1.626
78000	77054	174.4	174.4	1.492	1.522	1.119
80000	79006	165.7	165.7	1.008	1.028	7.563 - 3
82000	80956	165.7	165.7	6.744 - 3	6.877 - 2	5.058
84000	82904	165.7	165.7	4.512 - 3	4.601 - 2	3.384 - 3
86000	84852	165.7	165.7	3.020	3.079	2.265
88000	86798	165.7	165.7	2.021	2.061	1.516
90000	88743	165.7	165.7	1.353	1.380	1.015
92000	90687	168.4	168.4	9.074 - 4	9.253 - 3	6.806 - 4
94000	92630	176.1	176.2	6.172	6.294	4.630
96000	94572	183.7	183.9	4.270	4.354	3.203
98000	96512	191.4	191.7	3.000	3.059	2.250
100000	98451	199.0	199.5	2.138	2.180	1.604
102000	100389	206.6	207.2	1.544	1.574	1.158
104000	102326	214.2	215.0	1.128 - 4	1.151 - 3	8.463 - 5
106000	104261	221.8	222.7	8.341 - 5	8.505 - 4	6.256
108000	106196	248.4	249.6	6.274	6.398	4.706
110000	108129	286.7	288.2	4.906	5.003	3.680
112000	110061	325.0	326.9	3.957	4.035	2.968
114000	111991	363.1	365.5	3.270	3.335	2.453
116000	113921	401.2	404.1	2.755	2.809	2.066
118000	115849	439.1	442.6	2.358	2.404	1.768
120000	117777	477.0	481.2	2.044	2.085	1.533
125000	122589	571.3	577.4	1.497	1.527	1.123
130000	127395	664.9	673.6	1.151 - 5	1.174 - 4	8.632 - 6
135000	132192	757.8	769.5	9.167 - 6	9.348 - 5	6.876
140000	136983	849.9	865.3	7.502	7.650	5.627
145000	141766	941.0	961.0	6.272	6.395	4.704
150000	146542	1031.	1056.	5.334	5.439	4.001
155000	151310	1120.	1152.	4.602	4.693	3.452
160000	156071	1207.	1247.	4.018	4.097	3.014
165000	160825	1285.	1334.	3.544	3.614	2.658
170000	165572	1323.	1381.	3.145	3.207	2.359
175000	170311	1359.	1427.	2.803	2.858	2.102
180000	175043	1371.	1451.	2.505 - 6	2.554 - 5	1.879 - 6
185000	179768	1381.	1474.	2.243	2.287	1.682
190000	184485	1389.	1498.	2.013	2.052	1.510
195000	189196	1397.	1522.	1.809	1.845	1.357
200000	193899	1404.	1545.	1.629	1.661	1.222
205000	198595	1411.	1569.	1.470	1.499	1.102
210000	203284	1414.	1587.	1.328	1.354	9.959 - 7
215000	207965	1414.	1604.	1.201	1.225	9.009
220000	212640	1414.	1620.	1.088	1.109	8.159
225000	217307	1414.	1636.	9.863 - 7	1.006	7.398

81

Table 1-2 (cont.)

ALTITUDE		TEMPERATURE		PRESSURE		
Z, m	H, m'	T, °K	$T_{M'}$, °K	P, mb	P, kgf m^{-2}	P, mm H
230000	221968	1415.	1653.	8.953 - 7	9.129 - 6	6.715 - 7
240000	231267	1415.	1685.	7.401	7.547	5.551
250000	240539	1415.	1718.	6.143	6.265	4.608
260000	249782	1416.	1750.	5.120	5.221	3.841
270000	258998	1417.	1782.	4.284	4.369	3.213
280000	268185	1418.	1814.	3.598	3.669	2.699
290000	277345	1420.	1846.	3.033	3.092	2.275
300000	286478	1423.	1878.	2.565	2.615	1.924
310000	295583	1426.	1910.	2.176	2.219	1.632
320000	304661	1430.	1942.	1.853	1.889	1.390
330000	313711	1435.	1974.	1.582 - 7	1.613 - 6	1.187 - 7
340000	322735	1440.	2005.	1.355	1.382	1.016
350000	331731	1445.	2037.	1.164	1.187	8.729 - 8
360000	340701	1451.	2068.	1.002	1.022	7.518
370000	349644	1458.	2099.	8.656 - 8	8.827 - 7	6.492
380000	358561	1465.	2131.	7.495	7.643	5.622
390000	367451	1473.	2162.	6.506	6.634	4.880
400000	376315	1480.	2193.	5.661	5.773	4.246
410000	385152	1489.	2224.	4.938	5.035	3.703
420000	393964	1497.	2255.	4.316	4.401	3.238
430000	402749	1506.	2285.	3.782 - 8	3.856 - 7	2.837 - 8
440000	411509	1516.	2316.	3.320	3.386	2.491
450000	420243	1525.	2347.	2.921	2.979	2.191
460000	428951	1535.	2377.	2.576	2.626	1.932
470000	437634	1545.	2407.	2.275	2.320	1.707
480000	446291	1555.	2438.	2.014	2.053	1.510
490000	454923	1566.	2468.	1.786	1.821	1.339
500000	463530	1576.	2498.	1.586	1.617	1.190
510000	472111	1587.	2528.	1.412	1.439	1.059
520000	480668	1598.	2558.	1.258	1.283	9.438 - 9
530000	489200	1609.	2588.	1.123 - 8	1.146 - 7	8.427 - 9
540000	497707	1621.	2618.	1.005	1.025	7.536
550000	506189	1632.	2647.	9.000 - 9	9.178 - 8	6.751
560000	514647	1644.	2677.	8.075	8.234	6.056
570000	523080	1655.	2706.	7.255	7.398	5.442
580000	531489	1667.	2736.	6.528	6.657	4.896
590000	539874	1679.	2765.	5.882	5.998	4.412
600000	548235	1691.	2794.	5.308	5.413	3.981
610000	556571	1703.	2824.	4.796	4.891	3.597
620000	564884	1715.	2853.	4.339	4.425	3.255
630000	573173	1727.	2882.	3.931 - 9	4.009 - 8	2.949 - 9
640000	581438	1739.	2911.	3.566	3.636	2.675
650000	589680	1751.	2940.	3.239	3.303	2.429
660000	597898	1763.	2968.	2.945	3.003	2.209
670000	606092	1775.	2997.	2.681	2.734	2.011
680000	614263	1788.	3026.	2.444	2.492	1.833
690000	622411	1800.	3054.	2.230	2.274	1.673
700000	630536	1812.	3083.	2.037	2.077	1.528

82

ALTITUDE		ACCELERATION OF GRAVITY	SPECIFIC WEIGHT	DENSITY	MOLECULAR WEIGHT
Z, m	H, m	g, m sec^{-2}	ω, kgf m^{-3}	ρ, kg m^{-3}	M
64000	63362	9.6121	2.1467 - 4	2.1901 - 4	28.966
66000	65322	9.6061	1.6691	1.7039	28.966
68000	67280	9.6001	1.2851	1.3128	28.966
70000	69238	9.5942	9.7911 - 5	1.0008	28.966
72000	71194	9.5882	7.3744	7.5424 - 5	28.966
74000	73148	9.5822	5.4853	5.6137	28.966
76000	75102	9.576	4.025	4.122	28.97
78000	77054	9.570	2.909	2.981	28.97
80000	79006	9.564	2.068	2.120	28.97
82000	80956	9.558	1.382	1.418	28.97
84000	82904	9.553	9.243 - 6	9.489 - 6	28.97
86000	84852	9.547	6.182	6.350	28.97
88000	86798	9.541	4.135	4.251	28.97
90000	88743	9.535	2.767	2.846	28.97
92000	90687	9.529	1.824	1.877	28.96
94000	92630	9.523	1.185	1.221	28.95
96000	94572	9.517	7.848 - 7	8.087 - 7	28.93
98000	96512	9.511	5.288	5.452	28.92
100000	98451	9.505	3.619	3.734	28.90
102000	100389	9.499	2.514	2.596	28.88
104000	102326	9.493	1.770 - 7	1.829 - 7	28.87
106000	104261	9.488	1.262	1.305	28.85
108000	106196	9.482	8.466 - 8	8.759 - 8	28.83
110000	108129	9.476	5.730	5.930	28.82
112000	110061	9.470	4.073	4.218	28.80
114000	111991	9.464	3.008	3.117	28.78
116000	113921	9.458	2.291	2.375	28.76
118000	115849	9.452	1.789	1.856	28.74
120000	117777	9.447	1.426	1.480	28.71
125000	122589	9.432	8.687 - 9	9.032 - 9	28.66
130000	127395	9.417	5.717 - 9	5.953 - 9	28.59
135000	132192	9.403	3.979	4.150	28.53
140000	136983	9.389	2.892	3.020	28.45
145000	141766	9.374	2.173	2.274	28.36
150000	146542	9.360	1.679	1.759	28.27
155000	151310	9.345	1.326	1.392	28.16
160000	156071	9.331	1.068	1.123	28.04
165000	160825	9.317	8.794 - 10	9.256 - 10	27.91
170000	165572	9.302	7.524	7.932	27.75
175000	170311	9.288	6.479	6.841	27.57
180000	175043	9.274	5.688 - 10	6.015 - 10	27.36
185000	179768	9.260	5.004	5.300	27.12
190000	184485	9.246	4.412	4.680	26.85
195000	189196	9.231	3.899	4.142	26.59
200000	193899	9.217	3.452	3.673	26.32
205000	198595	9.203	3.063	3.264	26.06
210000	203284	9.189	2.731	2.914	25.80
215000	207965	9.175	2.442	2.610	25.54
220000	212640	9.161	2.186	2.339	25.29
225000	217307	9.148	1.959	2.100	25.04

83

Table 1-3 (Cont)

ALTITUDE		ACCELERATION OF GRAVITY	SPECIFIC WEIGHT	DENSITY	MOLECULAR WEIGHT
Z, m	H, m	g, m sec^{-2}	ω, kgf m^{-3}	ρ, kg m^{-3}	M
230000	221968	9.134	1.758 - 10	1.887 - 10	24.79
240000	231267	9.106	1.421	1.530	24.32
250000	240539	9.078	1.154	1.246	23.87
260000	249782	9.051	9.408 - 11	1.019	23.44
270000	258998	9.024	7.706	8.375 - 11	23.03
280000	268185	8.996	6.338	6.909	22.65
290000	277345	8.969	5.233	5.722	22.28
300000	286478	8.942	4.338	4.757	21.95
310000	295583	8.916	3.609	3.969	21.63
320000	304661	8.889	3.013	3.324	21.33
330000	313711	8.862	2.524 - 11	2.792 - 11	21.06
340000	322735	8.836	2.121	2.354	20.80
350000	331731	8.810	1.788	1.991	20.55
360000	340701	8.783	1.512	1.688	20.33
370000	349644	8.757	1.283	1.436	20.12
380000	358561	8.731	1.091	1.225	19.92
390000	367451	8.705	9.307 - 12	1.048	19.73
400000	376315	8.680	7.960	8.994 - 12	19.56
410000	385152	8.654	6.826	7.736	19.39
420000	393964	8.628	5.868	6.670	19.24
430000	402749	8.603	5.057 - 12	5.765 - 12	19.09
440000	411509	8.578	4.369	4.995	18.96
450000	420243	8.552	3.783	4.338	18.83
460000	428951	8.527	3.283	3.775	18.71
470000	437634	8.502	2.855	3.293	18.59
480000	446291	8.477	2.488	2.878	18.48
490000	454923	8.453	2.173	2.521	18.38
500000	463530	8.428	1.901	2.212	18.28
510000	472111	8.403	1.667	1.945	18.19
520000	480668	8.379	1.464	1.714	18.10
530000	489200	8.355	1.289 - 12	1.512 - 12	18.01
540000	497707	8.330	1.136	1.337	17.93
550000	506189	8.306	1.003	1.184	17.86
560000	514647	8.282	8.875 - 13	1.051	17.78
570000	523080	8.258	7.864	9.339 - 13	17.72
580000	531489	8.235	6.980	8.313	17.65
590000	539874	8.211	6.205	7.411	17.58
600000	548235	8.187	5.525	6.617	17.52
610000	556571	8.164	4.926	5.917	17.47
620000	564884	8.140	4.399	5.299	17.41
630000	573173	8.117	3.934 - 13	4.753 - 13	17.36
640000	581438	8.094	3.523	4.268	17.30
650000	589680	8.071	3.159	3.839	17.25
660000	597898	8.048	2.837	3.457	17.21
670000	606092	8.025	2.551	3.117	17.16
680000	614263	8.002	2.296	2.814	17.12
690000	622411	7.979	2.070	2.544	17.07
700000	630536	7.957	1.868	2.302	17.03

84

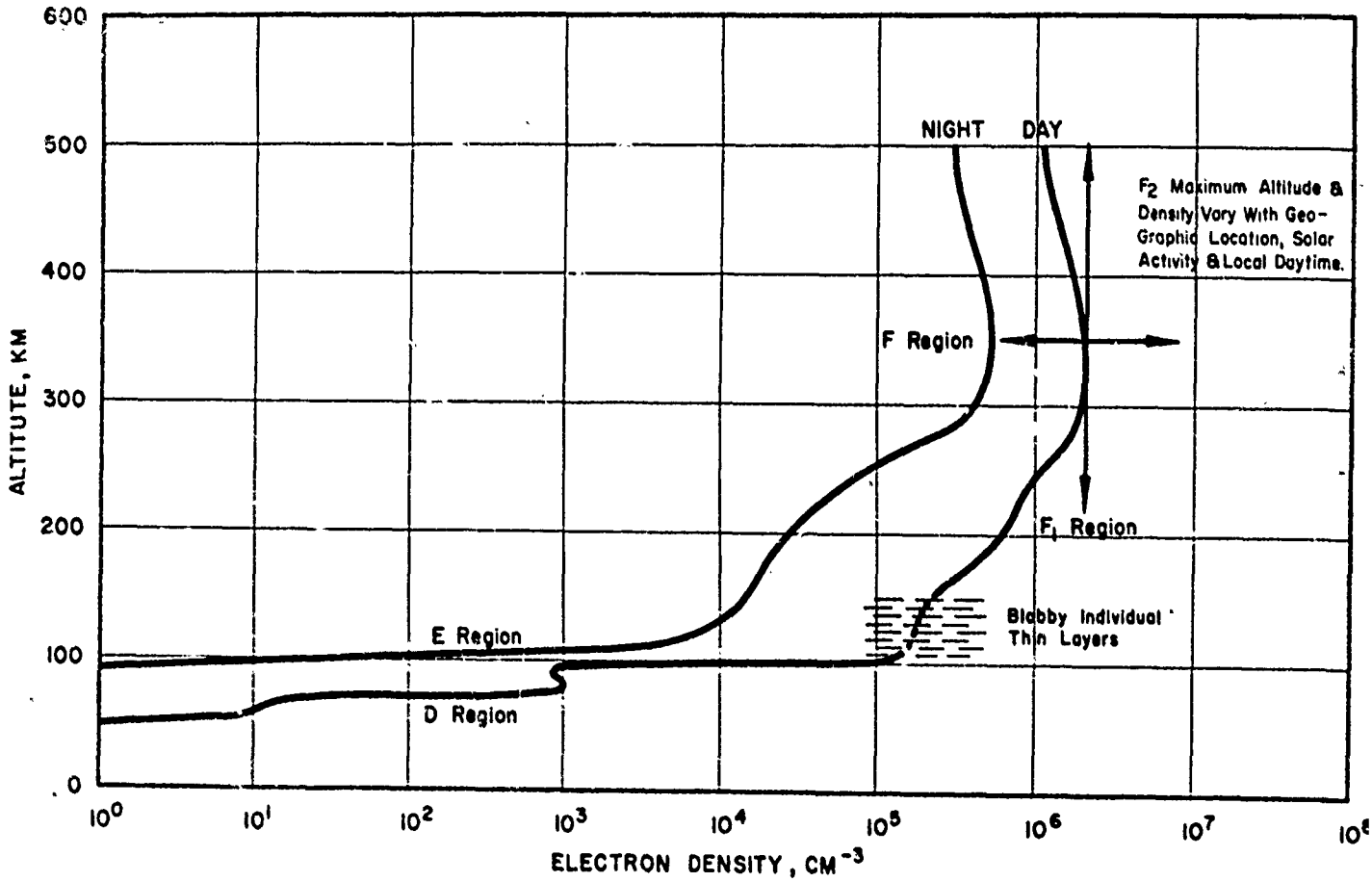

Fig. 15-2. An Electron Density Model in the Ionosphere

85

APPENDIX II

Ion Production and Acceleration Mechanisms.(Extract from Reference 13.).

2. PHYSICAL PROCESSES

All electric propulsion engines rely upon two basic processes:

1. Ion production
2. Ion acceleration

In accomplishing these ends, certain penalties must be paid, which are usually evaluated in terms of propellant mass utilization and electric power utilization. The axisymmetric Hall current accelerator, or MPD arc, accomplishes all of the three processes mentioned above by means of a dc arc struck between electrodes placed symmetrically in a solenoidal magnetic field. However, the measurements that can be made are such that it is virtually impossible to evaluate propellant mass utilization and power utilization independently. Thus, great simplicity of design is gained at the expense of great complexity in the interaction of the engine operating mechanisms.

One of the features of the MPD arc that appears most baffling to physicists is the apparently uncorrelated behavior of the arc current and the ion flux rate. Since the electrons can carry an appreciable fraction of the arc current, considerable energy from the electric field is transferred initially to the electron internal and kinetic energy, from where it can later be transferred to the ions. This allows the ions, under some circumstances, to leave the engine with energies greater than they could achieve by falling through the potential drop of the discharge. The detailed process by which this can be accomplished will be discussed in the following paragraphs.

86-A

2.1 Ion Production

The momentum conservation equations indicate that some torque and force reaction must occur on the engine (see Section 3). For this to happen, ions must be produced in and expelled from the motor with axial and angular velocity. The fewer the ions, the higher the resultant velocities must be and, consequently, the beam power must be higher. On the other hand, as the ion production and expulsion rate increases, the power in ion production becomes very high, hence some ion flow rate must exist at which the electrical power into the discharge is a minimum. If the arc current is held fixed, this implies that the discharge seeks a minimum voltage mode in which to operate. The above argument then indicates that the arc accomplishes this end by ionizing the optimum amount of propellant to expell in the exhaust beam. The key, then, to explaining the operating characteristics of the engine lies in determining the optimum ion exhaust rate and in understanding the production process for these ions throughout the volume of the discharge.

Previously (Ref. 1), it had been concluded that volume ionization away from the electrode surfaces could not account for all of the ions produced. At that time, it was assumed that the electron temperature was about 10,000°K. Since then, data on anode heating have indicated that the electron temperature may be much higher, e.g., $\approx$ 30,000 - 50,000°K. This raises the probability of volume ion production, through electron atom collisions, to values where it can account for most, if not all, of the ions used in the exhaust beam.

The atoms are not confined to any great extent by the electric discharge. Hence the flow field of the gas will be substantially the same as one would find for the gas issuing from the orifice with no discharge present. The discharge must now encompass this gas and adjust the electron temperature and density throughout its volume so as to ionize the optimum amount of propellant. Clearly, to get good propellant utilization, the injected flow rate should be close to the ion flow rate in the beam. However, in the interest of obtaining best

overall efficiency, it may be necessary to inject slightly more propellant than is used by the beam. This would help to restrict the volume of the discharge and perhaps keep the electron temperature to lower values, thus reducing power loss by electron energy convection to the anode.

Since a vast majority of atom-electron collisions are elastic collisions, the energy used to ionize one atom must be considerably greater than the ionization potential of the atom. The energy difference is transferred into the internal energy of the atoms and ions. If most of the injected mass is eventually ionized, this energy is not lost but is available to be transferred into beam kinetic energy by eventual expansion through the magnetic nozzle. It is obvious, of course, that this internal energy of the heavy particles can never be higher than that of the electrons. This argument indicates that the ionization process need not be efficient. However, the number of inelastic collisions that excite the electrons to states that can radiate should be minimized. This is basically a problem of propellant selection.

The electron internal energy results from the electron current passing through the potential drop and being randomized by collisions with heavy particles. For this reason it would be expected that the highest electron energy would be found in the anode sheath, after the electrons have fallen through most of the potential drop. This is fortuitous, since it is precisely in this region that the highest production rate is wanted, to let the ions gain a maximum of kinetic energy by falling through the potential back toward the cathode jet

2.2 Ion Acceleration

Momentum can be transferred to the ions from electric fields or from collisions with other particles. For convenience, the momentum exchange processes in a fully ionized gas through which an electric discharge is passing shall be discussed.

Locally, the force on each ion is given by the following expressions:

Axial: $$|e|\left\{E_z + u_I B_\theta - v_I B_r - \frac{J_z}{\sigma}\right\}$$

Radial: $$|e|\left\{E_r + v_I B_z - w_I B_\theta - \frac{J_r}{\sigma}\right\}$$

Azimuthal: $$|e|\left\{w_I B_r - u_I B_z - \frac{J_\theta}{\sigma}\right\}$$

If an electric discharge is established in a uniform axial magnetic field we shall call the region where the current flows downstream the anode sheath and the region where it flows upstream the cathode jet. If a cathode of maximum diameter R_c is surrounded by an anode ring of diameter R_A ($R_A > R_c$) we ask the questions:

1. Does the cathode jet expand out to meet the anode sheath?
2. Does the anode sheath contract in diameter to meet the cathode jet?
3. Do both (1) and (2) occur simultaneously?

Consider first the cathode jet. If the cathode jet is to expand outward, conservation of momentum states that the axial momentum of the jet must increase and the rotational momentum of the jet must increase. However, the local (E + v x B) axial and tangential electric fields are both in the wrong direction to accelerate the ions and the mementum must hence be transferred to them by electron collisions. This is a highly dissipative process, resulting in strong heating of the electrons. This increases the rates of entropy production over that caused by ion-electron drag in a purely dissipative plasma (no body force).

In the anode jet the situation is quite different. Both E_z and $u_I B_\theta$ are in the positive z direction, thus helping to accelerate the ions axially. The only dissipative or entropy producing

1. A uniform diameter cathode jet is established which carries only a small fraction of the injected mass flow rate.
2. An annulus of plasma is established off of the anode face. The injected mass is accumulated within this annulus. All of the discharge current passes through the annulus.
3. The average radius of this anode sheath decreases downstream. This causes the ions in the sheath to be accelerated slightly in the axial direction and to be spun up to high azimuthal velocities. The electrons are simultaneously heated, mainly by the ion-electron drag in the azimuthal direction, where the azimuthal electron motion is helping to spin up the ions.
4. The anode sheath eventually meets the cathode jet at $z = L$ and the current path is completed. No discharge current flows at axial positions beyond this point.
5. At positions of $z > L$, the magnetic field acts like a magnetic nozzle. As the field diverges the ions are accelerated axially by two processes:
    a. Conversion of angular momentum requires that as the jet radius increases, rotational ion energy must be transferred to axial and radial kinetic energy.
    b. The high energy electrons tend to expand out of the nozzle ahead of the ions, thus setting up a positive axial electric field that accelerates the ions. In this manner, all of the energy of the particles in the beam can be converted into the kinetic energy of the ions. Obviously, some of this energy will reside in the radial motion with the result that the expansion will not be 100 percent efficient.

An attempt to analyze the "heating" (constant magnetic field) region of such a device is made in Section 4 of this report.

3. INTEGRALS OF THE MOMENTUM EQUATIONS

There are a few cases where the net electromagnetic force in an axisymmetric body can be computed without detailed knowledge of the distributions of current and magnetic field. In the general case, the momentum equations must be integrated simultaneously with continuity, energy, Ohm's laws, Maxwell's equations and the equations of state. The cases chosen here are such that the integrand (force per unit volume) can be put into the form of a divergence, by using Maxwell's equations and simplified momentum equations. These forces can be integrated in terms of total current, radius, and applied magnetic field.

3.1 Pressure Due to $J_z B_\theta$ Pinch

Here the average pressure on the cathode is computed in terms of the current and radius of attachment. The equations used are a momentum equation

$$\frac{dp}{dr} = - J_z B_\theta, \quad p(r=R) = p_o \quad , \tag{1}$$

an induction equation

$$\frac{1}{r} \frac{d}{dr}(rB_\theta) = \mu_o J_z, \quad B_\theta(r = 0) = 0 \quad , \tag{2}$$

a total current integral

$$I = \int_o^R J_z(r)\ 2\pi r\ dr \quad , \tag{3}$$

91

and a definition of average pressure

$$p_{av} = \frac{1}{\pi R^2} \int_0^R p(r)\ 2\pi r\ dr \tag{4}$$

Combining the above relations, it follows that independent of the distribution of J_z, the average cathode pressure is given by:

$$p_{av} = p_o + \frac{\mu_o I^2}{8\pi^2 R^2} \tag{5}$$

The pressure given by Eq. 5 will act on the cathode to give a thrust. This thrust force is given by $\mu_o I^2/8\pi$ and is independent of the distribution of the current density at the cathode, and of the size of the cathode attachment.

3.2 Thrust Due to $J_r B_\theta$ Pumping

The amount of thrust in an axially symmetric volume due to radial currents and induced azimuthal magnetic field can be evaluated in terms of the magnetic field distribution at the boundaries. This, in turn can be evaluated from the total currents. The following relations are used:

$$\frac{1}{r}\frac{\partial}{\partial r}(r\ B_\theta) = \mu_o\ J_z \tag{6}$$

$$-\frac{\partial B_\theta}{\partial z} = \mu_o\ J_r \tag{7}$$

From Eq.7 it follows that $J_r\ B_\theta = -\frac{\partial}{\partial z}(B_\theta^2/2\mu_o)$

$$\text{Thrust} = \int_0^R \int_{z_1(r)}^{z_2(r)} J_r \, B_\theta \, 2\pi r \, dz \, dr \tag{8}$$

$$= \int_0^R 2\pi r \left[\frac{- B_\theta^2}{2 \mu_o} \right]_{z_1(r)}^{z_2(r)} dr$$

B_θ can be found by integrating (Eq. 6)

$$B_\theta(r, z) = \frac{1}{r} \int_0^r s \, J_z(s, z) \, ds \tag{9}$$

Equation 8 shows that thrust can be evaluated in terms of magnetic field and Eq. 9 shows that magnetic field depends only upon axial current. If:

a) Current leaves cylindrical anode of radius R_A

b) current enters circular cathode of radius R_c with uniform current density

then

$$\text{Thrust} = \frac{\mu_o I^2}{4\pi} \left(\frac{1}{4} + \ln \frac{R_A}{R_c} \right) \tag{10}$$

3.3 Torque Due to $(r J_z B_r - r J_r B_z)$

In an axially symmetric volume with radial and axial currents and magnetic fields, there will be a torque which occurs when the current crosses the magnetic field. To evaluate this torque, introduce the vector potential A_θ.

$$B_r = -\frac{\partial A_\theta}{\partial z} \; ; \quad B_z = \frac{1}{r}\frac{\partial}{\partial r}(r A_\theta) \tag{11}$$

The quantity $(r A_\theta)$ is constant along a magnetic field line. The torque per unit volume is given by:

$$r J_z B_r - r J_r B_z = -\left[J_r \frac{\partial (r A_\theta)}{\partial r} + J_z \frac{\partial (r A_\theta)}{\partial z}\right] \tag{12}$$

For the axially symmetric case, $\frac{\partial (r A_\theta)}{\partial \theta} = 0$, hence

$$\begin{aligned} \text{Torque} &= -\bar{J} \cdot \nabla (r A_\theta) \\ &= -\nabla \cdot (r A_\theta \bar{J}) \end{aligned} \tag{13}$$

where $\nabla \cdot J = 0$ has been used. Upon integration over a volume R of surface S, outward normal $\bar{n}$,

$$\int_R (\text{torque})\, d(\text{vol}) = \int_S (-r A_\theta)(\bar{J} \cdot \bar{n})\, dS \tag{14}$$

If $r A_\theta$ is constant at anode and cathode

$$\text{Torque} = I\left[(r A_\theta)_{\text{anode}} - (r A_\theta)_{\text{cathode}}\right]$$

$$= I \int_{\text{cathode}}^{\text{anode}} \left[\frac{\partial (r A_\theta)}{\partial r} dr + \frac{\partial (r A_\theta)}{\partial z} dz\right] \qquad (15)$$

$$= \frac{I \text{ (Magnetic Flux Between Cathode and Anode)}}{2\pi}$$

Finally for a point cathode, and an average axial field B_z through a circular anode of radius R_A,

$$\text{Torque} = \frac{1}{2} B I R_A^2 \qquad (16)$$

3.4 Max Thrust Due to $J_\theta B_r$

In an axially symmetric volume where J_θ is induced (by the Hall effect), the amount of axial force cannot be larger than for the case of a completely diamagnetic plasma. In this limiting case, the J_θ lies completely in the surface of the volume, and no magnetic fields exist inside the volume. Compute the currents and magnetic field as follows. Let $B = B_0 + B_1$ where B_0 is the applied field due to external magnets and B_1 is the field due to induced currents within the volume. Outside of the plasma, $\nabla \times B_1$ is zero, hence $B_1 = \nabla \Psi$, where Ψ is a scalar field. Since $\nabla \cdot B_1 = 0$, then

$$\nabla^2 \Psi = 0 \text{ (outside of plasma)} \qquad (17)$$

Since $\bar{B} \cdot \bar{n} = 0$ at the plasma surface

$$\frac{\partial \Psi}{\partial n} = - (\bar{B}_0) \cdot \bar{n} \text{ (at plasma surface)} \qquad (18)$$

Solve Laplace Eq. 17 with boundary condition Eq. 18. The force is given by

$$\text{Force} = -\int\int (\bar{B}_0 + \nabla \Psi)^2 \, \bar{n} \, d S$$

where $\bar{n}$ is an outward normal and S is the surface area of the plasma.

The same result can be obtained by the following method. Here we shall attempt to solve for the surface J_θ distribution for a particular plasma configuration shown in Fig. 3-1. We use a θ-Ohm's law (where Ψ_e is the Hall parameter for electrons).

$$J_\theta = -\frac{\Psi_e}{|B|} (J_z B_r - J_r B_z), \tag{19}$$

and the induction equations

$$\frac{\partial B_r}{\partial z} - \frac{\partial B_z}{\partial r} = \mu_o J_\theta \tag{20-a}$$

$$\frac{1}{r} \frac{\partial}{\partial r} (r B_r) + \frac{\partial B_z}{\partial z} = 0 \tag{20-b}$$

In Eq. 19, the coefficient $\frac{\Psi_e}{|B|}$ does not depend upon magnetic field, since Ψ_e is proportional to $|B|$. We assume J_z and J_r are known, based upon visual observations of the operation of the accelerator. It appears that $J_r = 0$, and J_z = total current divided by cross sectional area of the anode jet ($2\pi R_a \delta$). Thus Eq. 19 becomes

$$J_\theta = -\left[\frac{\Psi_e}{|B|} \frac{I_A}{2\pi R_A \delta}\right] B_r \tag{21}$$

From Eq. 21 we see that B_r (and not B_z) is important for calculating J_θ. We can use the integral solution of Eqs. 20-a and 20-b which assumes no magnetic material is present:

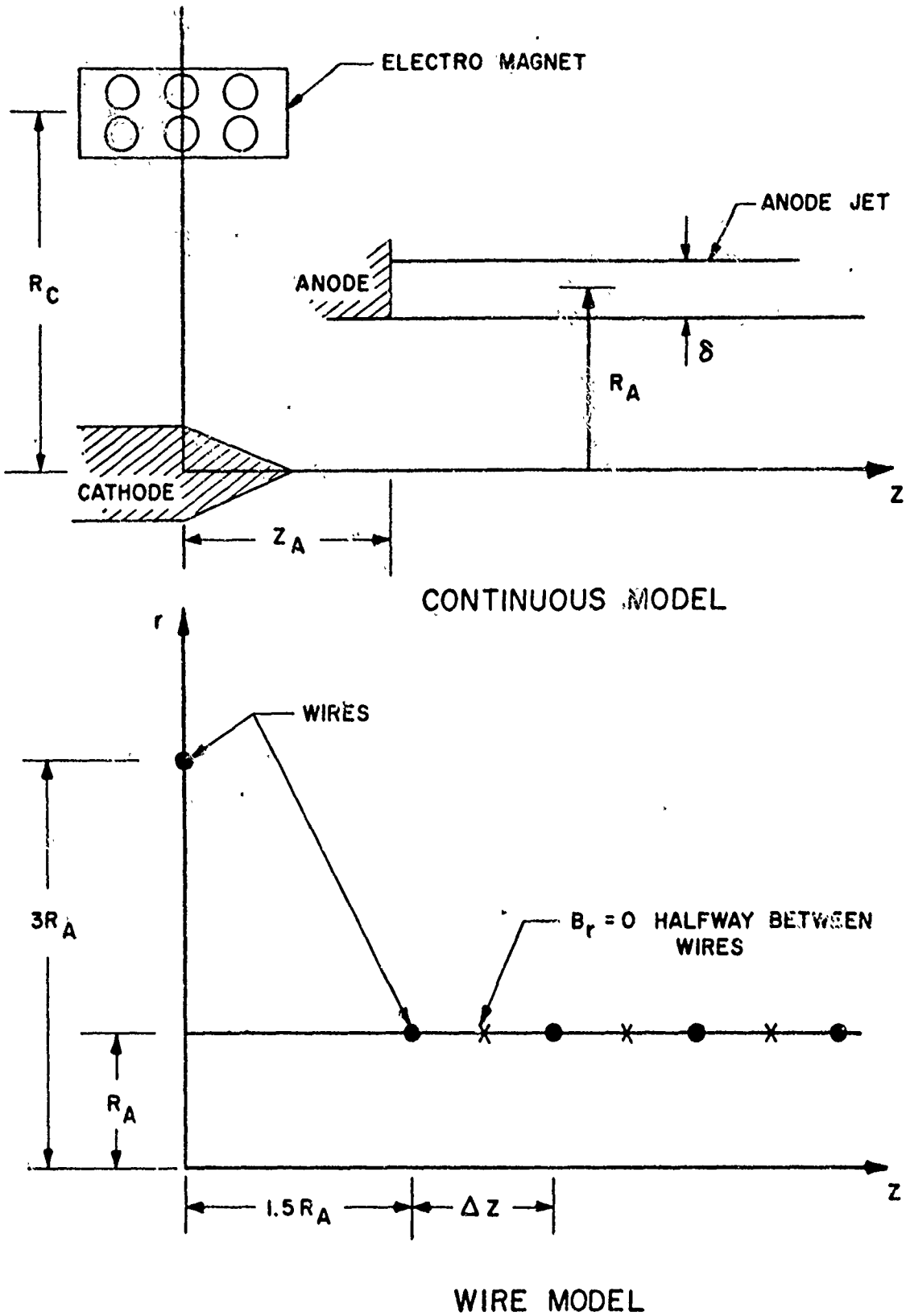

FIG. 3-1 MODELS FOR INDUCED FIELD ANALYSIS

$$B_r(r, z) = \frac{\mu_o}{2\pi r} \iint G(r; s; z-t)\, J_\theta\, , t)\, ds\, dt$$

where

$$G(r, s; z-t) \equiv \int_0^\pi \frac{r\, s\, (z-t)\, \cos\phi\, d\phi}{\left[r^2 - 2rs\cos\phi + s^2 + (z-t)^2\right]^{3/2}} \qquad (22)$$

When applying Eq. 22, we use Eq. 21 for the value of J_θ in the region of the anode jet, and the known J_θ in the electromagnet. Thus, Eq. 21 becomes:

$$J_{\theta,Hall} = \left[1 - \frac{\Psi_e}{|B|} \frac{I_A}{2\pi R_A \delta}\right] \frac{\mu_o}{2\pi r} \left\{ \begin{array}{l} \iint_{coil} G(r, s; z-t)\, J_{\theta,coil}(s,t) ds\, dt \\ \\ + \iint_{anode\ jet} G(r,s,z-t) J_{\theta,Hall}(s,t)\, ds\, dt \end{array} \right\} \qquad (23)$$

Eq. 23 is an integral equation for the Hall current in the anode jet.

Exact solutions are not available for Eq. 23. An approximate solution has been obtained by lumping the distributed Hall currents J_θ into concentrated currents. We will refer to this technique as the wire model. The Hall currents are replaced approximately by hoop currents in a set of wires. The error of the lumping has been estimated, by changing the number of wires per unit length of the anode jet, and shown to be small.

The solution found was for infinite conductivity, or more precisely $\lambda \to \infty$ where

$$\lambda = \frac{\mu_o \Psi_e I_A}{|B| (2\pi)^2 R_A} = \frac{\mu_o \sigma I_A}{|e| n_I (2\pi)^2 R_A} \qquad (24)$$

This is the limit of a completely diamagnetic plasma.

To solve the wire model, concentrate the current density into a set of wires (see Fig. 3-1). Thus, the wire for the electromagnet coil has a current I_c, where I_c is equal to the number of turns times the current in one conductor. The wires which carry the Hall currents in the anode jet carry a current of $J_{\theta,\,\mathrm{Hall}} \cdot \Delta z \cdot \delta$. The integral Eq. 23 is thus replaced by a set of simultaneous algebraic equations. In the infinite λ case, which corresponds to infinite conductivity, $B_r = 0$. Thus, $(B_r)_j = 0$, where j stands for one of the points shown in the wire model of Fig. 3-1.

$$0 = G(R_A, R_c, z_j)\, I_c + \sum_{i=1} G(R_A, R_A, z_j - z_i)\, I_i \tag{25}$$

Some solutions of Eq. 25 are shown in Fig. 3-2. The Kernel function G defined in Eq. 22 can be computed in terms of elliptic integrals.

$$G(r,s;t) = \frac{2rst}{\left[(r+s)^2 + t^2\right]^{3/2}} \; \frac{(2-k^2)\,E(k) - 2(1-k^2)\,K(k)}{k^2\,(1-k^2)} \tag{26}$$

where E and K are elliptic integrals and $k^2 = 4rs/\left[(r+s)^2 + t^2\right]$. To simplify the computations, a function G_{planar} based upon a flat geometry was used

$$G_{\mathrm{planar}}(r,s;t) = \frac{4r^2\,st}{\left[(r-s)^2 + t^2\right]\left[(r+s)^2 + t^2\right]} \tag{27}$$

This is a good approximation to the Kernel function near the coil.

The electromagnetic thrust can be computed either from the integral of the $J_\theta B_r$ forces in the jet or by the reaction on the coil.

$$\text{Thrust} = \iint_{\text{coil}} J_{\theta,\,\text{coil}}\, B_r\, 2\pi r\, dr\, dz = -\iint_{\text{anode jet}} J_{\theta,\text{Hall}} B_r\, 2\pi r\, dr\, dz \tag{28}$$

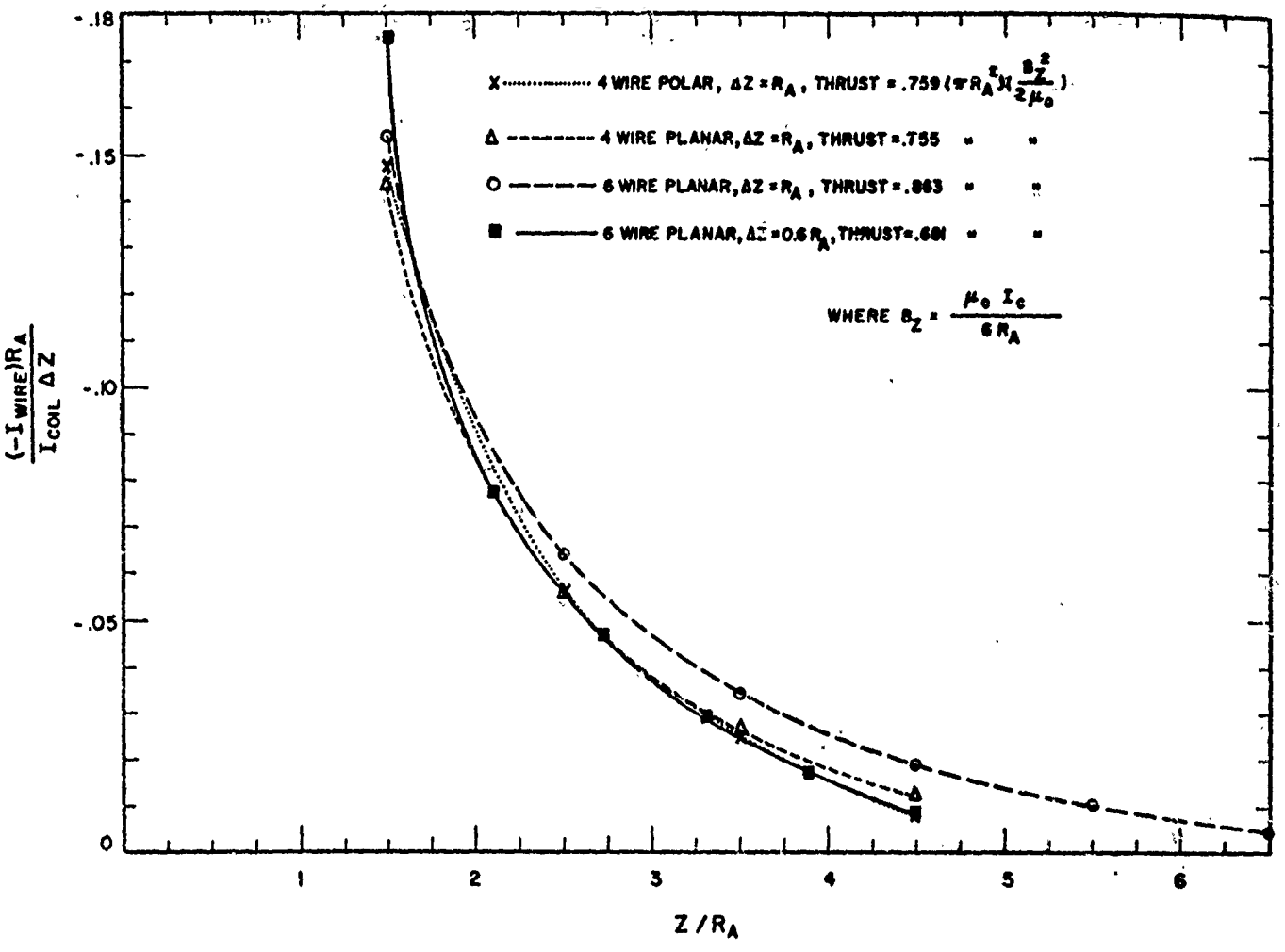

FIG. 3-2 COMPUTED HALL WIRE CURRENTS AND THRUSTS

For the example of Fig. 3-1, the integration was made over the coil. The thrust is approximately 80 percent of the product of the cross-section area of the anode jet times the magnetic pressure which would exist along the centerline if there were no Hall currents. This is probably an upper limit of the possible thrust.

12.4 Estimated Costs

Section	Labor	Hardware	Facilities * (Leased or Rented)	TOTAL
12.1	$12,500.	$ 3,700.	$ 3,200.	$19,400.
12.2	32,900.	5,800.	12,700.	51,400.
12.3	65,400.	12,900.	20,200.	98,500.

* (Not needed if USAF facilities are available)